NTNU
Norwegian University of
Science and Technology

Analysis and Design of Mooring and Turret Systems for Ship-shaped Floating Production Systems (FPSOs)

Analyse og design av forankrings- og
turretsystemer for flytende produksjonsskip
(FPSO)

Åse Kristin Danbolt
Svalastog

Marine Technology
Submission date: June 2017
Supervisor: Kjell Larsen, IMT

Norwegian University of Science and Technology
Department of Marine Technology

NTNU Trondheim
Norges teknisk-naturvitenskapelige universitet
Institutt for marin teknikk

MASTER THESIS SPRING 2017

for

Stud. tech. Åse Kristin Danbolt Svalastog

Analysis and Design of Mooring and Turret Systems for Ship-shaped Floating Production Systems (FPSOs)

Analyse og design av forankrings- og turretsystemer for flytende produksjonsskip (FPSO)

Background

Floating production concepts for oil and gas are often designed as turret moored ships; Floating Production, Storage and Offloading units (FPSOs). The purpose of the turret mooring system is to keep the vessel safely at a required position due to the integrity of the production risers. It normally consists of 12-20 mooring lines of heavy chain, steel wire ropes and/or synthetic polyester ropes connected to a seabed anchor.

During the past years, the requirements to the mooring and station keeping systems of mobile and permanent units have become more complex;
- The industry is moving into new frontiers (ultra-deep water down to 3000m depth and into arctic areas).
- There are more operations adjacent to other installations (floatel operations and tender support vessel operations).
- The new mobile units are becoming larger and many units are at the end of their lifetime.
- There are too many anchor line failures.
- The design lifetime of the units must in many cases be extended due to increased oil recovery.

The overall objective of this thesis is to assess and perform optimization for ULS design of the turret mooring system based on numerical simulations in the time domain. A typical FPSO unit designed for Norwegian Continental Shelf shall be studied.

Analysis methods for estimating ultimate mooring line tension and vessel offset can be divided into frequency domain (FD) methods and time domain (TD) methods. When using TD methods, all non-linearities in the dynamic system (stiffness and damping) and in the excitation may be taken into account. The result of TD simulations are time series of selected responses that must be carefully analysed by relevant statistical methods in order to establish a reliable estimate of the characteristic load effect. Simulations in the time domain shall be used as the basic method for the work in this thesis.

Scope of Work

1) Review relevant literature for mooring systems and in particular time domain simulation of mooring systems and describe the theory related to coupled and separated analysis methodology. Describe the relevant simulation tools available in SIMA and how SIMA can effectively be utilized.

2) Establish and verify a time domain simulation model for the given FPSO in SIMA for use in SIMO and RIFLEX. Perform simple design calculations according to requirements in rules and regulations.

3) Propose a ULS design methodology for the mooring lines and turret support forces based on time domain simulations using the contour line approach. Perform selected analyses and assess the variability in the line tensions and turret forces. Sensitivity studies shall be carried out as agreed with the supervisor.

4) Quantify, compare and describe the load effects in leeward and windward lines for typical ULS conditions. Make a comparison between tension in single lines and turret forces. For the turret support forces the required turret weight in order to prevent uplift shall be quantified.

5) Conclusions and recommendations for further work.

General information

The work shall build on the project work report "Design of mooring systems with focus on frequency domain analysis of a turret moored FPSO".

All necessary input files related to the FPSO for the simulation case will be provided by Statoil.

The work scope may prove to be larger than initially anticipated. Subject to approval from the supervisor, topics may be reduced in extent.

In the project the candidate shall present her personal contribution to the resolution of problems within the scope of work.

Theories and conclusions should be based on mathematical derivations and/or logic reasoning identifying the various steps in the deduction.

The candidate should utilise the existing possibilities for obtaining relevant literature.

Thesis report

The thesis report should be organised in a rational manner to give a clear exposition of results, assessments, and conclusions. The text should be brief and to the point, with a clear language. Telegraphic language should be avoided.

The report shall be written in English and edited as a research report including literature survey, description of relevant mathematical models together with numerical simulation results, discussion, conclusions and proposal for further work. List of symbols and acronyms, references and (optional) appendices shall also be included. All figures, tables and equations shall be numerated.

The original contribution of the candidate and material taken from other sources shall be clearly defined. Work from other sources shall be properly referenced using an acknowledged referencing system.

In addition to an electronic version, the report shall be submitted in two paper copies:

- Signed by the candidate
- The text defining the scope included
- In bound volume(s)
- Drawings and/or computer prints which cannot be bound should be organised in a separate folder.

Ownership

NTNU has according to the present rules the ownership of the project results. Any use of the project results has to be approved by NTNU (or external partner when this applies). The department has the right to use the results as if the work was carried out by a NTNU employee, if nothing else has been agreed in advance.

Thesis supervisor:

Prof. II Kjell Larsen, NTNU/Statoil

Deadline: June 11th, 2017

Trondheim, June, 2017

Kjell Larsen (date and signature) : June 8th 2017

Åse Kristin Danbolt Svalastog (date and signature):

June 8th 2017
Åse Kristin D. Svalastog

Preface

This master thesis is written as a part of a two-year Master of Science program with a specialization in Hydrodynamics at the Norwegian University of Science and Technology. The thesis is carried out from January to June 2017. I am intrigued by the dynamics between the moored floating structures and the forces acting on it, in addition the topic is highly relevant in the industry today, these are the main reasons for why I chose to write this paper.

My gratitude goes to my supervisor Kjell Larsen for his encouragement, helpful assistance and inspiration during this master thesis. I would also like to thank Statoil for providing the coupled SIMO-RIFLEX model used in the analyses.

The reader of this report should preferably have a basic understanding of marine hydrodynamics and dynamic analysis.

Trondheim, June 9th 2017

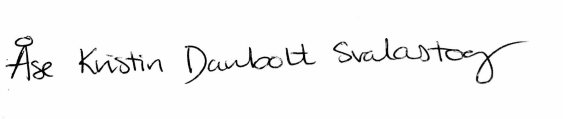

Åse Kristin Danbolt Svalastog

Summary

During the past years, the requirements to the mooring and station keeping systems of mobile and permanently moored units have become more complex. New frontiers are explored and therefore it is an increasing demand for safe and reliable mooring systems. In addition, the number of anchor line failures are too high, which implies that the industry has urgent needs for improvement.

From a marine operational point of view, a precise position and motion control of ships and other floating structures are important. In order to design a mooring system that can satisfy this, the top end motion of the mooring lines must be calculated. The excitation loads on a moored vessel are due to wind, waves and current. The wind is characterized as a static force excited by the mean wind speed, and as a low-frequency force excited by wind gusts. The waves are characterized by static mean forces, first order linear forces and second order non-linear wave forces. The current forces are considered as static forces.

The main categories of station keeping are pure mooring systems, such as spread and single-point moorings, dynamic positioning systems and thruster-assisted mooring systems. Typical arrangements are taut, semi-taut and catenary systems. Mooring lines can be divided into several segments, with different material and buoyancy elements along the line. Mooring lines are often made of chain, synthetic fibre rope, wire rope or a combination of them. Three limit states are described; intact (ULS), accidental (ALS) and fatigue (FLS).

Generally there are three different methods to compute the response of a floating structure; the frequency domain, time domain or a combined time and frequency domain approach. In the frequency domain, the non-linear restoring terms and damping terms are linearised and the low- and wave-frequency load effects are decoupled. The total contribution is then found by use of the superposition principle. In the time domain, the motions are solved simultaneously and

non-linear effects are directly accounted for in the restoring and damping terms.

The FPSO in question is located in the Barents Sea on the Norwegian Continental Shelf. The ship-shaped unit has a passive turret mooring system consisting of three bundles with five anchor lines each, resulting in 15 mooring lines. The vessel has in total 11 risers, with opportunity for future risers. A coupled SIMO-RIFLEX model provided by Statoil has been used to perform simple ULS and ALS analyses in the software SIMO, by use of the time domain approach. In this thesis three following limitations are considered valid; three environmental conditions are tested, the risers are disabled and the number of required simulations are found to be 14. In addition, the turret model is simplified to a beam element with zero torsional stiffness.Two important functional requirements for the FPSO are that the integrity of the risers are maintained, provided by an offset requirement, and that the safety factor for the moorings are fulfilled.

Several analyses for the intact condition are performed for different 100-years conditions for the loaded vessel. Four additional ALS analyses are conducted for the case with the most loaded line in ballast condition; one and two anchor line failure, and two definitions of the ALS extreme weather with 10 000-year return period. The vessel offset, the mooring line tensions and the dynamic turret support forces for all cases are discussed and compared with the respective acceptance criteria. In addition, simple uplift calculations are derived for the intact condition and the condition most sensitive towards uplift.

Ship-shaped units are sensitive to low-frequency motion, and therefore the sea state with the shortest period is the most critical one. The results show that the in-line condition leads to the highest tension in the mooring lines, hence this condition is further investigated for the accidental limit states. Both one and two line failures fulfils the requirements for permanent structures operating on the Norwegian Continental Shelf provided by DNV GL (2015). Statoil has an internal requirement for the extreme weather conditions, both extreme conditions fulfils the criteria. Comparing two definitions of the ALS extreme weather with 10 000-year return period, for the waves and wind, the waves were found to be the most critical extreme condition giving the highest responses of the ship-shaped unit and mooring system. Units with large topsides, such as semi-submersibles, are often more sensitive towards extreme wind. The dimensioning parameter for the FPSO is the tension in the heaviest loaded line in the two anchor line failure analysis, with a margin of 0.27.

Samandrag

Krava til posisjons- og forankringssystem av mobile og permanente einingar har dei seiste åra blitt meir komplekse. Nye grenser som ultra-djupt vatn og arktiske områder utforskast, difor er det ein aukande etterspurnad etter sikre og pålitelege forankringssystem. Antal linebrot er for høgt og tilseier at næringa har eit stort og akutt behov for forbetringar.

Presis posisjon og rørslekontroll av skip og flytande einingar er utruleg viktig sett frå eit maritimt operasjonelt ståstad. For å kunne utforme eit forankringssystem som kan tilfredsstille dette, må den øvre rørsla til ankerlinene bereknast. Eksitasjonslastene på eit fortøyd fartøy skuldast påkjenning frå bylgjer, vind og straum. Bølgjene er karakterisera av statiske middelkrefter, fyrste ordens lineære og andre ordens ikkje-lineære bylgjekrefter. Vinden er karakterisera av statiske middelkrefter eksitert av den gjennomsnittlege vindhastigheita, og av lågfrekvente krefter eksitert av vindkast. Straumkreftene er karakterisera som statiske middelkrefter.

Generelt sett er det tre forskjellige metodar for å berekne responsen for ein flytande konstruksjon. Dette er frekvensplanet, tidsplanet eller ein kombinera tids-og frekvensplansanalyse. I frekvensplanet vert dei ikkje-lineære tilbakeføringskreftene og dempingskreftene linearisera, og dei låg-og bylgjefrekvente kreftene vert kopla frå kvarandre. Det totale bidraget vert då utrekna ved hjelp av superposisjonsprinsippet. I tidsplanet derimot vert alle rørslene løyst samstundes og dei ikkje-lineære effektane er tatt direkte i betraktning i tilbakeførings- og dempingskreftene.

Hovudkategoriane for posisjonssystem er reine forankringssystem, til dømes spredningsog enkeltpunktsfortøyingssystem, dynamisk posisjonering og thruster-assistert fortøyingssystemer. Såkalla *"taut"* (stramt), semi-taut og kjedelinje er typiske systemarrangement. Ankerliner kan delast inn i fleire segmenter med forskjellige material- og oppdriftselement langs lina. Ankerliner er ofte laga av kjetting, syntetisk taug, vaier eller ein kombinasjon av dei. Tre kondis-

joner er beskrive; intakt (ULS), skade (ALS) og utmatting (FLS).

Produksjonsskipet i denne oppgåva er lokalisert i Barentshavet på den norske kontinentalsokkelen. Den skipsforma FPSOen har et passivt turret forankringssystem er satt opp av tre klasar med fem forankringsliner kvar, til saman vert det 15 ankerliner. Fartøyet har totalt 11 stigerøyr, med moglegheit for framtidige stigerøyr.

Ein kopla SIMO-RIFLEX-modell av FPSOen i ballast kondisjon levert av Statoil har blitt brukt til å utføre enkle tidsplansanalyser i programvara SIMO i både intakt og skada kondisjon. I denne oppgåva, grunna tidsavgrensing og kapasitet, er tre fylgjande begrensingane er sett på som gyldige; kunn tre miljøtilstander vert testa, stigerøyra er fråkopla og antall krevde simuleringar er 14 stykk. I tillegg er turret-modellen forenkla til ein vertikal bjelke med null torsjonsstivleik. Nokre av dei viktigaste funksjonelle krava til produksjonsskipet er at stigerøyra vert helde intakte, av den grunn må eit krav til forskyving av skipet overhaldast, i tillegg må sikkerheitsfaktoren for ankerlinene overhaldast.

Dei intakte analysane vert utført for forskjellige hundreårskondisjonar, funne ved hjelp av konturlinjemetoden. I tillegg vert fire ALS-analyser utført for kondisjonen med den mest belasta lina i ballasttilstand. Her vert ein og to ankerliner kutta, og to definisjonar av ALS ekstremvær med 10 000 års returperiode analysera. Fartøyets forskyving, ankerlinestrekket og dei dynamiske turret opplagerkreftene for alle testar diskutera og samanlikna med dei tilhøyrande kriteriane. Til slutt vert enkle oppløftsberekningar utført for den analysa som er mest sensitiv for oppløft.

Skipsforma einingar er spesielt sensitive for lågfrekvente rørsler, og difor er sjøtilstanden med den kortaste perioden mest kritisk. Resultata visar at når miljøet vert sendt direkte inn i ei lineklynge, er den tilstanden som fører til den mest belasta lina, difor vert denne tilstanden granska vidare for skadekondisjonane. Både ein og to linebrot oppfyller krava frå DNV GL (2015) satt til permanente konstruksjonar som opererer på norsk sokkel. ALS ekstremvær med 10 000års returperiode for anten bylgjer eller vind vert analysera. Her gjer bylgjene mest kritiske responsar, som er forventa for skipsforma einingar. Einingar med stort areal over vatn, som til dømes halvt nedsøkkbare plattformar, er ofte meir sensitive ovanfor ekstrem vind. Statoil har eit internt krav til linestrekket under ekstremvær, FPSOen ligg godt innanfor dette kriteriet. Den dimensjonerande parameteren for FPSOen er strekket i den tyngst belasta lina ved to ankerlinebrot, med ein margin på 0.27.

Contents

List of Figures

List of Tables

Nomenclature

Acronyms

2D	Two dimensions
3D	Three dimensions
ALS	Accidental Limit State
BOG	Bogies
CALM	Catenary Anchor Leg Mooring
CT	Chain Table
DNV GL	Det Norske Veritas Germanischer Lloyd
DOF	Degree Of Freedom
DP	Dynamic Positioning
FEM	Final Element Method
FK	Froude-Krylov
FLS	Fatigue Limit State
FPSO	Floating Production and Offloading
GIL	Gas Injection Lines
JONSWAP	Joint North Sea Wave Project

LF Low Frequency

MBS Minimum Breaking Strength

MPM Most Probable Maximum

NPD Norwegian Petroleum Directorate

PDF Probability Density Function

PLEM Pipe Line End Manifold

PM Pierson-Moskowitz

PR Production Riser

R3S and R4 Raw Material Strength R3S and R4

RAD Radial Wheels

RAO Response Amplitude Operator

SALM Single Anchor Leg Mooring

SBM Single Buoy Moorings

SIMO/SIMA Simulation of Marine Operations

SPM Single Point Moorings

SSSW Sheeted Spiral Strand Wire

STL Submerged Turret Loading

STP Submerged Turret Production

TLP Tension Leg Platform

ULS Ultimate Limit State

UMB Umbilical

WF Wave Frequency

WIR Water Injection Riser

Greek Letters

α_{cu}	Current direction	[deg]
α_{wa}	Wave direction	[deg]
α_{wi}	Wind direction	[deg]
β	Variance of the Gumbel distribution	[dependent on response]
η_1	Surge	[m]
η_2	Sway	[m]
η_3	Heave	[m]
η_4	Roll	[deg]
η_5	Pitch	[deg]
η_6	Yaw	[deg]
γ	Euler-Mascheroni constant	[−]
Λ	Logarithmic decrement	[−]
λ	Wavelength	[m]
μ	Expectation of the Gumbel distribution	[dependent on response]
ω	Frequency	[rad/s]
ϕ	Angle between tension and horizontal plane	[deg]
θ	Pitch	[deg]
ξ	Damping ratio	[−]

Symbols

$\overline{q}_{cu}$	Mean current force	[N]
$\overline{q}_{wi}$	Mean wind force	[N]
A	Cross-section area	[m^2]
$A(\omega)$	Frequency-dependent added mass matrix	[kg]
$C(\omega)$	Frequency-dependent potential damping matrix	[Ns/m]
C_{cr}	Critical damping	[Ns/m]
C_{cu}	Current force coefficient	[−]
C_{wa}	Wave drift force coefficient	[−]
C_{wi}	Wind force coefficient	[−]
D	External force in radial direction	[N]
d	Water depth	[m]
D_q	Quadratic damping matrix	[Ns/m]
E	Elastic modulus	[Pa]
F	External force in tangential direction	[N]
F_X^{CT}	Force in horizontal direction at chain table	[N]
F_X^{RAD}	Force in horizontal direction at radial wheels	[N]
F_Z^{BOG}	Force in vertical direction at bogies	[N]
F_Z^{CT}	Force in vertical direction at chain table	[N]
$F_{support}^{BOG}$	Support force at bogies	[N]
g	Gravity of earth	[m/s^2]

H_S	Significant wave height	[m]
i, j and k	Unit vectors along the x-, y- and z-axis respectively	[-]
I^{COG}	Inertia at turret	[tm^2]
$K(r)$	Non-linear stiffness matrix	[N]
k_E	Elastic stiffness	[N]
k_G	Geometric stiffness	[N]
k_{TOT}	Total stiffness	[N]
M	Mass matrix	[kg]
M^{BOG}	Moment at bogies	[N]
M^{BOG}	Moment at chain table	[N]
M_{req}	Required turret mass to prevent uplift	[kg]
N_{req}	Number of required simulations	[−]
$Q(t, r, \dot{r})$	Excitation forces	[N]
q_{cu}	Current forces	[N]
q_{th}	Thruster forces	[N]
q_{wa}	Wave forces	[N]
q_{wi}	Wind forces	[N]
$r, \dot{r}$ and $\ddot{r}$	The position, velocity and acceleration vectors respectively	[m], [m/s], [m/s^2]
S_{MBS}	Minimum breaking strength of mooring lines	[N]
sf	Safety factor	[−]
T_H	Horizontal tension	[N]

T_n	Natural period	[s]
T_{char}	Characteristic tension	[N]
T_P	Peak period	[s]
U	Vessel speed	[m/s]
V_{cu}	Current velocity	[m/s]
V_{wi}	Wind velocity	[m/s]
W	Weight	[kg]
x	Offset	[m]
X_l	Distance to anchor	[m]
$q_{wa}^{2.ord}$	Second order wave drift force	[N]

Chapter 1

Introduction

1.1 Background

During the past years, the requirements to the mooring and station keeping systems of mobile and permanently moored units have become more complex. The industry is moving into new frontiers, as ultra-deep water down to 3000m depths, Arctic areas, also fish farms are moving into offshore areas, this introduces new design challenges. Station keeping capabilities are critical for operations adjacent to other installations, such as flotel operations and tender support vessel operations. In addition, new mobile units are becoming larger and many units are at the end of their lifetime.

In the period from 2010 to 2014 a number of 16 anchor line failures were registered on the Norwegian Continental Shelf (Kvitrud 2014). The failures are due to fatigue, overload, mechanical damage or manufacturing errors, the errors in winches or brakes are not included. The amount of failures are too high and this implies that the industry has an urgent need for improvements.

The mooring system has a purpose to keep a floating vessel safely at a required position. Often the system consists of 12-20 mooring lines of heavy chain, steel wire ropes and/or synthetic polyester ropes to a seabed anchor. In addition the market has a large focus on cost efficient operations and design cost. The challenge today is to be able to design a mooring system at a low expense, but at the same time ensure that safety and standard requirements are fulfilled.

A mooring system can be analysed in the frequency or time domain, or a combination of

both. Based on the selected approach, the vessel offset, maximum tension in the mooring lines and other responses can be estimated. In the frequency domain the non-linear restoring terms and damping terms are linearised, and the low-frequency and wave-frequency load effects are decoupled. Then the superposition principle is used to sum these contributions. The time domain, on the other hand, takes the non-linearities from the dynamic system and the excitation loads directly into account, and solves the responses simultaneously. A main disadvantage of time domain simulation is the need for high computational effort.

1.2 Scope of Work

The overall objective of this master thesis is to assess and perform analyses for ULS and ALS design of the turret mooring system based on numerical simulations in the time domain. A typical FPSO unit designed for Norwegian Continental Shelf shall be studied.

The objectives are listed as

1. Review relevant literature and describe possible mooring and station keeping systems for mobile and permanent units, with focus on the station keeping principles and main hardware components. Describe the relevant simulation tools available in SIMO and how SIMO can effectively be utilized.

2. Describe the design limit states for mooring systems with corresponding acceptance criteria outlined in rules and regulations.

3. Propose a ULS design methodology for the mooring lines and turret support forces based on time domain simulations using the contour line approach. Perform selected analyses and assess the variability in the line tensions and turret forces. Sensitivity studies shall be performed.

4. Quantify, compare and describe the load effects in leeward and windward lines for typical ULS and ALS conditions. Make a comparison between tension in single lines and turret forces.

5. Describe and perform an estimate of the turret uplift.

1.2.1 Approach

This master thesis is a continuation of the project thesis report *"Design of mooring systems with focus on frequency domain analysis of a turret moored FPSO"* written autumn 2016. Hence large parts of the literature study were produced in the project thesis.

The first three objectives are based on reviewing relevant literature and extracting the theory of importance. The topic *station keeping and mooring systems* is a large and complex subject and a thorough investigation would take tremendous lot of time, therefore in this thesis an overall glance of the topic is covered. The part concerning SIMO theory and calculations are based on the manual provided by MARINTEK. The two last objectives involves the coupled numerical simulations in SIMO.The model has been simplified and tested for several weather conditions, the responses are then compared for the different cases.

1.2.2 Limitations

- The numerical model provided by Statoil is in ballast condition, hence the loaded condition of the ship is not investigated.
- The number of simulations are chosen with respect to the Gumbel parameters for some responses. Since not all responses in the analyses are used to find the required simulations, the amount of simulations may not be representative for all responses.
- The number of different design cases are constrained, the complexity of the turret design and numerical model is simplified due to time limitation in this master thesis
- The duration of the time series are of 3 hours, hence a more complete long-term analysis will provide more reliable results.

1.3 Structure of the Report

The rest of the report is organized as follows

- Chapter 2 describes the hardware components of a mooring system and typical mooring systems, in particular for the turret mooring system concept.

- In Chapter 3 the principles of the environmental loads acting on marine constructions and methods for computing responses are studied. The equations of motions, mooring line equilibrium, restoring and damping terms are characterized.
- Chapter 4 addresses the simulation tools SIMO and RIFLEX, including the definitions of the coordinate system and extreme value statistics for time domain results.
- Chapter 5 provides a model description of the FPSO in question, including vessel, turret, mooring and riser particulars. In addition the numerical model is verified and constrained. The design considerations and requirements are also presented in this chapter.
- Chapter 6 presents and discusses the results from analyses performed in SIMO.
- Chapter 7 is the final chapter providing a summary and conclusion of the project thesis and recommendations for further work.

It should be noted that the name of the FPSO in question is confidential, hence referred to as *the FPSO* in this master thesis.

Chapter 2

Station Keeping and Mooring Systems

This chapter describes the design considerations and hardware components for a mooring system, and the possible mooring and stationkeeping systems for permanent and mobile units. Since the ship-shaped FPSO is a permanent turret moored unit, this will be of main interest.

2.1 Mooring Systems

This section is based on the references ISO (2013) and Larsen (2016).

A mooring and station keeping system for a floating structure can be of many different types and shapes, depending on the purpose and characteristics of the structure, and the environmental conditions. A mooring system consists of a number of lines attached to the floating structure at different points with the lower ends of the lines anchored to the seabed.

2.1.1 Permanent and Mobile Mooring Systems

Permanent moorings are typically used for production operations with longer design lives (API 2008). The mooring system for production units, such as FPSOs and FSOs, are normally a permanent mooring since the design lives is often over 10 years. Mobile moorings on the other hand, stays in one location for a short period.

2.1.2 Design Considerations

The primary design considerations associated with a mooring system are according to API (2008) the design criteria, design loads, design life, operation and maintenance considerations and so on.

The riser system is often a governing limitation on the allowable offset of the vessel. This is because the riser transfer fluids between the seabed and the production or drilling vessel, therefore the system is sensitive towards large and rapid movements. If extreme vessel offsets should appear, mooring line adjustments such as slackening the leeward lines are sometimes performed to avoid damage on the risers (API 2008). A consideration that is of main importance, is the interference between the mooring lines and risers, during both operation and extreme weather conditions. Therefore, the mooring and risers systems must be designed to accommodate each other, and coordination of these two design efforts is essential.

Mooring lines should be clear of subsea equipment such as flowlines, templates, riser base and so on. Contact between mooring lines and subsea equipment during installation, operation or maintenance is often prone to damage to both the mooring line and equipment. The coordination of the mooring system and the subsea equipment layout relative to each other is vital.

2.1.3 Hardware Components

The mooring lines can be divided into several segments, with different material and buoyancy elements along the line. Mooring lines are often made of chain, synthetic fibre rope, wire rope or a combination of them. The hardware components of a mooring system are illustrated in Figure 2.1 and can be listed as

- Winch
- Fairlead
- Chain, steel-wire ropes or synthetic (polyester) fibre ropes
- Buoyancy elements and/or clump weights
- Connection links

- Anchor

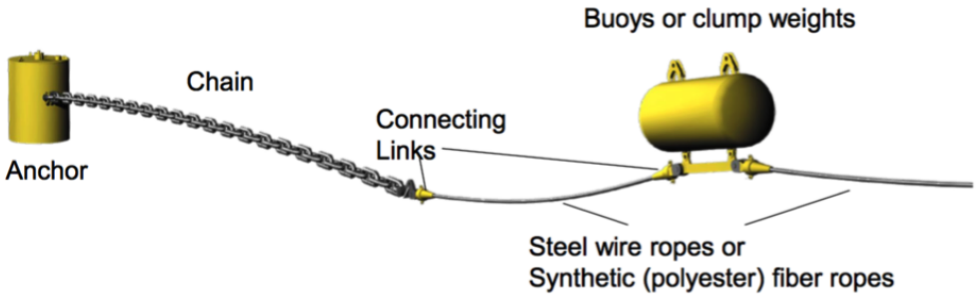

Figure 2.1: Mooring system components (Larsen 2016)

A more detailed description of the components is given below.

Chain

Typically, chain consists of studless or studded chain links, it has a large weight which provides high stiffness and good abrasion characteristics. Therefore chain is often used in segments in the top and end of the mooring lines. An all-chain system in deep water imposes an increasing penalty on the floating structure's payload because of its weight and pre-tension requirements. Also, chain contributes significantly to the anchor holding capacity.

Synthetic Fibre Ropes

This type of rope is made of polyester, HMPE or aramid fibre which results in a lighter submerged weight and high elasticity compared to steel wire ropes. In addition, the ropes have long fatigue lives.

Steel Wire Ropes

Steel wire ropes can be of spiral strand, which may be covered with plastic sheet, or six-strand (also called multi strand) which is uncovered. This material is much lighter than chain, hence provides a greater restoring force for a given pre-tension. It is often used in the water span, due to low abrasion qualities, and at the sea floor.

Buoyancy Elements and Clump Weights

Sometimes clump weights are incorporated in the mooring line design, this is to optimize the performance. Spring buoys can also be connected into the mooring line design as surface buoys or sub-surface buoys. Some of the benefits are the reduced weight, reduced effect of line dynamics in deep water, and reduced floating structure offset, for given size and pre-tension. Some less beneficial effects of the spring buoys is that there will be more connecting links and other components in the mooring line system, which results in a far more complex installation and maintenance plan. Also, buoys in heavy sea can provide increased environmental actions on the mooring lines.

Anchors

There are many different types of anchors; fluke anchors, plate anchors, suctions anchors et cetera. The different criteria for choosing the anchor system is the seabed foundation (e.g. clay, sand or rock) and if it is a permanent or mobile mooring system. One essential condition is if the anchor must be able to obtain vertical loads or not. Insufficient line length can introduce vertical actions at the anchor.

For deepwater mooring systems suction anchors is often used, these are designed for very high mooring line tensions. Typically, suction anchor are tall cylindrical piles. They are installed by lowering the unit into the soil to self-penetration depth. The water inside the cylinder is pumped out, creating a pressure difference driving the anchor further into the soil. When the desired penetration is gained, the water outlet is closed. The suction anchor is able to resist vertical and horizontal forces, moments and combinations of these.

2.2 Main Categories of Station Keeping Systems

In this section ISO (2013) is used as the main reference.

The main categories of station keeping systems are mooring systems such as spread and single-point mooring, dynamic positioning (DP) system and thruster-assisted mooring system.

The station keeping system for a floating structure can be either a single-point mooring or

a spread mooring. For ship-shaped vessels, single-point moorings tend to be used more frequently (API 2008). While spread moorings are used mostly for semi-submersibles and spars. A third type of station keeping system is dynamic positioning (DP). Dynamic positioning can be used as the one and only station keeping source, or to assist a catenary mooring system.

Typical arrangements of mooring systems can be as shown in Figure 2.2.

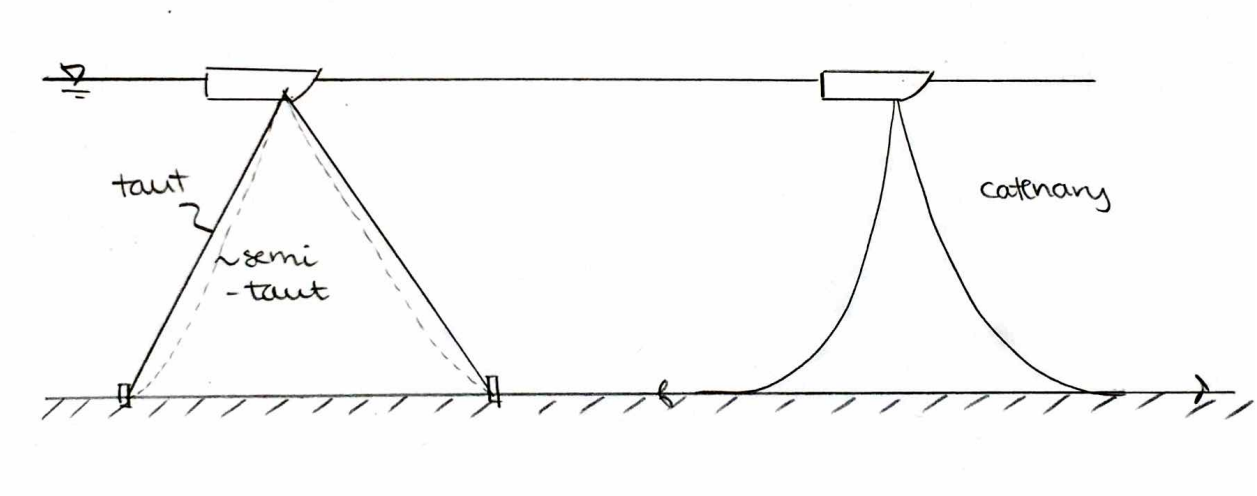

Figure 2.2: Typical arrangement of mooring systems (Svalastog 2016)

Spread Moorings

The main advantage of a spread mooring system is that it fixes the orientation of the floating structure, in this way drilling or other operations can be carried out on subsea equipment directly below the floater. The spread of the system is rather large, it can be several times the water depth, which can be a disadvantage in many situations; trawlers, thugs and other ships operating in the area can then damage or break the lines.

Spread mooring systems can be of catenary, taut-line and semi-taut line. The lines can be of chain, wire rope, synthetic fibre rope, or a combination of the three. Drag anchors and anchor piles are typically used.

Single Point Moorings (SPM)

Typically, SPM is used for ship-shaped floating structures such as FPSOs and FSOs. A main advantage for these systems, are that they allow the structure to weathervane. There are many

different types of single point mooring systems, but the function is essentially the same. Turret mooring, catenary anchor leg mooring (CALM) and single anchor leg mooring (SALM) are frequently used systems.

Dynamic Positioning (DP) Systems

DP systems uses thrusters and propellers to automatically maintain the position of a floating structure. They are tailor made for structures leaving and arriving locations and performing operations of short duration. It is very costly to set up a mooring system for short periods, in these cases a DP system may be a better alternative compared to an anchored system. While for a permanent structure the DP systems are both expensive and not environmentally friendly, hence not a favourable solution. Dynamic positioning can be used with either ship-shaped or semi-submersible vessels (API 2008).

Thruster Assisted Mooring Systems

These systems uses mooring lines, thrusters and propellers to maintain position. The thrusters can be used to control the heading of the structure, in addition it can reduce mooring forces in harsh environments, or increase the workability of the floating structure.

2.3 Turret Mooring System

In this thesis the FPSO in question is turret moored, therefore a closer look at this system is performed.

2.3.1 General

A turret mooring system is defined as any mooring system where a number of catenary mooring lines are attached to the turret, here bearings are included to allow the vessel to rotate around the anchor lines (API 2008).This means that the moored part of the turret is fixed relative to the sea bottom, hence a global coordinate system (Paik & Thayamballi 2007). From this fixed part, flexible risers are suspended and connected to Pipe Line End Manifold (PLEM) arrangements or directly to wellheads.

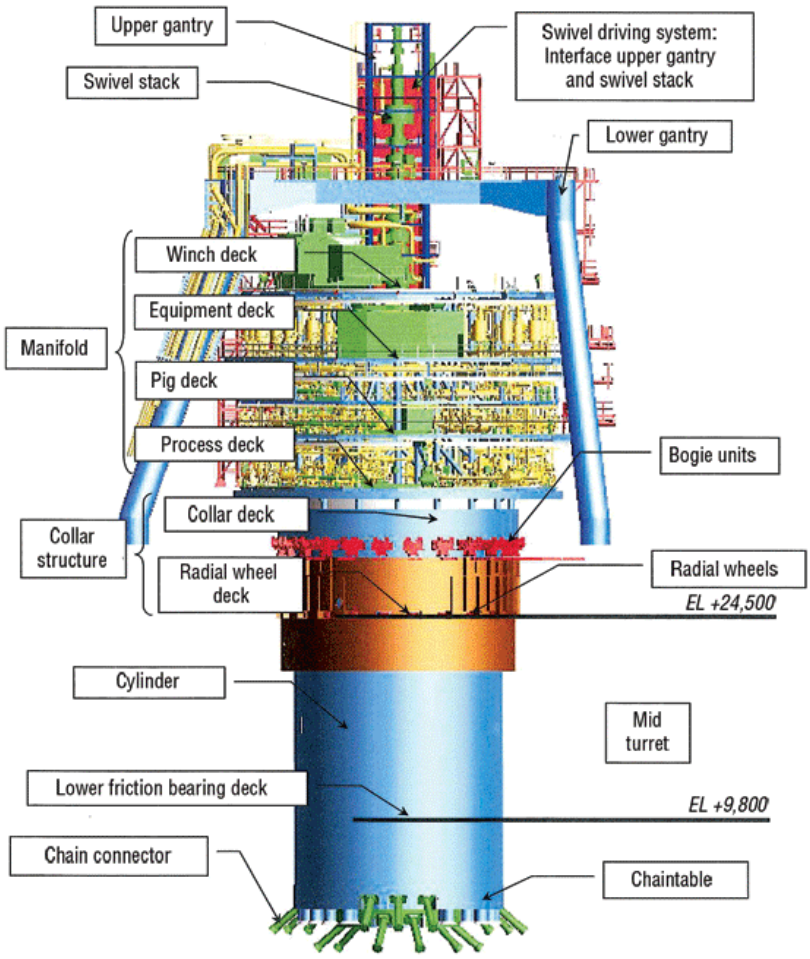

Figure 2.3: Conceptual arrangement of a turret system (Naciri et al. 2011)

A swivel is situated on top of the turret to connect the flexible risers to the fixed piping mounted on the vessel. This allows the vessel to weathervane and at the same time produce oil and gas, also water and gas injection can be inserted into the reservoir. The swivel is the connection between the fixed global mooring lines, and the body-fixed weathervaning ship-shaped FPSO. A conceptual arrangement of a turret system is illustrated in Figure 2.3.

2.3.2 Turret Solutions

According to Paik & Thayamballi (2007) turrets can be grouped into two main types: permanent and disconnectable. This distinguish between a turret permanently built in the floating vessel and being able to disconnect if certain environmental design conditions and associated limits are exceeded.

There are different solutions for internal turrets, either a small buoy turret or large turret. Large turrets can accommodate a considerable number of risers, hence the turret must be large and penetrates the whole ship. Therefore large turrets are only of permanent type. The small buoy turrets accommodates a couple of risers and can be of both permanent and disconnectable type. Small buoy turrets are often classified as STL (Submerged Turret Loading) and STP (Submerged Turret Production), used on tankers and production units respectively, but is essentially the same in use. External turrets are of permanent type. A principal sketch of the turret solutions are shown in Figure 2.4.

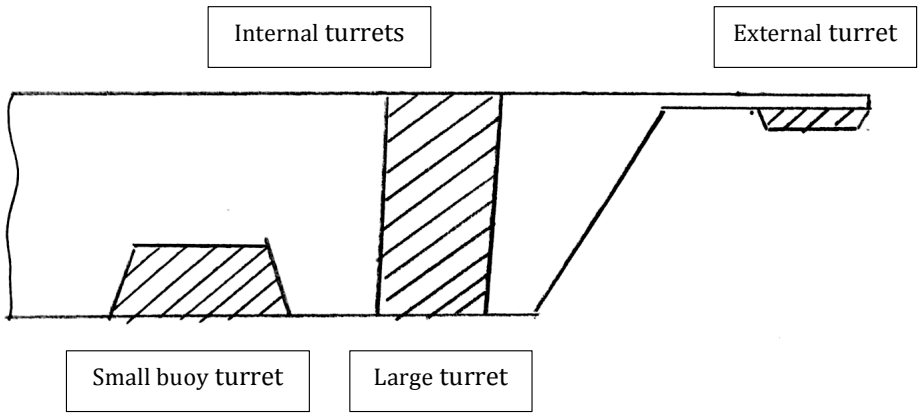

Figure 2.4: Principal sketch of the different types of turrets

When the turret is integrated into the hull of the structure, the internal position of the turret provides protection for the risers in the wave zone. The structural steel of the vessel's hull is directly used to support the turret (de Boom 1989). The remaining cross section of the vessel at the centre line of the turret has to be adequately designed to provide sufficient strength and to limit deformations, according to de Boom (1989). The optimal longitudinal position of the turret is a continuous compromise between minimizing the vertical motions of the turret and

providing sufficiently weathervaning capability. An important aspect in this context is the riser considerations.

The vertical ship motions due to pitch and heave becomes smaller towards midships, and largest at the bow. This is important to have in mind for conditions where there are expected large dynamic loads in the riser and the mooring lines, such as harsh weather conditions and large water depths (de Boom 1989). Another natural constraint is if the turret location is too close to midships, the vessel loses its natural weathervaning capability, which is the essential function for single point moored units. It's also important to have in mind that an internal turret can reduce the available deck area.

The structural behaviour of the turret is often established by finite element stress analysis in conjunction with structural strength and fatigue codes of practice (Barltrop 1998). The finite element model needs to consider the flexibility and deformations induced by the direct loading on the ship's hull as well as the turret behaviour itself.

The turret has important local loading from the mooring system, accelerations of the ship hull and hydrostatic and dynamic pressure loads. Slamming may be an important design consideration for turrets mounted near the bow.

Chapter 3

Theoretical Background

The theory in this chapter is based on the references Faltinsen (1990) and Larsen (2016).

In order to design a mooring system, the principles of defining the environmental loads and methods for analysing a mooring system are investigated. From a marine operational point of view, a precise position and motion control of ships and other floating structures are extremely important. One crucial parameter to be calculated is the top end motion. The FPSO has several pipelines, and is therefore sensitive towards heave movement in addition to offset in the horizontal direction. The equation of motions is solved in all six degrees of freedoms (DOFs) to determine the responses and the tensions in the mooring lines. A time and frequency domain analysis are required in order to achieve a reliable analysis of the motions and loads in a mooring system.

3.1 Motions and Forces

The motions for a mooring system are divided into static and dynamic motions. The definition of motion of floating structures is commonly divided into wave frequency (WF) motion, low frequency (LF) motion and mean drift motion. The oscillating rigid-body translatory motion modes are referred to as surge, sway and heave, denoted as η_1, η_2 and η_3 respectively. The oscillation rigid-body angular rotations are referred to as roll, pitch and yaw, denoted as η_4, η_5 and η_6 respectively. The rigid-body motions, definitions of coordinate system and wave propagation

direction can be seen from Figure 3.1, where U is the forward speed of the ship.

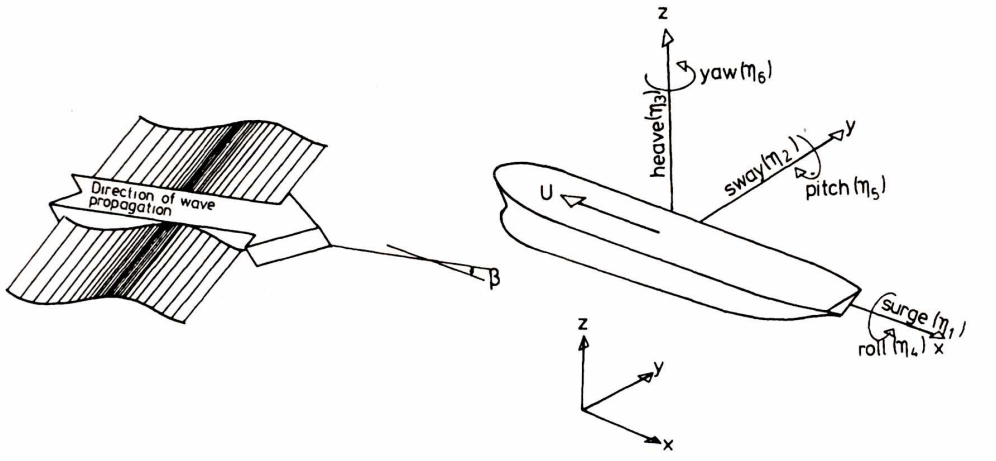

Figure 3.1: Rigid-body motion modes (Faltinsen 1990)

The static force has contributions from the average force from wind, waves and current. These forces are in most cases independent of the configuration of the anchor system, and determined by the size, shape and orientation of the anchored vessel. The static forces causes an offset of the vessel and the static mooring line forces can be directly computed from the anchor system characteristics (Fylling 1980).

The dynamic forces has a more complicated form and can depend strongly upon the mooring system. The mean, WF and LF motions are important for the design of the mooring system for the FPSO. The motion of an arbitrary position on the floater can be expressed as

$$s = \eta_1 i + \eta_2 j + \eta_3 k + \omega \times r \tag{3.1}$$

where $\omega = \eta_4 i + \eta_5 j + \eta_6 k$ and $r = xi + yj + zk$, and i,j,k are unit vectors along the x-, y- and z-axis, respectively. This leads to

$$s = (\eta_1 + z\eta_5 - y\eta_6)\, i + (\eta_2 - z\eta_4 + x\eta_6)\, j + (\eta_3 + y\eta_4 - x\eta_5)\, k \tag{3.2}$$

By use of these equations, the motion of the fairlead can be found.

3.1.1 Equation of Motion

When the hydrodynamic forces are established, the equations of motion in six degrees of freedom can be written as

$$(M + A(\omega)) \cdot \ddot{r} + C(\omega) \cdot \dot{r} + D_l \cdot \dot{r} + D_q \cdot \dot{r}|\dot{r}| + K(r) \cdot r = Q(t, r, \dot{r}) \tag{3.3}$$

Where M represents the mass matrix, $A(\omega)$ is the frequency-dependent added mass matrix, and $r, \dot{r}$ and $\ddot{r}$ are the position, velocity and acceleration vectors respectively. $C(\omega)$ is the frequency-dependent potential damping matrix, D_l represents the linear damping matrix, D_q is the quadratic damping matrix, $K(r)$ is the non-linear stiffness matrix and $Q(t, r, \dot{r})$ are the excitation forces.

The first term to the left in Equation 3.3 represent the inertia forces. The next three terms represents the damping forces, that are primary the drag forces on the hull of the floating structure. The last and fifth term on the left hand side represents the stiffness and restoring forces provided by the mooring lines. The right hand side of the equation is the excitation forces, caused by the sea state, defined as

$$Q(t, r, \dot{r}) = q_{wa} + q_{wi} + q_{cu} + q_{thr} \tag{3.4}$$

The wave forces, q_{wa}, are characterized by 1^{st} order forces proportional with wave amplitude, mean value due to 2^{nd} order wave loads and LF forces excited by 2^{nd} order wave loads. The wind forces, q_{wi}, are characterized by a mean value due to mean wind velocity and LF forces excited by wind gusts. The current forces, q_{cu}, are characterized by a mean value due to mean current velocity, while the current turbulence is neglected. The thruster forces, q_{th}, are characterized by mean forces and/or dynamic forces dependent on automatic or manual control. The FPSO only has thrusters in the transverse direction, hence $q_{thr} = 0$. The environmental loads have different frequencies and can be divided into excitation regimes shown in Table 3.1.

Table 3.1: Excitation regimes for wave, wind and current forces (Larsen 2016)

Excitation	**Mean**	**30-500s: LF**	**5-30s: WF**
Waves	Mean wave drift force	2nd order difference frequency (wave drift)	1st order forces
Wind	Mean wind speed	Wind gust	-
Current	Mean current speed	-	-

A limiting factor for drilling operations is the heave motion. The vertical motion of the risers, which means the heave and pitch modes, are not affected by a catenary mooring system. Therefore the dimensioning and location of the risers, hence the turret, are extremely important design considerations.

By designing the structure with a low heave motion, the drilling operation can be carried out for as high percentage of the time as possible. Two important design parameters are the breaking strength of the mooring lines and the flexibility of the risers.

Table 3.2: The "preferred" natural oscillation periods in general for different structures(Larsen 2016)

Response	**Surge**	**Sway**	**Heave**	**Roll**	**Pitch**	**Yaw**
FPSOs	$\approx > 100s$	$\approx > 100s$	$10-15s$	$10-20s$	$10-15s$	$\approx > 100s$
Semi-subs	$\approx > 100s$	$\approx > 100s$	$20-25s$	$45-60s$	$45-60s$	$\approx > 100s$
TLPs	$70-100s$	$70-100s$	$2-3s$	$2-3s$	$2-3s$	$70-100s$

3.1.2 Time and Frequency Domain

This part is based on Larsen (2014) and ISO (2013).

Generally there are three methods used to solve the equations of motions, hence compute the floating structure responses. These are the frequency domain, time domain and combined time and frequency domain approach. The methods involve different degrees of approximations and are affected by different limitations. Therefore they may not necessarily give a consistent result.

Frequency Domain Approach

The equation of motion describing the response of the structure are decoupled and analysed separately for mean, LF and WF responses. Mean responses are calculated from static equi-

librium between the steady environmental actions and the restoring forces from the mooring system. WF and LF structure motions are calculated by the frequency domain approach, which yields motions response statics. The extreme values, such as significant and most probable maximum responses are evaluated based on the Gaussian and Rayleigh peak probability density distributions. Then the extreme values of the WF and LF responses are combined with the mean static response.

When performing a frequency domain analysis of a weathervaning structure, the heading of the structure shall be fixed. The fixed design heading where the mooring system responses are calculated shall be determined, taking into consideration the mean equilibrium heading and LF yaw motions. To ensure that the largest maximum has been identified, normally more than one fixed heading shall be considered.

Time Domain Approach

The equation of motion describing the combined mean, LF and WF responses of the floating structure are solved simultaneously in the time domain. The mean, LF and WF actions due to wind, waves and current (and thrusters, if present) are included in the force functions. The time domain simulation include all behaviours and interactions from the equations describing the floating structure, mooring lines, risers and thrusters. From the simulation the total time series are obtained defining the total response, which in general is non-gaussian. By performing statistical analyses of the time series, the extreme values can be found. The time domain simulation should be long enough to obtain stable statistical values. The time domain approach is often used for complex structures where the finite element method (FEM) is used to describe the lines, which represent the stiffness, damping and inertia properties of the structure.

Combined Time Domain and Frequency Domain Approach

A fully coupled time domain simulation is complex and takes large computational effort. In order to reduce this, often a combined time and frequency domain approach is performed. The time and frequency domain can be combined in different ways. Typically it is performed by simulating the mean and LF responses in the time domain while the WF responses are solved separately in the frequency domain.

3.2 Restoring Forces and Stiffness

The following section is based on Larsen (2016).

The mooring system creates stiffness, thus a mooring system can be seen as the interaction between elastic and geometrical stiffness. A freely floating structure will not experience any stiffness in surge, sway and yaw, as opposed to an anchored structure. A very tight mooring system can therefore affect the displacement of a ship, a very heavy mooring system will therefore affect the loading capacity of the ship. One can say that the mean offset and partly the low-frequency (LF) motion is "controlled" by the stiffness. In addition, the WF motions must be absorbed by the mooring system.

There are two contributions to the total stiffness, the geometric and elastic stiffness. These can be modelled as springs in series. The total stiffness can be found as

$$\frac{1}{k_{TOT}} = \frac{1}{k_G} + \frac{1}{k_E} \tag{3.5}$$

Generally a catenary system is applicable for shallow or medium shallow water, where chain or steel wire ropes are commonly applied. Taut mooring is best for deep water and consists of synthetic fibre ropes, often polyester.

The riser can handle larger motions in deep water than in shallow water. Based on the riser requirements a more rigid mooring system is needed in shallow water, such as catenary mooring. If a taut mooring system is applied for shallow water, the lines would have to be extremely long in order to absorb the large motions. Long mooring lines are both expensive and unpractical with respect to weight and vulnerability (outside the 500 m safety-zone). An advantage of the taut system relative to a catenary system is that the taut mooring lines do not achieve large drag forces and is generally a light-weight system.

3.2.1 Catenary System: Geometric Stiffness

The geometric stiffness and tension are provided by the weight of the mooring lines in the water. Chain is heavy, and often used in catenary systems and will therefore induce geometric stiffness. Figure 3.2 shows the principle for calculating the restoring force for one line in a catenary sys-

tem. The figure shows how the offset x affects the system, where point 1 represents the initial position and point 2 is the offset position. W_1 and W_2 represents the weight of the mooring line in point 1 and 2 with associated moments arms defined as a_1 and a_2 respectively. The water depth is defined as d, and the horizontal tension is defined as T_H^1 and T_H^2 respectively. One important aspect for a catenary system is that the anchor cannot obtain vertical loads.

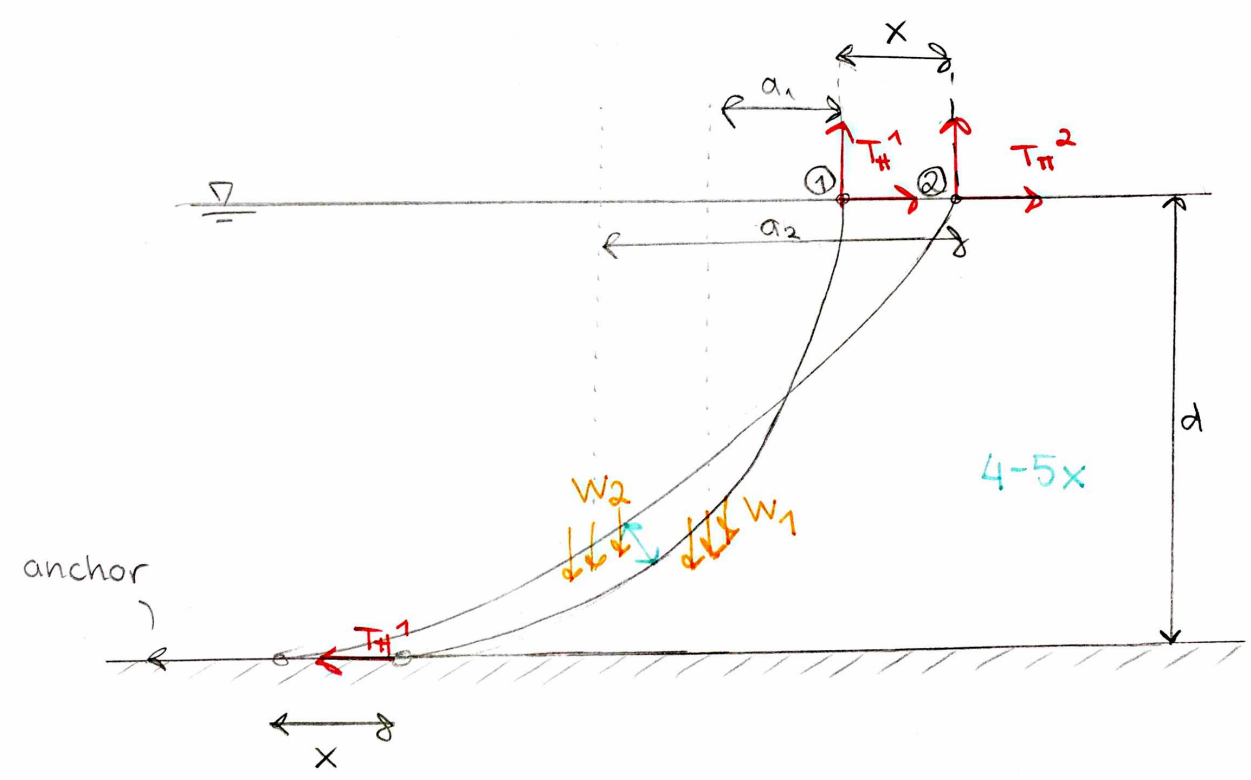

Figure 3.2: Geometrical stiffness of a catenary system (Svalastog 2016)

The moment equilibrium about water plane connection points (1) and (2), seen in Figure 3.2, gives

$$T_{H,1} \cdot d = W_1 \cdot a_1 \rightarrow T_{H,1} = \frac{W_1 \cdot a_1}{d} \tag{3.6}$$

$$T_{H,2} \cdot d = W_2 \cdot a_2 \rightarrow T_{H,2} = \frac{W_2 \cdot a_2}{d} \tag{3.7}$$

The difference between these two points results in the geometrical stiffness

$$k_G = \frac{T_{H,2} - T_{H,1}}{x} \tag{3.8}$$

A very stiff system, for example a catenary system, will experience drag loads and therefore also be exposed for the so-called drag lock-in phenomena. This means that the drag forces from the anchor lines *locks* the geometrical stiffness, this is illustrated by springs in Figure 3.3. For a geometrically dominated system, typically a catenary system, the elastic stiffness is usually much larger relative to the geometric stiffness, i.e. $k_E >> k_G$. The stiffness k is a measurement of how well the member resists deformation, and in a geometrically dominated system, the geometrical parts of the mooring line absorbs the motions to a much larger extent than the elastic parts of the line. Hence, at drag lock-in it will only be the elastic stiffness that absorbs the environmental forces.

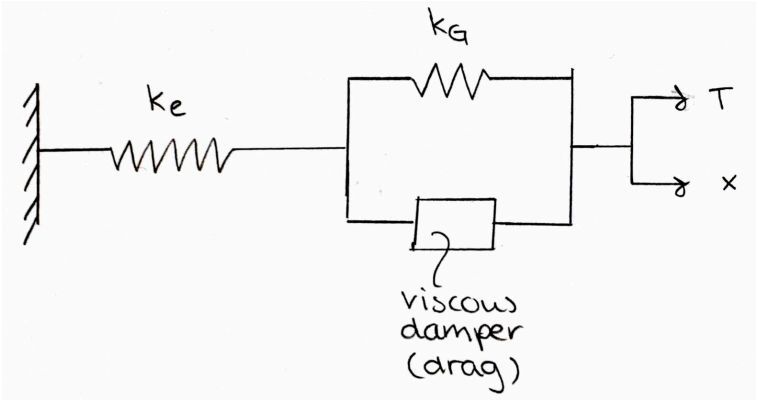

Figure 3.3: Illustration of a dynamic mooring line analysis (Svalastog 2016)

3.2.2 Taut System: Elastic Stiffness

For a taut system the anchor is much bigger and has other characteristics than for a catenary system, this is because the anchor must be able to obtain vertical loads. Synthetic fibre ropes are approximately neutral buoyant when submerged, and geometrical sagging in water will not appear in a significant extent as opposed for a chain line. Thus, the phenomena drag lock-in will not occur.

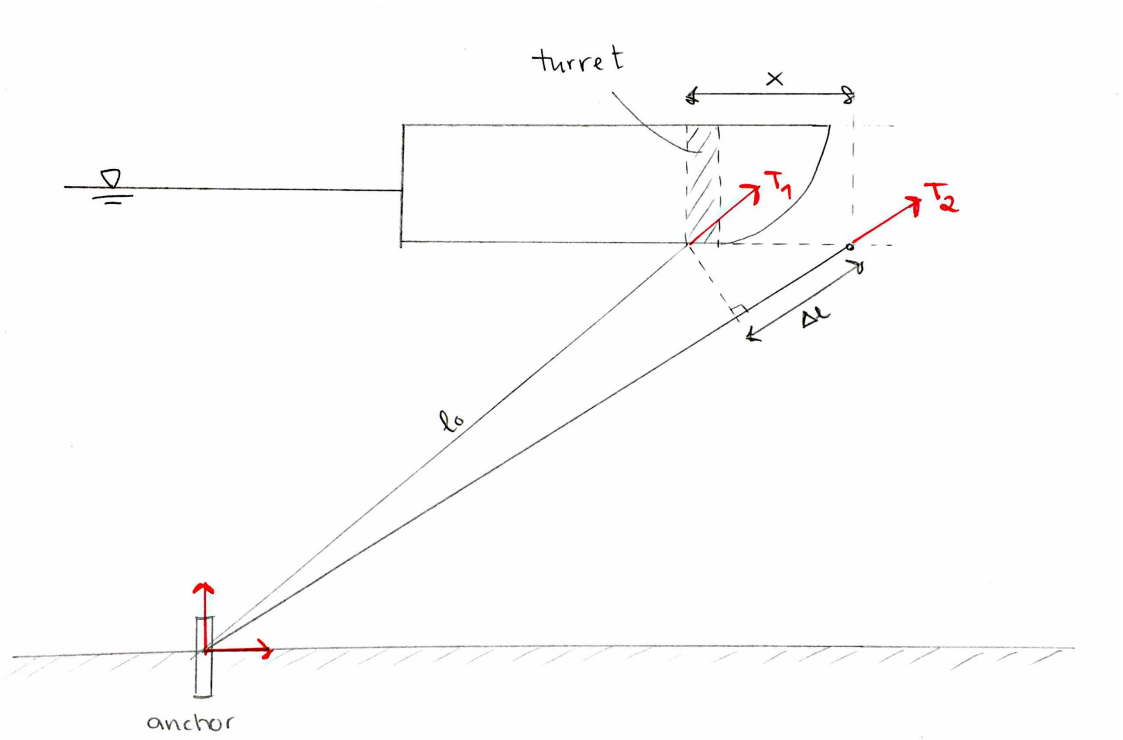

Figure 3.4: Elastic stiffness of a taut system (Svalastog 2016)

In order for the system to absorb the environmental forces, the rope must be able to elongate a distance Δl described in Figure 3.4. At the initial starting point (1), the length of the line is l_0, the axial stiffness of the line is defined as EA and the tensions in the two points are defined as T_1 and T_2 respectively.

The elastic stiffness can then be derived as

$$\Delta T = T_2 - T_1 = \frac{EA}{l_0} \cdot \Delta l \quad \text{where} \quad k_E = \frac{EA}{l_0} \tag{3.9}$$

Figure 3.5 illustrates the components of a taut mooring line, typically the elastic stiffness is much smaller relative to the geometrical stiffness for this system, i.e. $k_E << k_G$. The elastic part of the line, k_E, is the stiffness absorbing the environmental loads. The more flexible the elastic parts of the mooring lines are, the less stiff they are, hence they can absorb larger environmental loads. The geometric stiffness, k_G, can represent small parts of chain in the ends of the lines due to abrasion.

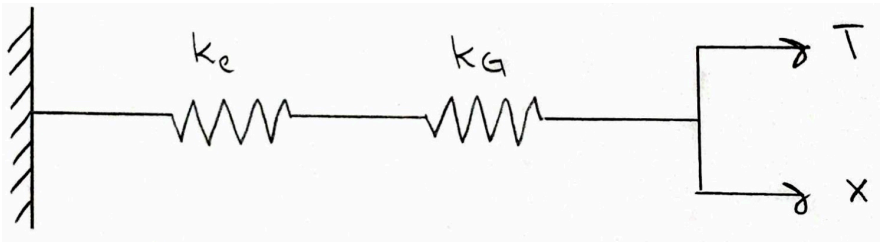

Figure 3.5: Illustration of a quasi-static mooring line analysis (Svalastog 2016)

3.2.3 Static Equilibrium of a Mooring Line

This part is based on the references (Larsen 2016) and (Faltinsen 1990).

A two-dimensional mooring line as seen in Figure 3.6, with zero bending stiffness, has the following notation; D and F are external forces on the line in radial and tangential direction respectively, and are current forces. The weight per unit length is denoted as w, EA is the axial stiffness of the line per unit length, with A as the cross section area of the line and E as the elastic modulus. T is the tension of the mooring line and φ is the angle between the tension and horizontal plane. The bending stiffness is neglected, which is a good approximation for chains and also appropriate for wires with a large radius of curvature. The dynamic effects in the line are also neglected.

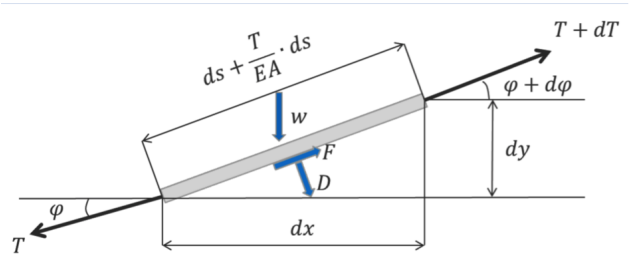

Figure 3.6: An illustration of the forces acting on a 2D mooring line (Larsen 2016)

The static equilibrium of a segment of length ds (zero tension) can be calculated in both tangential and normal direction. Equation 3.10 and 3.11 are often referred to as the catinary equations. Tangential direction:

$$dT = \left[w \cdot sin(\varphi - F\left(1 + \frac{T}{EA}\right) \right] \cdot ds \tag{3.10}$$

Normal (radial) direction:

$$T \cdot d\varphi = \left[w \cdot cos(\varphi + D\left(1 + \frac{T}{EA}\right) \right] \cdot ds \tag{3.11}$$

Equation 3.10 and 3.11 are non-linear and in general it's not possible to find an explicit solution. For the normal mooring line components, the tension is much less than the axial stiffness, hence it can be assumed that $\frac{T}{EA} << 1$ (inelastic line), and the term can be neglected.

Equations for an Inelastic Mooring Line

Of interest is the so-called line characteristics. The touch-down point is moving considerably when moving the top end of the line, and therefore its appropriate to choose an earth-fixed point as reference, e.g. the anchor point. This can be seen from Figure 3.7.

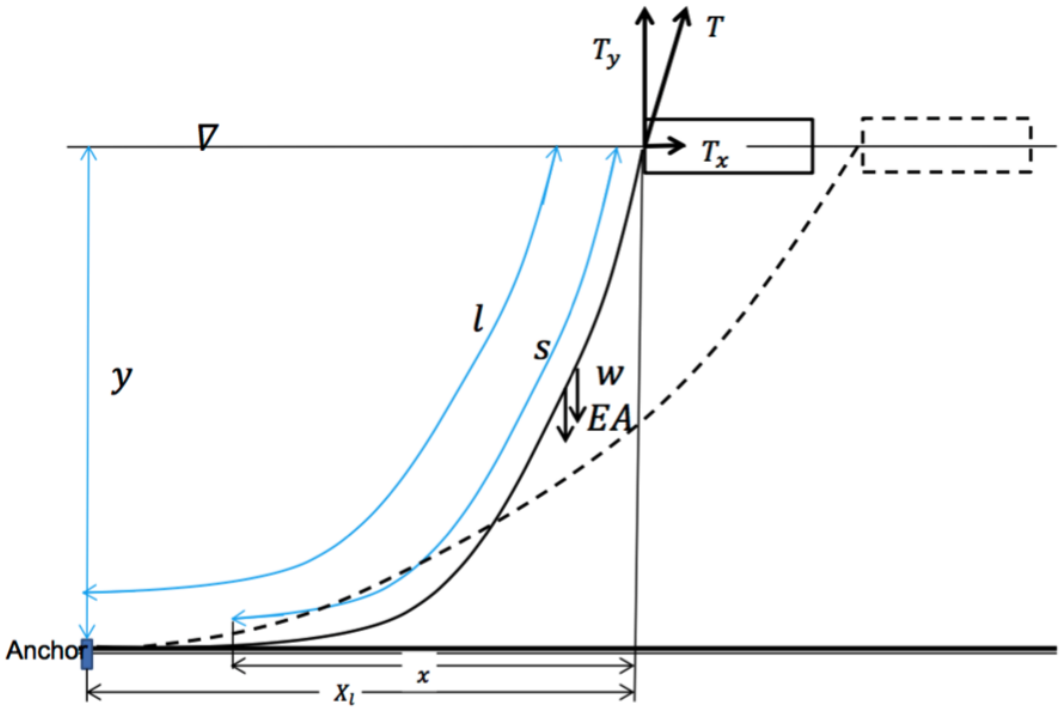

Figure 3.7: Illustration of the notation defining the line characteristics (Larsen 2016)

The distance to the anchor, X_l, is often known, and then it is of interest to calculate the tension, or more specifically, the horizontal tension at the top of the line. By manipulating the catenary equations, Equation 3.10 and 3.11, and combining several equations, the following

expression can be written for an inelastic mooring line

$$X_l = l + \frac{T_x}{w} \cdot cosh^{-1}\left(1 + \frac{w \cdot y}{T_x}\right) - \sqrt{y \cdot \left(y + \frac{2 \cdot T_x}{w}\right)} \tag{3.12}$$

This is often denoted as the line characteristics, which is a relation between the horizontal tension at the top end, T_x, and the offset of the floating structure, X_l, for a given water depth, y, and line weight, w. The horizontal stiffness from one mooring line is determined from line characteristics. This concept is not applicable for large water depths, this is due to the fact that a catenary system is very heavy with increasing water depths.

Line Characteristics with Line Elasticity Included

For high tension levels and/or long lines and/or more elastic line segments, the line elasticity, EA, must be accounted for. The line characteristics for a line where the elasticity is included are presented in Eq. 3.13 and Eq.3.14.

$$T_x = EA \cdot \left[\sqrt{\left(\frac{T}{EA} + 1\right)^2 - \frac{2 \cdot w \cdot y}{EA}} - 1\right] \tag{3.13}$$

and

$$x = \frac{T_x}{w} \cdot sinh^{-1}\left(\frac{T_y}{T_x}\right) + \frac{T_x \cdot T_y}{w \cdot EA} \tag{3.14}$$

The complete derivation of Equation 3.12 and the Equations 3.13 and 3.14 can be found in Larsen (2015).

Chapter 4

SIMO Theory and Definitions

In this chapter some essential SIMO and RIFLEX theory are presented, as the definition of coordinate system. A brief explanation of the Gumbel distribution is also provided. In this chapter the SIMO theory manual provided by MARINTEK (2016*b*) is used as a foundation to explain the basic theory of SIMO operations.

4.1 SIMO

SIMO is an application within the software SIMA which is a module in the Sesam Marine software. SIMO is a computer program for simulation of motions and station keeping behaviour of complex systems of floating vessels and suspended loads (MARINTEK 2016*b*). A couple of the most essential features are the ability to perform flexible modelling of multi-body systems and non-linear time domain simulation of wave-frequency as well as low-frequency forces. The results from the program are presented as time series, and in the post-processor option statistics, spectral analysis and more can be created for the forces and motions of the bodies in the analysed system.

4.1.1 Coordinate Systems

In SIMO several right-handed Cartesian coordinate systems with positive rotations counter-clockwise. The global earth-fixed coordinate system, notated as XG, is defined in Figure 4.1. The z-axis is directed upwards, defined as $XG(3)$, and the xy-plane ($XG(1)$ and $XG(2)$) coincides

with the calm water. The positions of all local body systems are referred to the global system. The local body-fixed coordinate system, XB, follows the body motions and is used to describe the coordinates of positioning elements and coupling elements. The body-related coordinate system, XR, is also a local coordinate system that follows the body's horizontal motion for floating vessels. Also, here the xy-plane is parallell to the calm water plane with the z-axis pointing upwards. Most coefficients, i.e. forces and motion transfer functions, are referred to this coordinate system. An illustration of the three coordinate systems are shown in Figure 4.2.

There is also an initial coordinate system, XI, which coincides with the body-related system when the time domain simulation starts, and remains fixed during the simulation. In this coordinate system first-order wave forces and wave drift forces may be pre-generated.

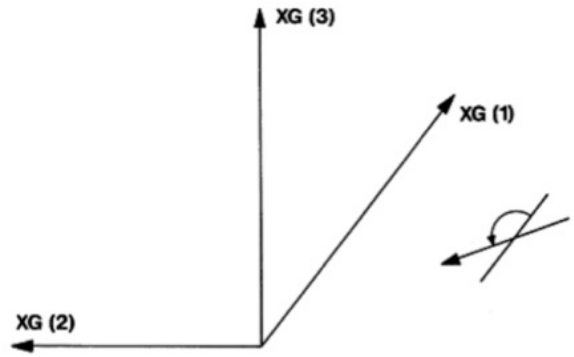

Figure 4.1: The global earth-fixed coordinate system

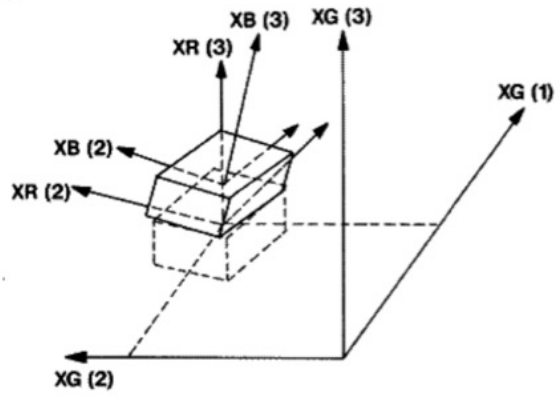

Figure 4.2: The local body-fixed and body-related coordinate system

4.1.2 Definition of Forces

Waves

According to MARINTEK (2016*c*) the direction of wave propagation equal to zero corresponds to wave propagation along the positive x-axis. There are many different ways to define the waves in SIMA. In this thesis the double peaked JONSWAP unidirectional wave spectrum is used. Compared to the Pierson-Moskowitz (PM) spectrum there will be more energy concentrated near the peak frequency, and less energy further away from the peak frequency when using the JONSWAP spectrum (Myrhaug & Lian 2009).

Wind

The wind field in SIMA is assumed to be 2-dimensional, i.e. propagating parallel to the horizontal plane. The model includes gust spectra both in the mean direction and normal to the mean wind direction. The wind gust (the varying part of the wind velocity) is assumed to be a Gaussian stochastic process. The varying part of the wind velocity in the mean direction can be described by a number of various wind gust spectra.

In this thesis the spectrum is defined by the guidelines given by the Norwegian Petroleum Directorate (NPD).

Current

In SIMA the current is described by a profile with specified directions and speeds at different levels. Linear interpolation is used. The current is taken to be constant from the lowest level specified to the bottom.

In this thesis the current is described at one water level with a corresponding velocity.

Station Keeping Forces: Anchor Lines

The implementation of a catenary mooring line model in SIMO is based on the model used in the mooring analysis program MIMOSA. The line dynamics model in MIMOSA, however, operates in the frequency domain and is therefore linearised. In SIMO, the model is extended to time domain. The mooring lines are treated individually. They may therefore have completely different properties, like material, dimension, length and so on. The mooring lines are assumed to form catenaries, modelled by the catenary equations.

4.2 RIFLEX

RIFLEX is a computer program for analysis of flexible risers and other slender structures, such as pipelines, mooring lines, fish cage systems and also conventional steel risers (MARINTEK 2016*a*). The structural analysis part in RIFLEX is based on finite element modelling. So-called *supernodes* in the model represents fairlead and anchors. Different cross-sections are defined

for the various types of wire, chain and rope. The line types consist of segments. In this thesis beam and bar elements, based on small strain theory, are used to model the slender system.

One of the finite element analysis techniques available in SIMO is the non-linear time domain analysis. Here, a step-by-step numerical integration of the incremental dynamic equilibrium equations are conducted for each time step. In this way the described non-linearities are properly treated. However, the non-linear dynamic analysis is quite time consuming due to repeated assembly of system matrices (mass, damping and stiffness) and triangularisation during the iteration process at each time step.

4.3 Coupled SIMO and RIFLEX

In a coupled SIMO-RIFLEX analysis the equation of motions, presented in Equation 3.3, for the moorings, risers and vessel are solved simultaneously. The frequency dependancy in SIMO is expressed by retardation functions. All the dynamic effects are taken into account. The paper Ormberg & Larsen (1998) compares the motions and mooring line tensions from models tests and simulations by use of coupled and separated analyses. A finding is that for the coupled approach, typical shortcomings are avoided, such as low-frequency damping contributions from moorings and risers. The separated approach may be severely inaccurate, especially for floating structures operating in deep waters. For that reason the coupled analysis method should be used for concepts in deep water based on that particular article.

4.4 Extreme Value Statistics

The results from time domain in SIMO are given in time series. The characteristic values for the different responses are obtained by using extreme value statistics.

The Gumbel distribution is often well suited to model the extreme value distribution. This method is based on recording global extreme values and fitting these to a corresponding Gumbel distribution (Naess & Gaidai 2008). Often, a specified fractile value of the fitted Gumbel distribution is extracted and used as a characteristic load in design consideration.

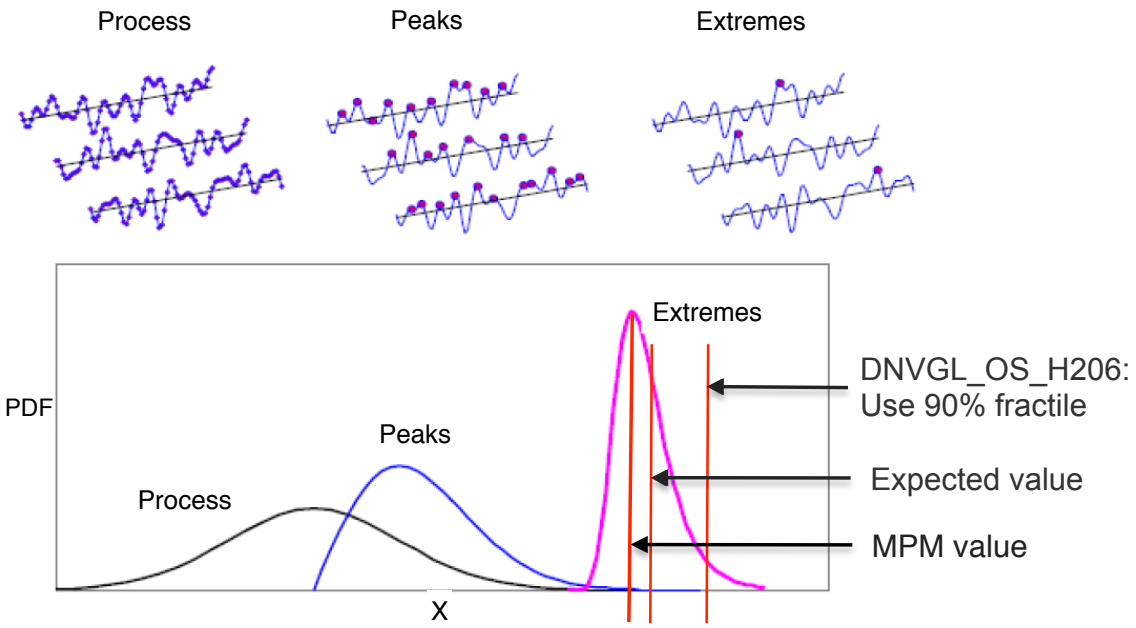

Figure 4.3: Illustration of the probability density functions for sample, peak and extreme values (Statoil 2016)

Depending on the response in question, the most probable max (MPM) value or the 90% fractile of the Gumbel distribution is used to find the characteristic value in this thesis. These characteristic design limits are illustrated in Figure 4.3. The MPM value of the Gumbel distribution corresponds to the 37% percentile, hence the 63% probability of exceedance (DNV GL 2015).

The Gumbel probability density function (PDF), modelling the distribution of the maximum value, is defined as

$$PDF_{Gumbel} = \frac{1}{\beta} e^{-(z+e^{-z})} \tag{4.1}$$

where

$$z = \frac{x-\mu}{\beta} \tag{4.2}$$

x is the response of interest, and μ and β are moment estimators of the Gumbel distribution.

The variance and the mean are found from the samples of the extreme values

$$Var(x)_{Gumbel} = \frac{\pi^2}{6}\beta^2 \tag{4.3}$$

$$E(x)_{Gumbel} = \mu + \beta \cdot \gamma \tag{4.4}$$

where $\gamma \approx 0.5772$ is the Euler-Mascheroni constant.

Chapter 5

Model and Numerical Simulation

In this chapter the model description and system performance of the numerical model in SIMO is presented and discussed. In addition, the uplift phenomena, number of simulations and riser contribution are considered. At the end, the focus in the analyses and the design requirements are provided.

5.1 Model Description

A model of the FPSO in SIMA was provided by Statoil, this is a coupled SIMO - RIFLEX model.

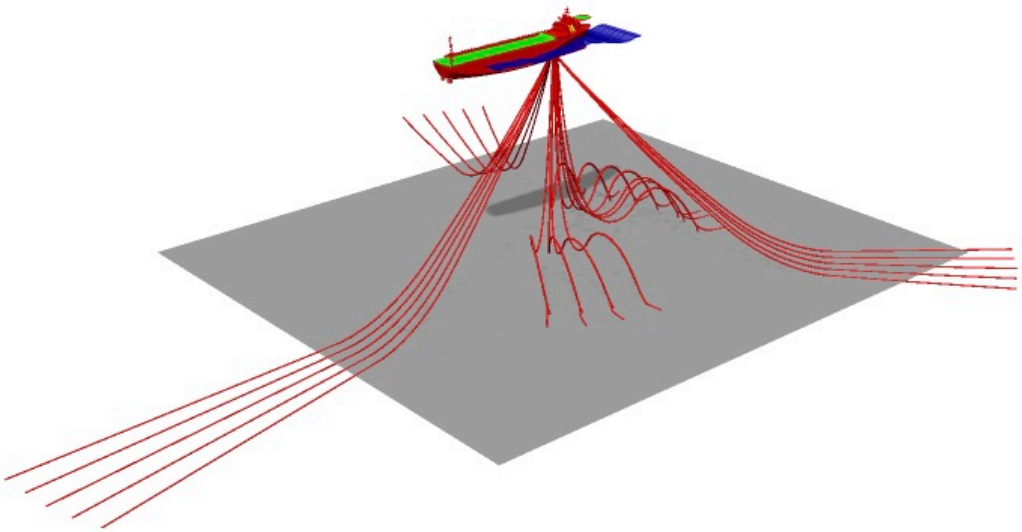

Figure 5.1: Illustration of the numerical model in SIMA

The BODY in the model represents the ship itself, while the mooring and riser system is defined as slender systems in RIFLEX. An illustration of the model is shown in Figure 5.1.

The vessels loading conditions are listed in Table 5.1. In this thesis only the ballast condition is examined, this is due to limitations of the master thesis.

Table 5.1: Vessel particulars (Statoil n.d.)

	Parameter	**Unit**	**Loading Conditions**	
			Full	*Ballast*
Hydrostatic properties	Length LPP	m	273.2	
	Breadth, moulded	m	54.8	
	Depth, moulded	m	30.0	
	Lightship weight	tonnes	91.000	
	Draft	m	21.3	16.6
	Heel	m	0.0	0.0
	Trim	m	1.4	1.8
	Displacement	tonnes	281552	218798
	LCG from AP	m	136.4	137.9
	TCG	m	0.0	0.0
	VCG from BL	m	22.7	20.2
	GM_s	m	2.4	4.6
	GM_f	m	0.6	4.1
Inertia	Rxx	m	18.9	23.8
	Ryy	m	65.0	75.3
	Rzz	m	65.0	75.6
	Rxx	% B	34.4	43.4
	Ryy	% Lpp	23.8	27.6
	Rzz	% Lpp	23.8	27.7
Natural periods	Heave: Tn3	s	12.5	11.7
	Roll: $T_{n,4}$	s	55.8	25.5
	Pitch: $T_{n,5}$	s	11.0	11.0

In order to connect the slender system with the BODY, i.e. the FPSO, a slender system connection is used. To do this a so-called *dummy line* for the vessel created in the slender system, and this dummy line is connected to the BODY. An illustration of the dummy lines are provided later, in Figure 5.4. The risers consists of beam elements, while the mooring lines are build up by bar elements.

5.1.1 Mooring and Riser System Description

The mooring system is passive and consists of three bundles with five anchor lines at each bundle, resulting in 15 mooring lines. In total 11 risers are included in the analysis, with opportunity for future risers. The FPSO has three aft thrusters, each with a power of 3 MW.

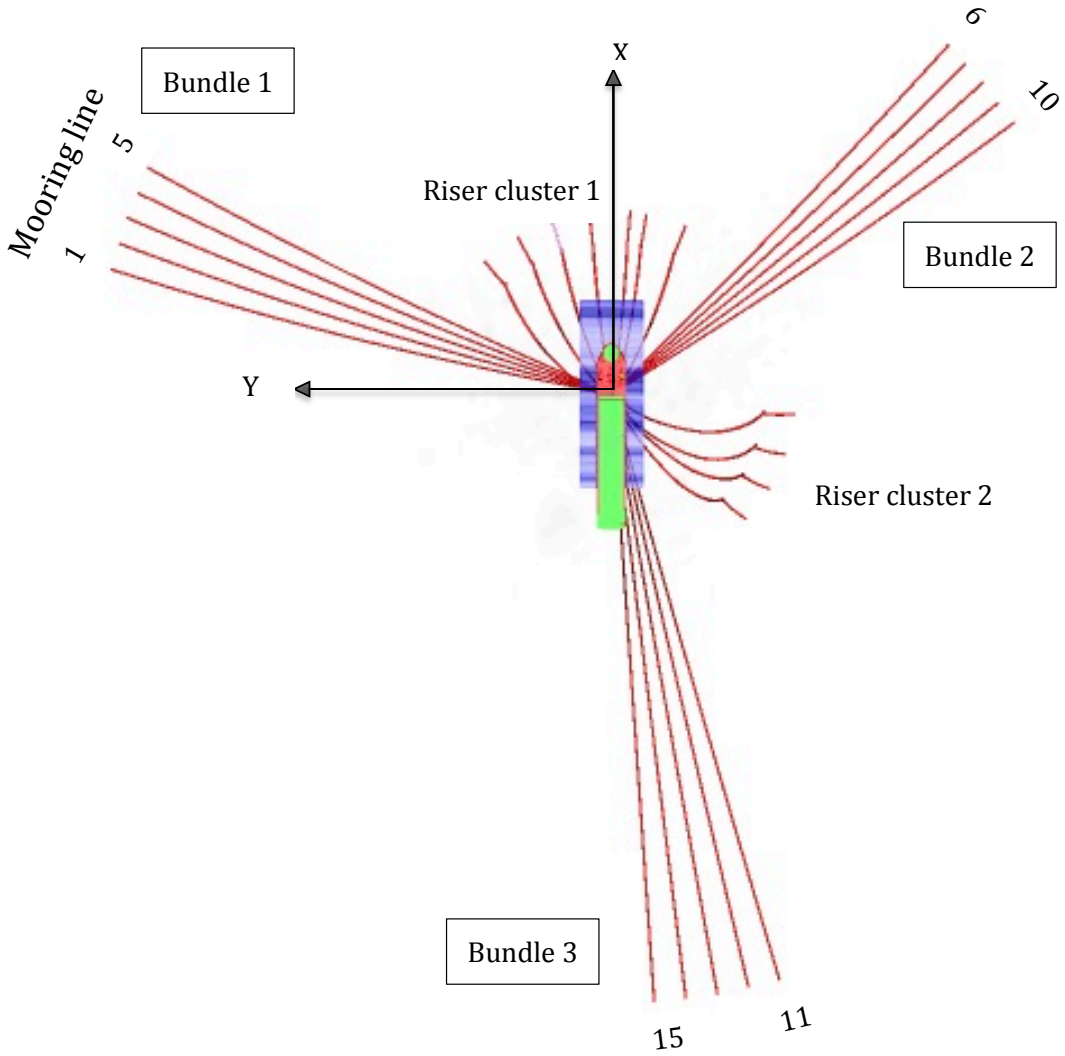

Figure 5.2: Illustration of bundles and risers in relation to the vessel modelled in SIMO

Figure 5.2 shows how the bundles and risers are located. It is approximately 120° between the centre of each bundle. The two riser clusters are both placed between two bundles, this is to enable better access for control and maintenance. Bundle 1 consists of mooring line 1-5, bundle 2 consists of mooring line 6-10 and bundle 3 consists of mooring line 11-15. There are two gas injection lines (GIL), five production lines (PR), two umbilicals (UMB) and two water injection risers (WIR), all with a length of 612m. The diameters are given in Table 5.2.

Table 5.2: Diameter of risers and injection lines

	PR	**WIR**	**GIL**	**UMB**
Diameter [m]	0.5	0.5	0.5	0.3

Each mooring line consists of three segments, the length of the bottom chain segment vary for the different bundles. In Table 5.3 the segments with associated length and type are listed. In the model 85 m has been added to the bottom chain lengths listed in Table 5.3. This results in a total length of 960 m, 910 m and 1110 m for bundle 1, bundle 2 and bundle 3 respectively.

Table 5.3: Segment lengths (Aas 2017)

Segment		**Bundle 1**	**Bundle 2**	**Bundle 3**
Top chain	[m]		50	
Mid Wire Rope	[m]		345	
Bottom chain	[m]	480	430	630
Total	[m]	875	825	1025

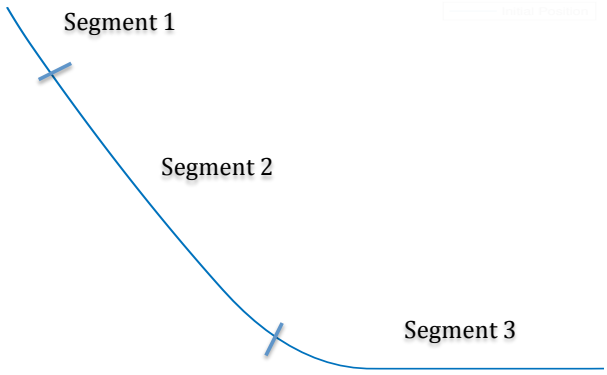

Figure 5.3: Illustration of the segments on a mooring line

The mooring line segments are illustrated in Figure 5.3, the associated segment properties for the mooring lines are given in Table 5.4. In addition, the adjustments for marine growth according to DNV GL (2015) is provided in Table 5.5.

Table 5.4: Segment properties (Statoil n.d.)

Parameter	**Unit**	**Bottom Chain**	**Mid Wire Rope**	**Top Chain**
Type	-	R3S	SSSW	R4
Nominal diameter (new)	mm	175	148	175
Linear mass	kg/m	618.6	115.9	618.6
Linear weight in water	kg/m	537.8	92.7	537.8
Stiffness (EA)	kN	1.5E+06	2.0E+06	1.4E+06
MBL (new)	kN	22876	22000	25173
MBL (corroded over 32 years)	kN	21597	N/A	23765
Drag coefficient - transverse	-	2.4	1.2	2.4
Drag coefficient - axial	-	1.15	0	1.15
Added mass coefficient - transverse	-	1	1	1
Added mass coefficient - axial	-	0.5	0	0.5
Note: SSSW outer diameter is taken as 170 mm (148+2 · 11mm sheathing)				

Table 5.5: Adjustments for marine growth (DNV GL 2015)

Parameter	**Unit**	**Bottom Chain**	**Mid Wire Rope**	**Top Chain**
Thickness marine growth	mm	30	30	30
Line type factor	-	2	1	2
Density of marine growth	kg/m3	1325	1325	1325
Density of water	kg/m3	1025	1025	1025
Mass of marine growth	kg/m	51.20	24.98	51.20
Weight in water of marine growth	kg/m	11.59	5.65	11.59
Weight in water of marine growth	kN/m	0.11	0.06	0.11
Drag coefficient - transverse	-	3.2	1.6	3.2
Drag coefficient - axial	-	1.5	0.0	1.5

Each of the risers are divided into three parts with different lengths and properties in the numerical model. In total, over the three riser segments for every riser type, it's on average 60 elements for each riser. Hence the numerical integration for all riser elements in RIFLEX will result in large computational time.

The weight of the risers will contribute to the vertical loading on the turret. Depending on the analysis, and the contribution from the risers, it is recommended to simplify the riser model. If this is reasonable in this case, will be addressed later.

5.1.2 Turret Description

In the numerical model the turret system is simplified by describing the turret as a dummy line. This line is a beam element with zero torsional stiffness to permit free rotation between the top end (node 2) and the lower "geo-stationary" end (node 1) (Statoil n.d.). The top end is fixed to the vessel dummy line, the mooring lines and risers are connected to the lower turret end as shown in Figure 5.4.

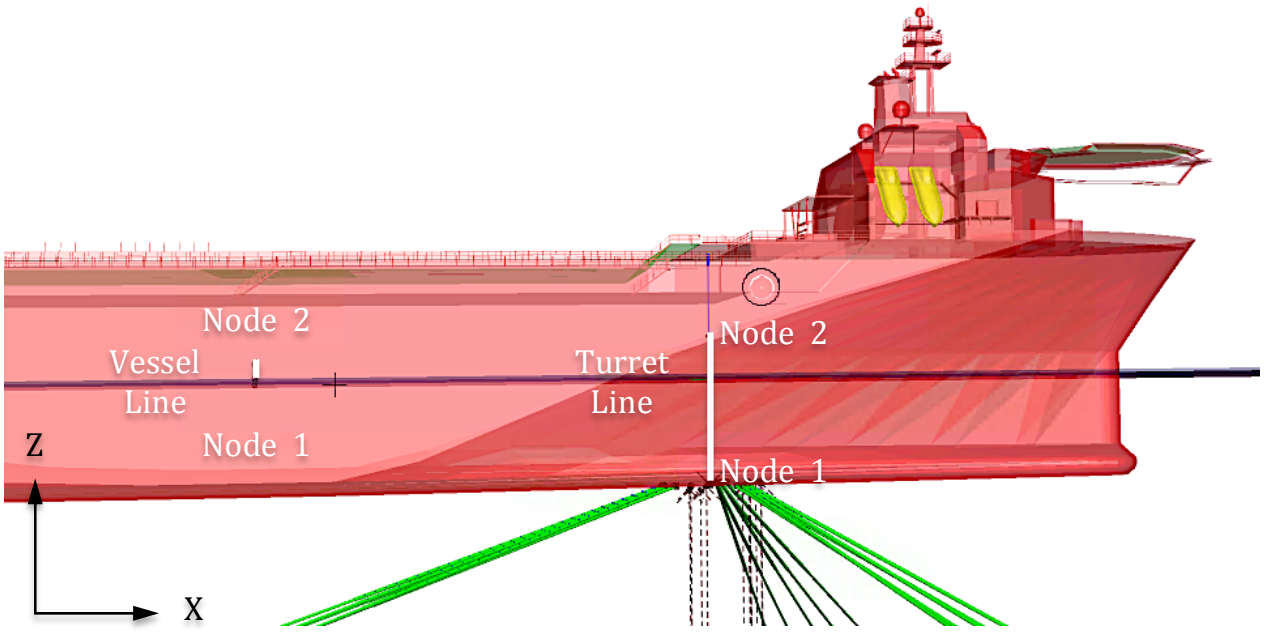

Figure 5.4: Illustration of the turret and vessel dummy lines in SIMO

The entrapped water refers to the volume of water inside the turret cylinder (Statoil n.d.). Its inertia due to the vessel accelerations induces loads at the turret. Industry practice is to consider

the water in the turret as a fixed mass of water, such as frozen water. A common approach is to add the inertia effect from entrapped water when post-processing the results, hence it's not modelled explicitly in the SIMO-RIFLEX model. The mass of entrapped water and other turret specifics are given in Table 5.6. Some of the main parameters are shown in the 2D cross sectional sketch of the turret, given in Figure 5.5. Similarly to the entrapped water, the effect of the turret weight is excluded from the SIMO-RIFLEX model and post-processed. The effect of the turret inertia can be discussed, but for this case focusing on the loads at the radial wheels and bogies, this is considered as a decent approximation.

Table 5.6: Turret mass properties

Parameter	**Unit**	**Value**
Diameter between bogies, D	m	20
Turret cylinder diameter	m	17.8
Elevation of radial wheels above keel (denoted a)	m	23.5
Mass of fixed part (turret dry mass)	tonnes	6100
Mass of entrapped water	tonnes	4357
Elevation of turret fixed part COG above keel	m	33.2
Rxx	m	28.6
Ryy	m	28.6
Rzz	m	9.10
Ixx	tm^2	4.98E+06
Iyy	tm^2	4.98E+06
Izz	tm^2	5.07E+05

Turret Support Forces

From the lower turret line end, i.e. node 1 in Figure 5.4, the loads at chain table, hence loads at the top of the mooring lines, can be extracted and transformed to the radial wheels and bogies. The dynamic global turret model can be simplified to a force equilibrium presented in Figure 5.6, that supposes three main equations of importance in this thesis.

The turret will be produced by SBM Offshore. In this design an axial bogie and radial wheel

system replaces the conventional roller bearing system (SBM Offshore 2012). Bogies and wheels run on bolted rail sectors in such a way that all components can be replaced where they are situated. The axial bogies and radial wheels are illustrated in Figure 5.5.

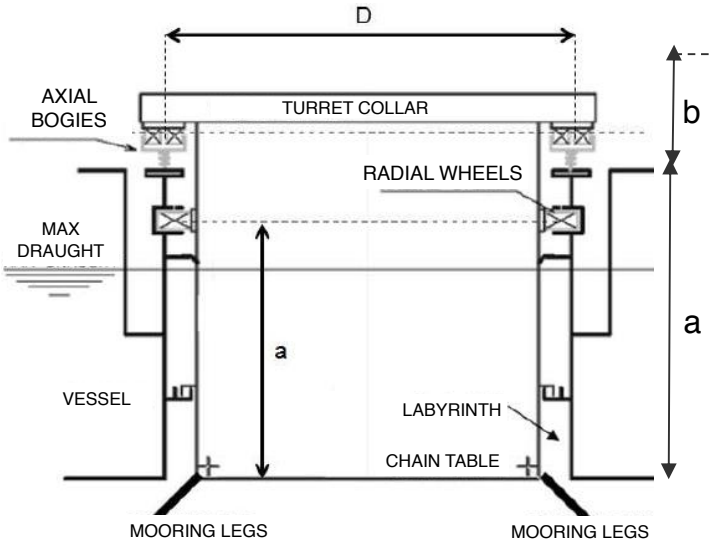

Figure 5.5: Cross-section of turret including the main particulars of the turret (Statoil n.d.)

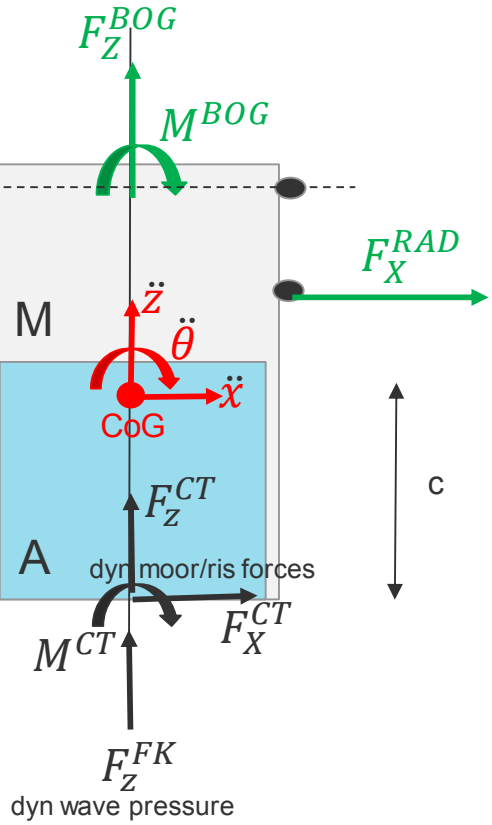

Figure 5.6: Simplified dynamic equilibrium of turret (Larsen 2017)

The unknown variables from Figure 5.6 are

- F_X^{RAD}: Force in the horizontal direction at the radial wheels
- F_Z^{BOG}: Force in the vertical direction at the bogies
- M^{BOG}: Moment at bogies

The known variables found from dynamic analyses in SIMO, are

- F_X^{CT}: Force in the horizontal direction at chain table (CT) from moorings and risers
- F_Z^{CT}: Force in the vertical direction at chain table (CT) from moorings and risers

- M^{CT}: Moment at chain table (CT) from moorings and risers
- F_Z^{FK}: Dynamic Froude-Krylov force in the vertical direction
- $\ddot{x}, \ddot{z}$ *and* $\ddot{\Theta}$: Acceleration of turret COG in horizontal, vertical and pitch direction respectively

In addition the lengths *a,b* and *c*, and the inertia at turret COG (I_{COG}) are calculated from the given parameters in Table 5.6. Turret dry mass and mass of entrapped water are denoted M and A respectively. The Froude-Krylov force is the force due to the unsteady pressure field generated by the undisturbed waves (Faltinsen 1990). The Froude-Krylov forces together with the diffraction force, is the total non-viscous forces acting on a floating body in regular waves. The dynamic pressure force is neglected for the simplified turret model, i.e. $F_Z^{FK} = 0$.

The unknowns are derived from the dynamic equilibrium of the turret, in Appendix A the complete derivation is given, resulting in the three main equations

$$F_X^{RAD} = (M + A) \cdot \ddot{x} - F_X^{CT} \tag{5.1}$$

$$F_Z^{BOG} = (M + A) \cdot \ddot{z} - F_Z^{CT} - F_Z^{FK} \tag{5.2}$$

$$M^{BOG} = I^{COG} \cdot \ddot{\Theta} - M^{CT} - F_X^{CT} \cdot a + (M + A) \cdot \ddot{x} \cdot (b + c) \tag{5.3}$$

In the numerical model in SIMO, only the length of the turret is implemented. The dynamic results are post-processed in SIMO and MatLab. It should be noted that F_X^{RAD}, F_Z^{BOG} and M^{BOG} are pure dynamic forces, based on contributions from wave- and low-frequent motions. The static mean forces are not included.

Uplift of Turret

The bogies consists of non-linear springs embracing the whole turret. The bogie support force $F_{support}^{BOG}$ is the force provided by the springs at the bogies. The turret collar rests upon the axial bogies, hence the turret weight keeps the turret from uplift. This is illustrated in Figure 5.7.

If the time series of the turret support forces are so large that the time series of the turret support force at bogies becomes zero or negative, uplift will happen. It is safety-critical that the

swivel situated on top of the turret does not experience uplift, due to the fluid and/or gas pipes to or from the reservoir, situated in the connection between the global and local coordinate system. If these are broken or damaged, different fluid and/or gas will be of danger for both crew and environment. Therefore the turret must have a certain weight in order to prevent uplift.

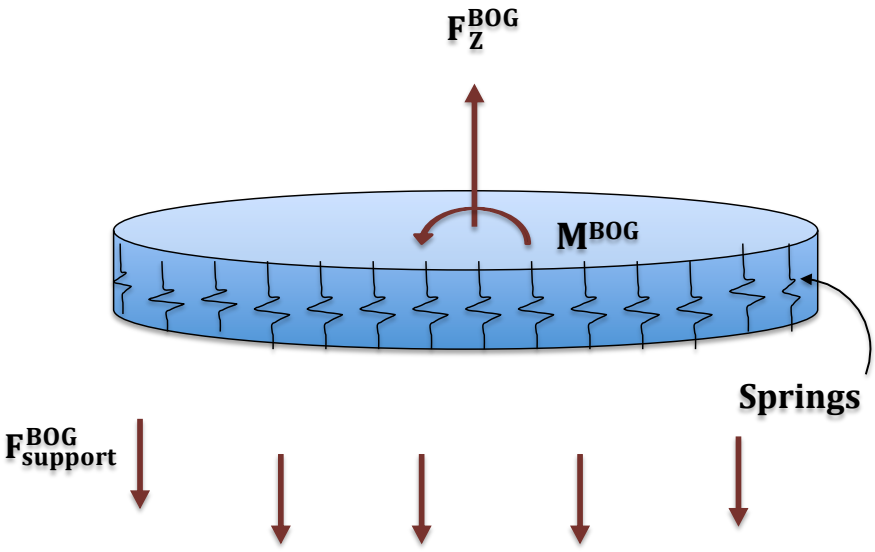

Figure 5.7: Illustration of the forces when considering turret uplift at bogies

The problem requires an advanced complete 3D turret model, where the time series of the support force at bogies is calculated. All springs are individual with regards to their characteristics and how they behave at different time steps. The model design and force calculation are considered as extremely complicated and time consuming, and beyond the scope of this master thesis.

Alternatively, a simplified 2D estimation can be done by looking at the bogies from the side, reducing the circular bogie to a single beam with supports. Two different support suggestions are illustrated in Figure 5.8 and 5.9 denoted alternative 1 and 2 respectively. The length of the beam equals the diameter, D, of the turret, given in Table 5.6. F_Z^{BOG} and M^{BOG} are situated exactly in the centre of the beams, at $D/2$.

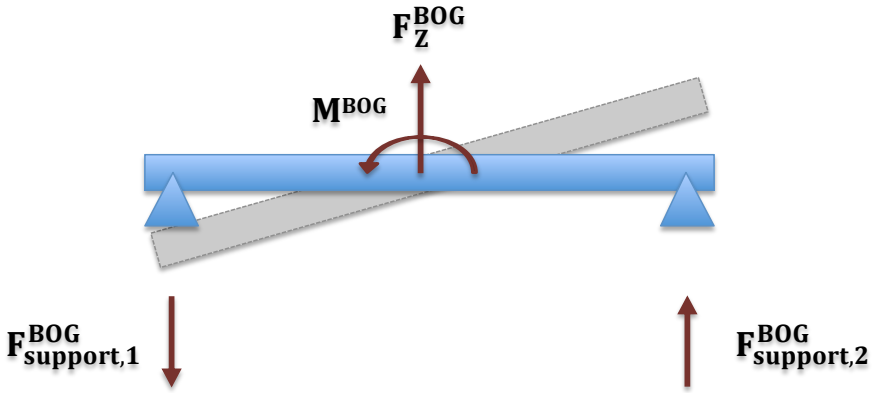

Figure 5.8: Alternative 1: Illustration of the forces at bogies for a simplified 2D expression, using roller bearing supports

where the support forces are defined as

$$F^{BOG}_{support,1} = \frac{F^{BOG}_Z \cdot \frac{D}{2} - M^{BOG}}{D} \quad and \quad F^{BOG}_{support,2} = -\frac{F^{BOG}_Z \cdot \frac{D}{2} + M^{BOG}}{D} \tag{5.4}$$

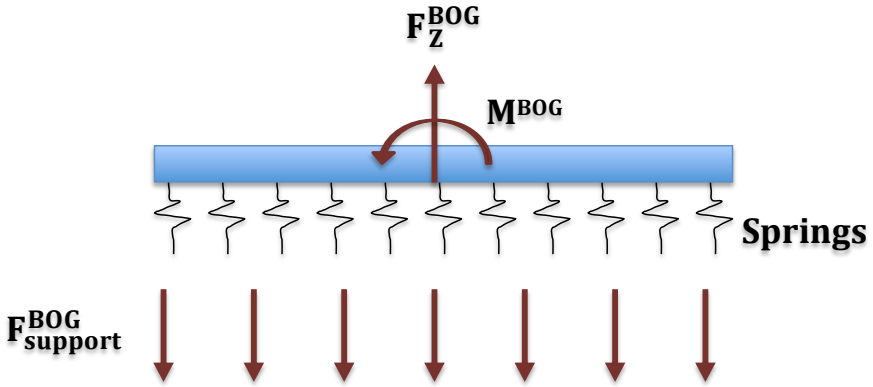

Figure 5.9: Alternative 2: Illustration of the forces at bogies for a simplified 2D expression, using springs as supports

In alternative 1, the axial bogies are simplified into two roller bearing supports in each beam end. Then, simple beam theory can be used to calculate the turret support force, presented in Eq. 5.4. However, this procedure is considered as far too simple for a design case, but provides a rough estimate. Alternative 2 on the other hand is somewhat more advanced compared to alternative 1. Here the axial bogies are represented by springs supporting the whole length of the beam. In real life the springs are non-linear, and the stiffness at the ends are more rigid than

those located in the middle. Hence this alternative is a large simplification compared to the 3D model. From the support forces at bogies the turret mass can be quantified.

5.2 Verification of Numerical Model

In order to document and verify that the model is within reasonable values, several tests are performed and force coefficients plotted. The wave drift, wind and current force coefficients, RAOs, free-decay and static pull-out tests are described and discussed.

The surge, sway and yaw motions are affected by the mooring system, since the moorings imposes stiffness in these DOFs, these are the degrees of freedom of particular interest. The frequency region of interest for a ship is the wave frequent region. Typically, for a ship-shaped FPSO, these are periods within an interval of $T\epsilon[5,30]s$.

5.2.1 Wind and Current Force Coefficients

The wind and current force coefficients are obtained by wind tunnel test, subsequently the results are imported to SIMO.

The dynamic wind will excite LF motions of moored floating structures. Wind gusts have significantly energy at surge, sway and yaw natural periods. The wind coefficients are plotted as a function of the vessels heading in degrees from $0-180°$, for surge, sway and yaw. Since the ship is almost symmetrically about the x-axis, it's representative to plot only one half of the ship, therefore the coefficients are plotted for the range $0-180°$. The mean wind force is defined as

$$\overline{q}_{wi} = C_{wi} \cdot \overline{V}^2_{wi} \tag{5.5}$$

where C_{wi} is the wind force coefficient and $\overline{V}^2_{wi}$ is the mean wind velocity.

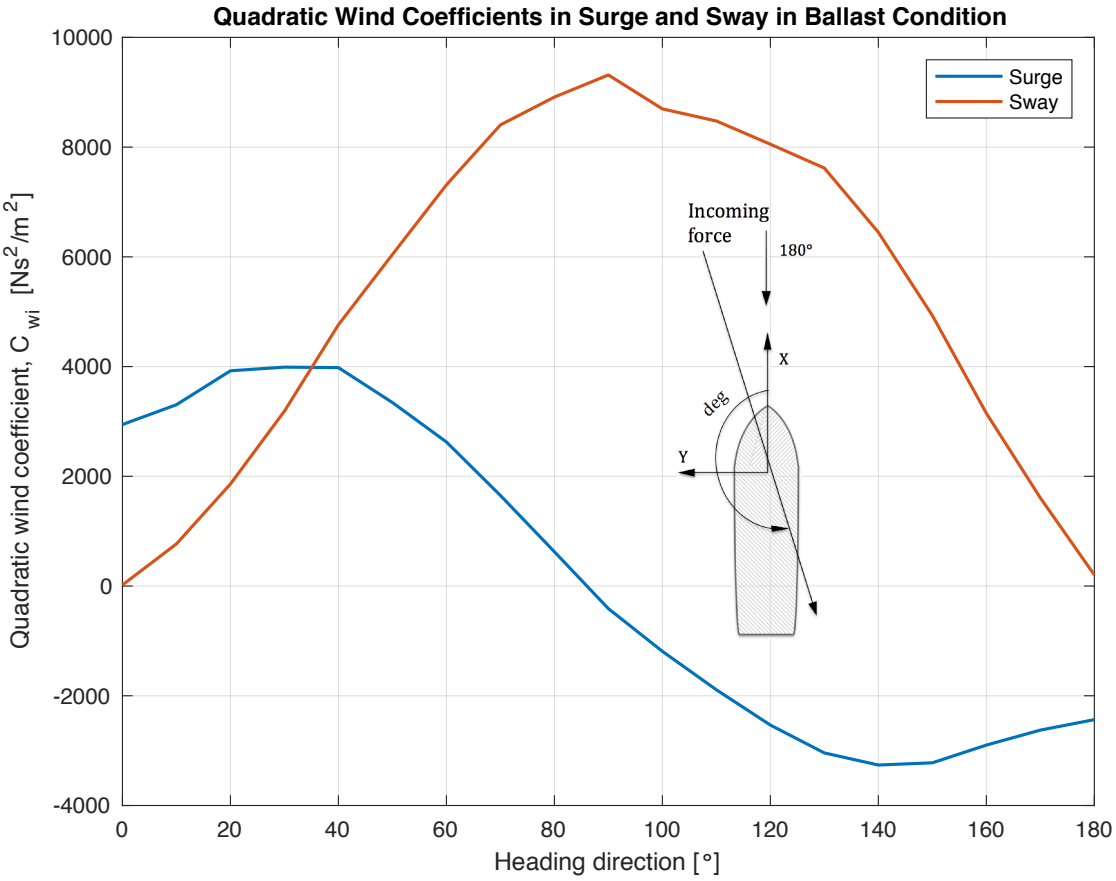

Figure 5.10: Quadratic wind coefficients in surge and sway

The coefficient in surge from Figure 5.10 indicates that the vessel's impact in surge is large for wind incoming at the bow, i.e. 180°. Then the impact increases and reaches a peak at 40° relative to the bow. It should be noted that the force is negative at 180° since it travels in the negative x-direction. Also, at a heading of 90° there is practically no impact in surge motion, which fits well with physical laws. The surge coefficient is somewhat larger in magnitude in the aft of the ship. This can be due to the location of the vessel's origo. The contact area behind origo may be much larger than in front of origo, hence larger impact from the applied wind.

The wind coefficient in sway has a large impact on the vessel at a heading of 90°. This is natural since the contact area for the wind is at its most in the y-direction. The wind coefficient is approximately zero for the heading towards the bow and stern of the vessel, i.e. 180° and 0° respectively. At 180°, i.e. the bow, the wind coefficient in surge is not quite zero. This can be due to shadow effects from the topside.

The quadratic wind coefficient in yaw is plotted in Figure 5.11, this shows that a heading of 140°, thus 40° relative to the bow, has a severe impact on the vessel. Since this is a weathervaning ship, it is most likely that the ship will stay within $0-50°$, hence a direction of 30° will have the highest impact in yaw. The magnitude of the force is much larger in front of origo compared to the aft of origo, as mentioned for the surge force, this is due to an unsymmetrical topside. Following the right hand rule, the positive direction of rotation for yaw is anti-clockwise.

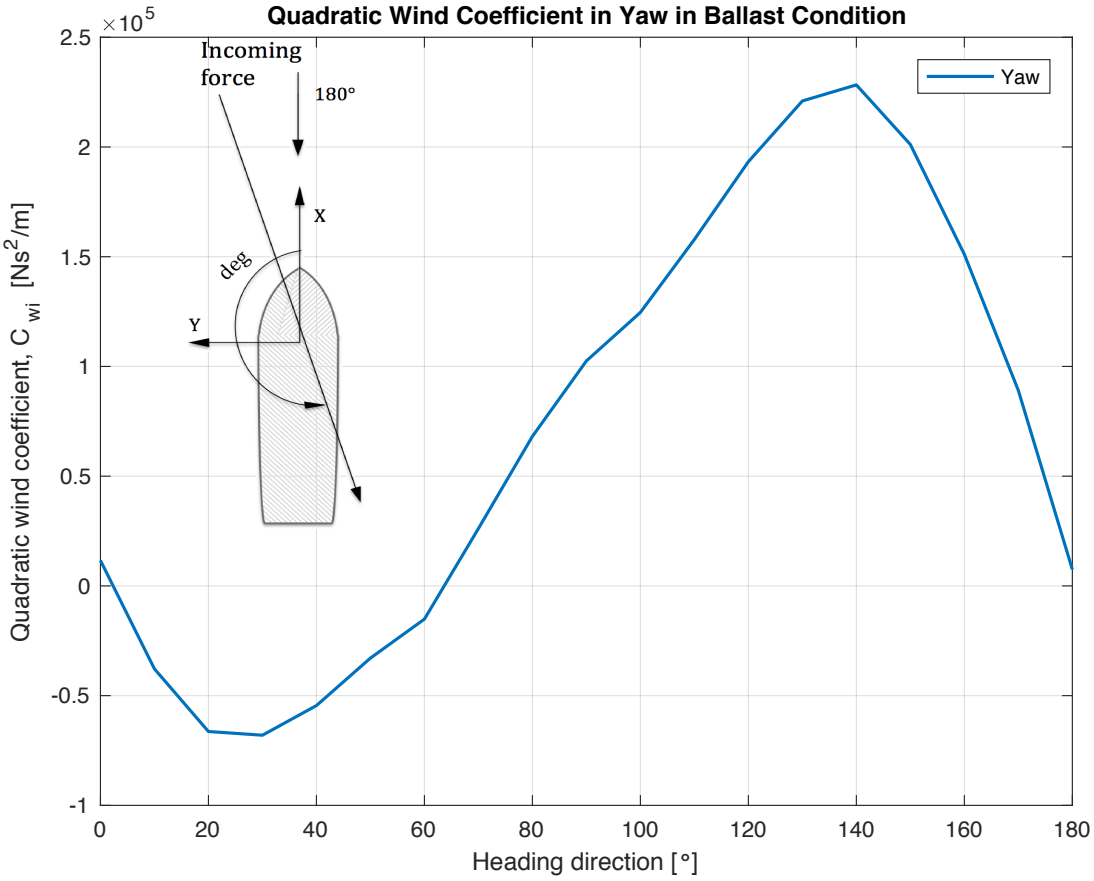

Figure 5.11: Quadratic wind coefficient in yaw

In contrast to the wind coefficient which applies to the topside of the vessel, the current coefficient is applied on the submerged part of the vessel. The submerged hull is utterly symmetrical and streamlined, thus the current coefficient will be more symmetrical in comparison with the wind coefficient. The current force coefficient is plotted as a function of the vessels heading from $0-180°$, for surge, sway and yaw. The current velocity is assumed to be constant

for the time period of interest. The mean current force can be expressed as

$$\overline{q}_{cu} = C_{cu} \cdot V_{cu}^2 \tag{5.6}$$

where C_{cu} is the current force coefficient and V_{cu}^2 is the current velocity.

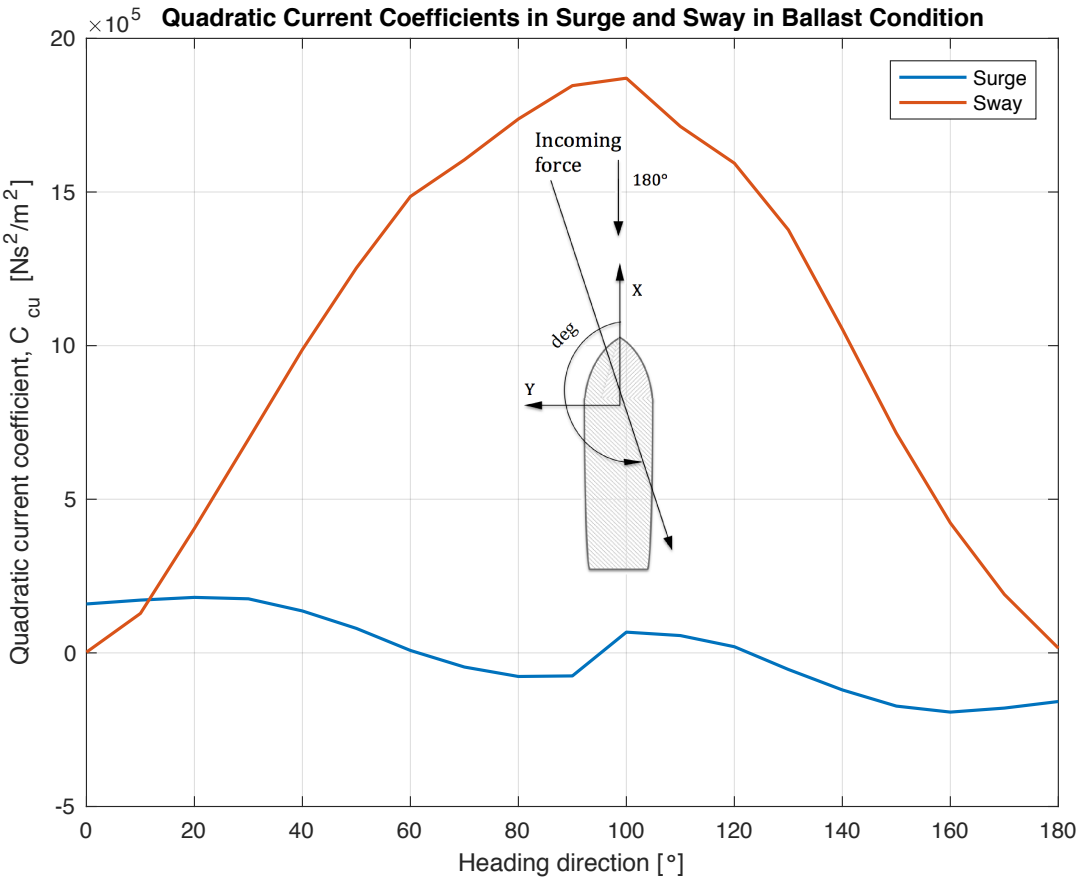

Figure 5.12: Quadratic current coefficients in surge and sway

The interpretation of the current coefficients impact on the vessel is quite similar as for the wind coefficient in principle. Comparing the magnitude of the force coefficients, the current has a much larger impact on the vessel. The reason for this is mostly due the difference between the two elements, air and water. The density and drag coefficient is much larger for water than air.

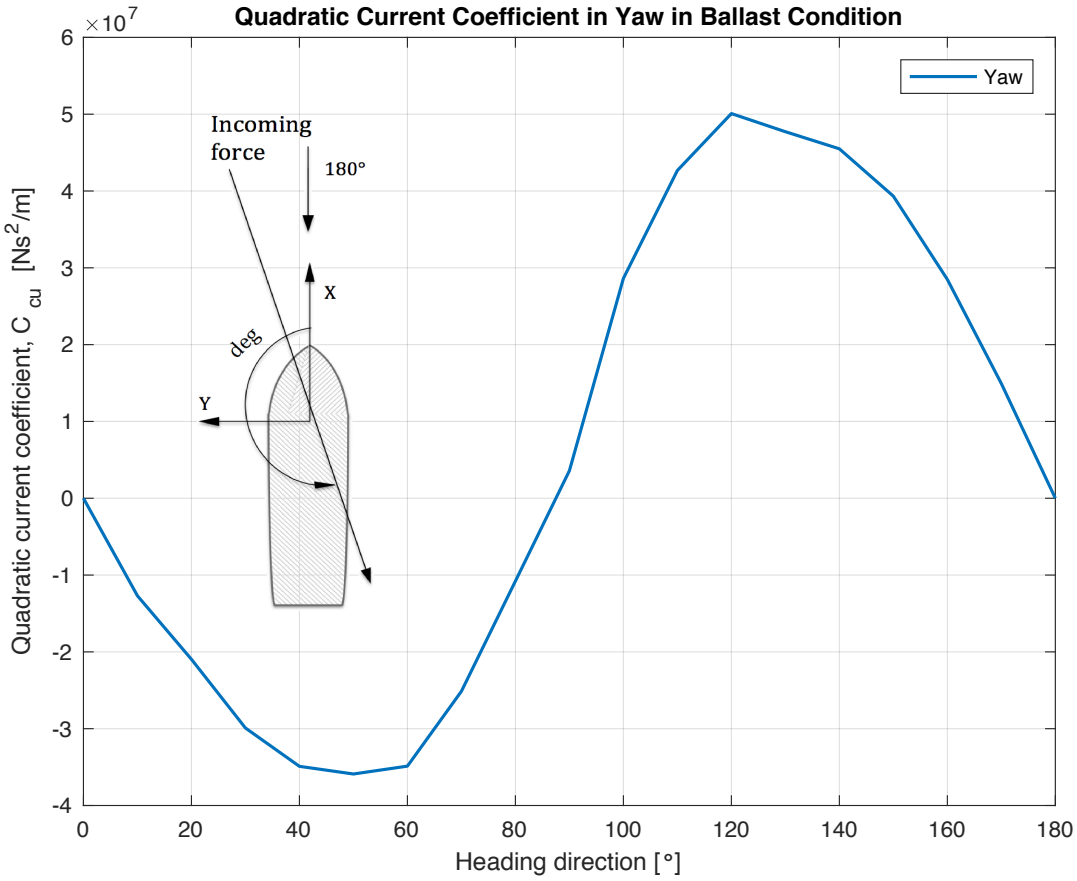

Figure 5.13: Quadratic current coefficient in yaw

On the whole, the wind and current force coefficients in surge, sway and yaw are considered as physically sound.

5.2.2 Wave Drift Force Coefficient

For a regular wave, the vessel experiences a mean drift force proportional to the square of the wave height. Mean wave drift force is given from the wave spectrum

$$\overline{q}_{wa}^{2.ord} = 2 \cdot \int_0^{\infty} C_{wa}(\omega) \cdot S_{\zeta_a}(\omega) d\omega \tag{5.7}$$

where $\overline{q}_{wa}^{2.ord}$ is the 2.ord mean wave drift force, C_{wa} is the wave drift force coefficient, and ω is the wave frequency. $S_{\zeta a}(\omega)$ is the wave spectrum shown in Figure 5.14 and the wave height, ζ_a, can be written as

$$\zeta_a^2 = 2 \cdot S(\omega) d\omega \tag{5.8}$$

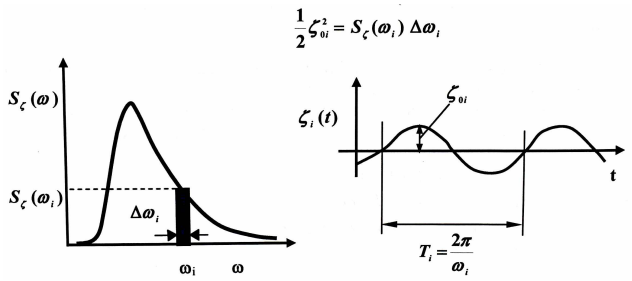

Figure 5.14: Wave spectrum and a harmonic component (Larsen 2014)

Hence, the wave drift coefficient can be written as

$$C_{wa} = \frac{\overline{q}_{wa}^{2.ord}}{\zeta_a} \tag{5.9}$$

The turret moored FPSO is continuously weathervaning, and therefore it's the directions towards the bow area which are of main interest. A range of $0-50°$ relative to the bow corresponds to wave coefficients from $180-130°$ in the SIMA notation. The wave drift force coefficients are plotted as a function of frequency for different directions.

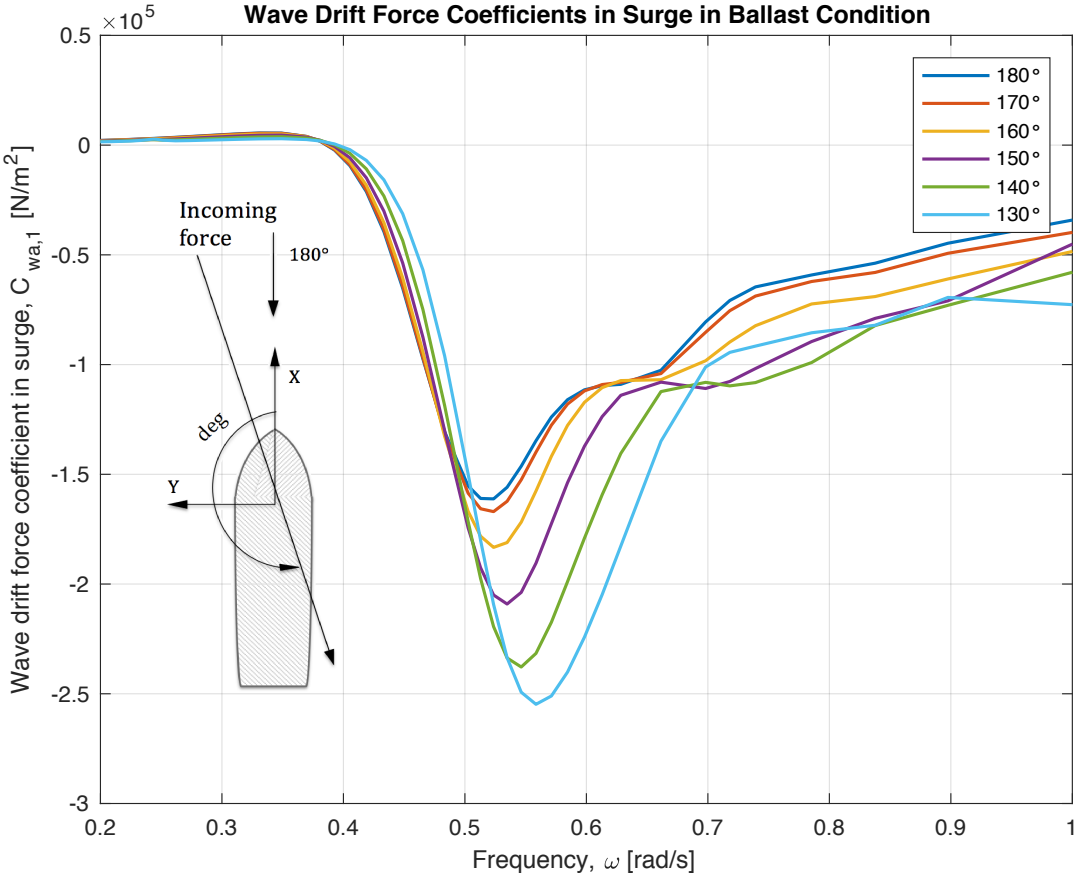

Figure 5.15: Wave drift coefficients in surge for 0-50 degrees relative to the units bow

In Figure 5.15 the wave force coefficients in surge are shown. At frequencies smaller than 0.4 rad/s, which are large periods, the body of the vessel floats with the wave. In such cases the waves has no impact on the vessel, hence the wave drift coefficient is zero. In the frequency interval between 0.4-0.7 rad/s, corresponding to wave periods of 9-16 s, is the area where the surge motions of the vessel is at its maximum. The peak of the wave drift force coefficients often corresponds to the peak in heave and pitch RAOs, due to the coupling of the forces. The RAOs are discussed later. At smaller frequencies the vessel acts like a wall relative to the incoming waves, and reflects the waves. Hence the wave drift coefficient goes asymptotically towards a value.

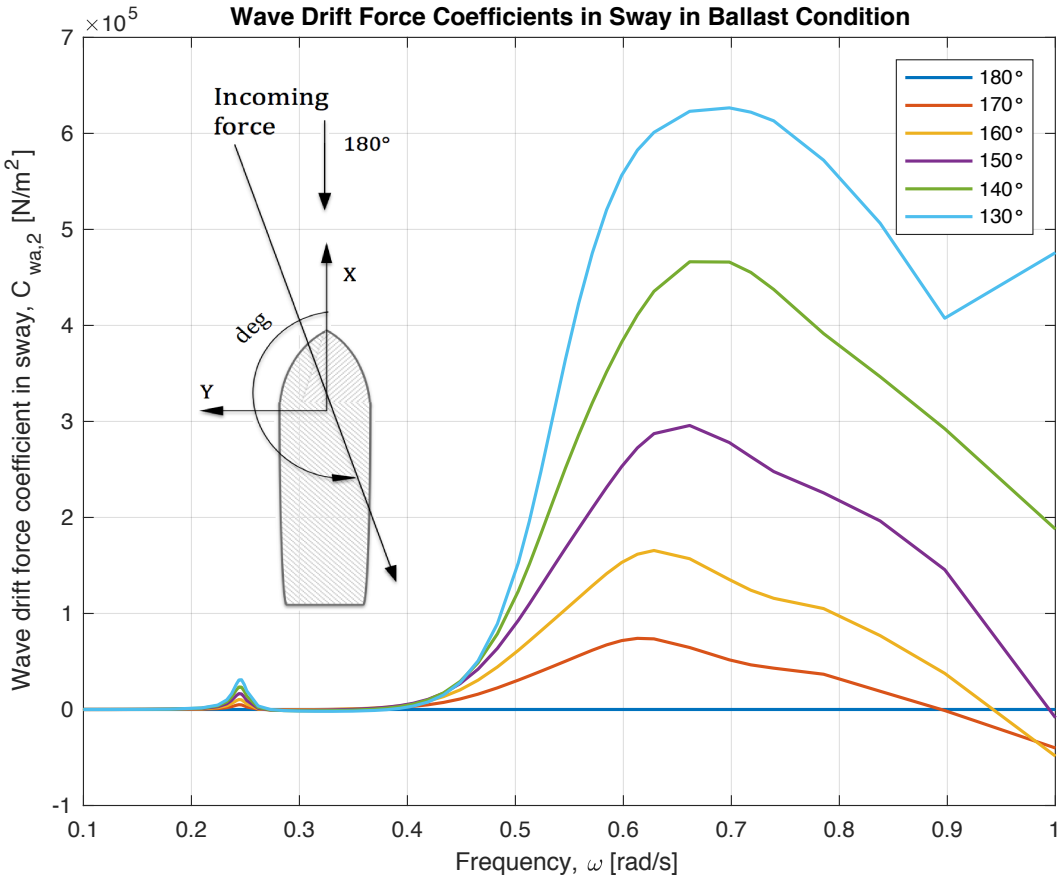

Figure 5.16: Wave drift coefficients in sway for 0-50 degrees relative to to units bow

For the wave coefficients in sway, represented in Figure 5.16, a force coming directly towards the bow has zero impact for all frequencies. By gradually increasing the direction relative to the bow, and for frequencies larger than 0.4 rad/s, the impact in sway increases. This seems natural. At frequencies between $0.6 - 0.7$ rad/s, the peaks from the different directions are located, this corresponds to periods of $9 - 10.5$ s. The curve representing the wave drift force at 130°, for high frequencies, are not logical. This is due to numerical instability in WAMIT, and can be a result of too large panel size. However, this corresponds to a period of approximately 6-7 s, and are therefore not important for the ship-shaped FPSO.

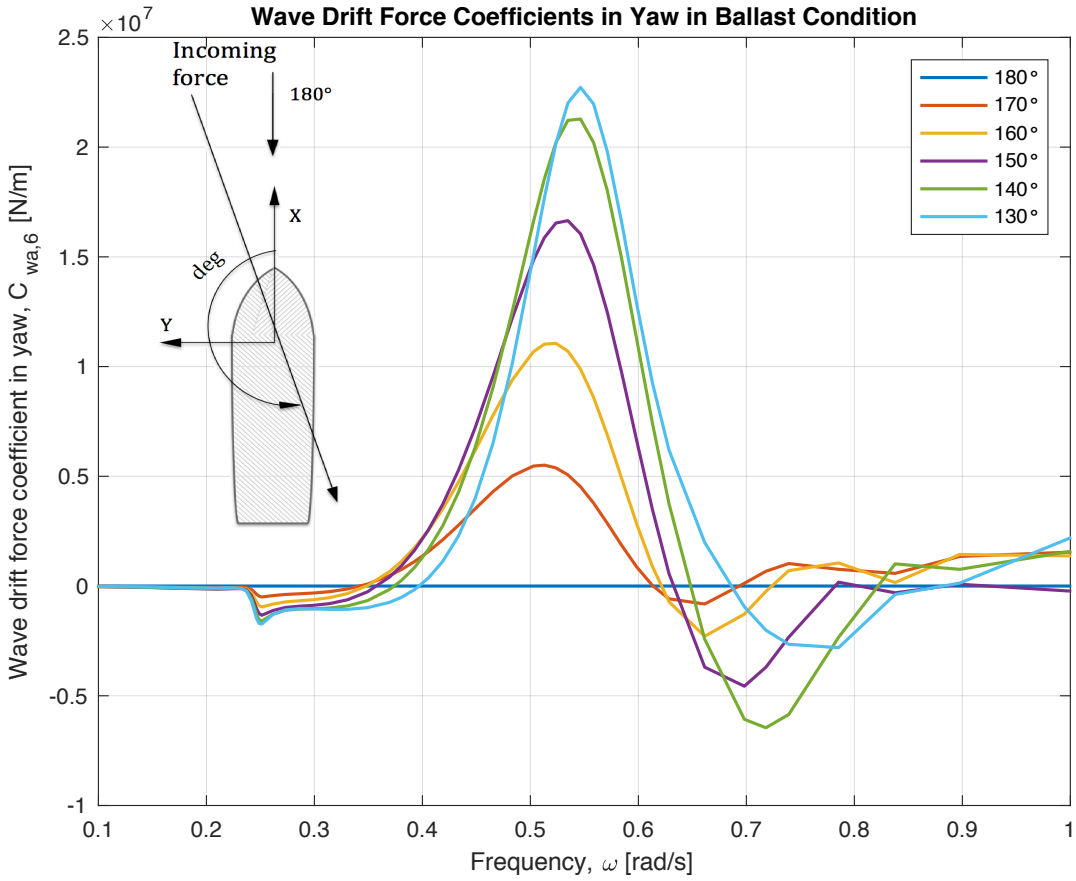

Figure 5.17: Wave drift coefficients in yaw for 0-50 degrees relative to the units bow

The wave drift force coefficients in yaw in Figure 5.17 shows that the vessel is not affected by the long periods. In addition, the impact in yaw of the vessel is greatest at frequencies between 0.5 and 0.6 rad/s for all directions.

Overall, the wave force coefficients in surge, sway and yaw are considered physically sound.

5.2.3 Response Amplitude Operator (RAO)

The motion RAOs are transfer functions which explains how the sea state will affect the motion of the ship. The RAO for all six degrees of freedoms are plotted as a function of frequency for $0-90°$ relative to the bow, thus $180-90°$ in the SIMO definition. In each plot, a sample of directions in this range are chosen as representative for the motion in question.

The motion RAOs in surge are presented in Figure 5.18. For long waves in head sea the surge

motion of the FPSO goes towards one, which means that the motions applied equals the vessel's motion. For short wave periods, hence high frequencies, the motion RAO is approximately zero. This is because the waves passes the vessel before the structure becomes affected, therefore the vessel surge motion is unaffected by the sea state.

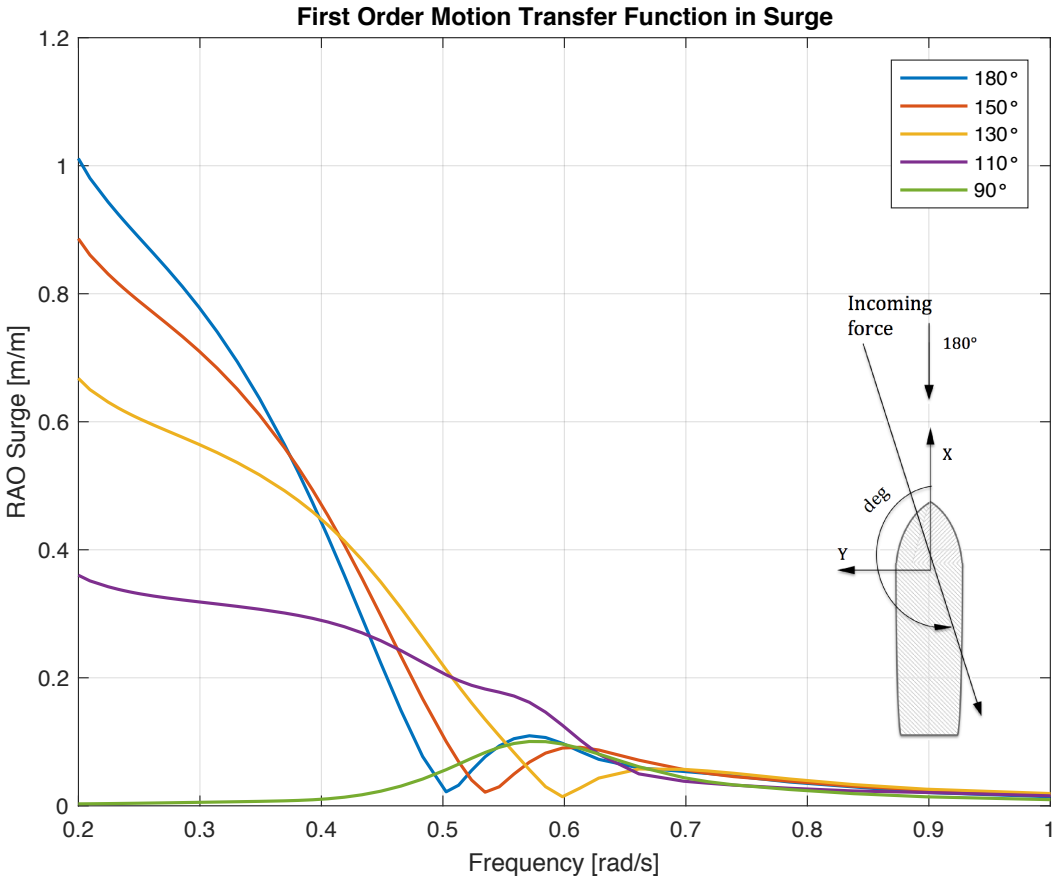

Figure 5.18: Motion RAOs in surge for 0-50 degrees relative to the units bow

In Figure 5.19 the motion RAOs in sway are shown. In beam sea, the motion RAO is quite large for all frequencies. On the contrary, head sea does not affect the ship motion in sway.

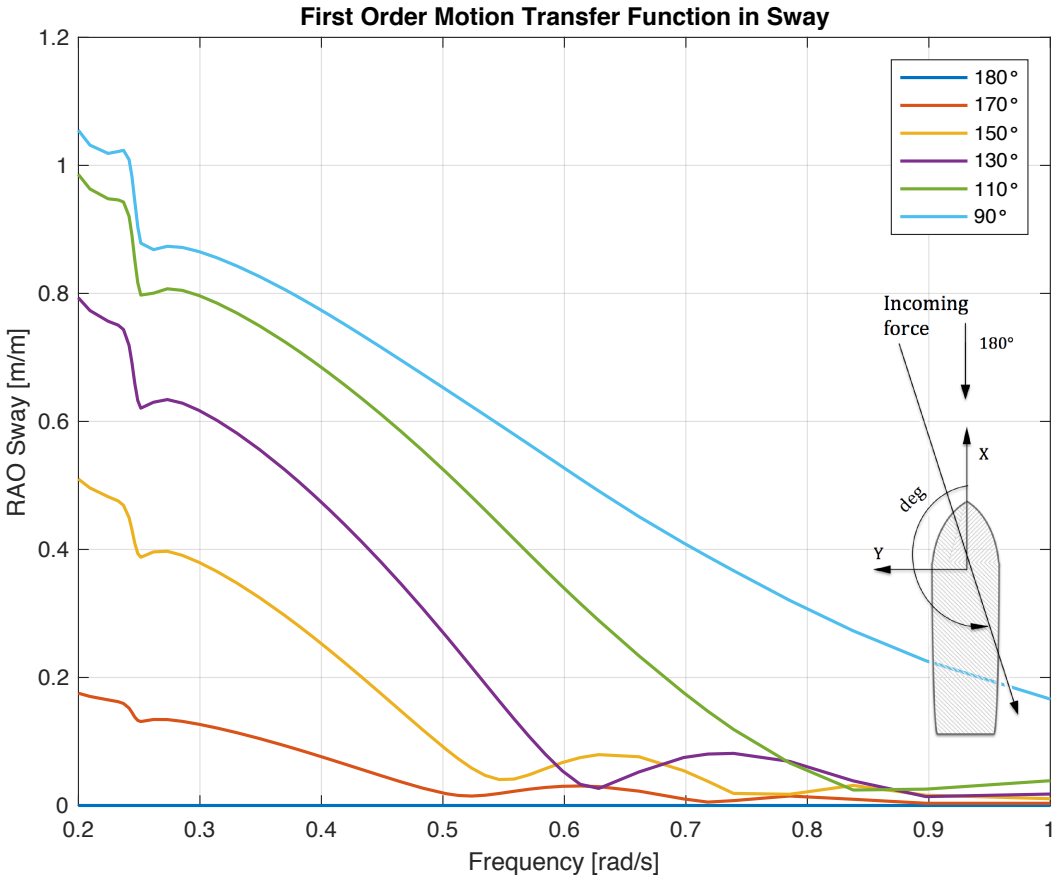

Figure 5.19: Motion RAOs in sway for 0-50 degrees relative to the units bow

As explained before, the structure follows the waves for long wave periods, hence small frequencies. In these cases the RAO goes asymptotically towards one. This can be seen from the heave RAO in Figure 5.20. When the motion RAO ≈ 1, it means that the heave amplitude coincides with the heave RAO.

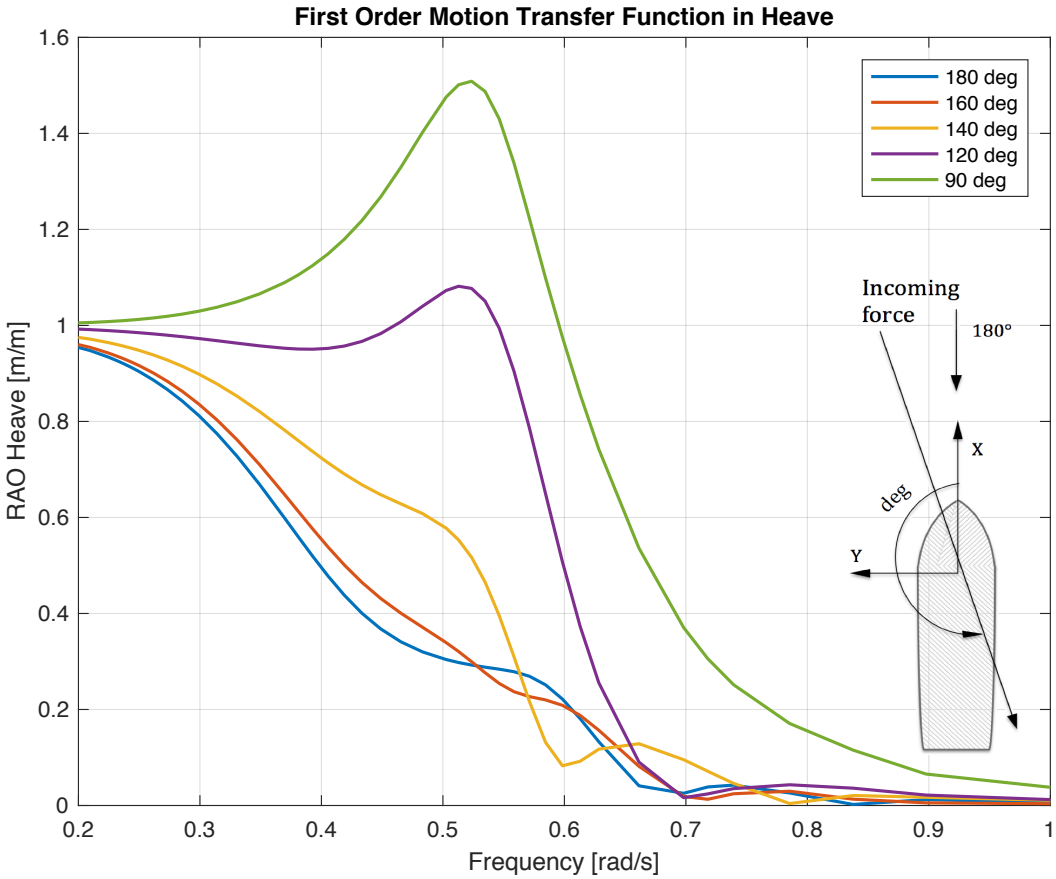

Figure 5.20: Motion RAOs in heave for 0-50 degrees relative to the units bow

In addition, the heave motion has large amplifications for frequencies around $0.5-0.6$ rad/s which equals $12-10.5$ s, especially in beam sea. The eigenfrequency in heave of the structure is located in this area, and must be accounted for when designing the mooring system with respect to risers and other heave sensitive equipment. From Table 5.1 the heave natural period in ballast condition is 11.9s, this coincides well with the motion RAO in heave. For head sea around the eigenfrequency it is not generated heave motions in particular, this is due to cancelling of the heave force. At a frequency of 0.6 rad/s, the wavelength $\lambda = g/2\pi T^2 \simeq 160m$. Compared to the vessel length, $L_{PP} = 273m$, this results in approximately 2 wave crests along the vessel hull.

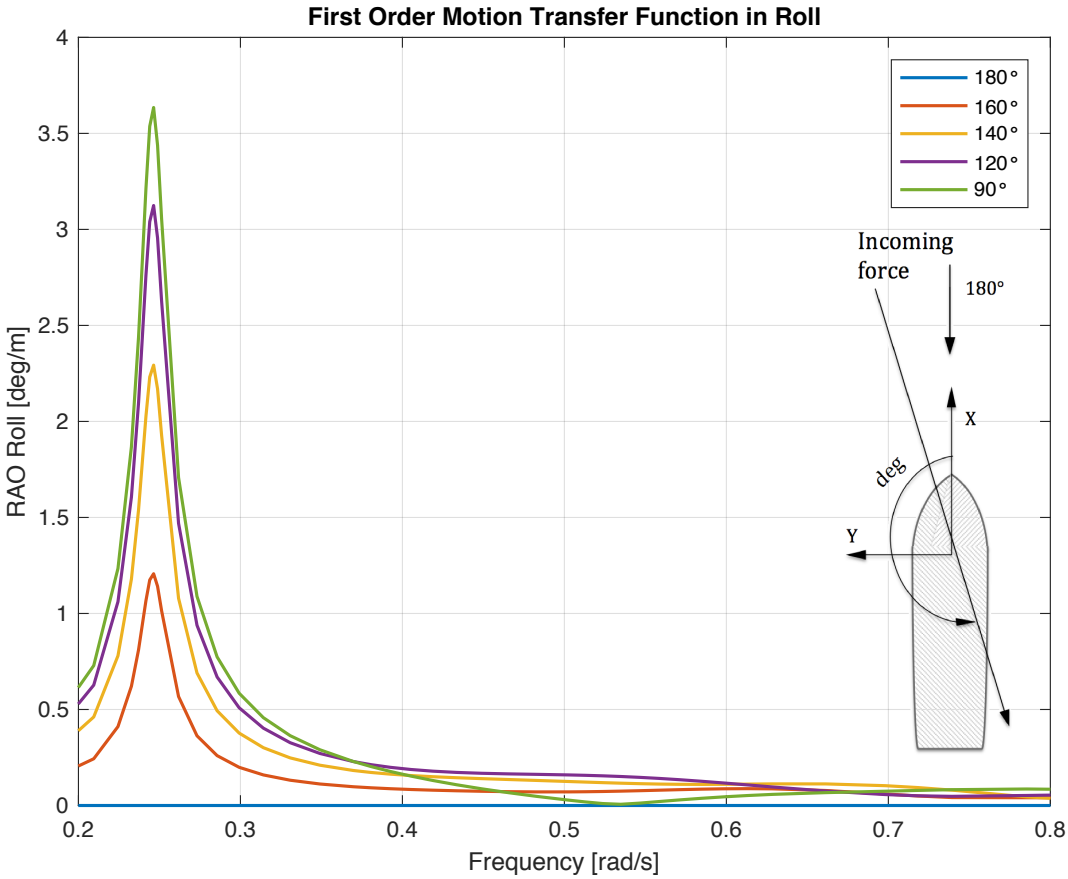

Figure 5.21: Motion RAOs in roll for 0-50 degrees relative to the units bow

From Figure 5.21 it's evident that the natural period in roll in ballast condition is approximately $\frac{2\pi}{0.25 rad/s} \approx 25$ s. This coincides well with Table 5.1, where the ballast natural period in roll is specified as 25.5s. In addition, one can see that the beam sea provides a considerable amplification to the roll motion, in contrast to head sea that does not affect the ship at all in roll.

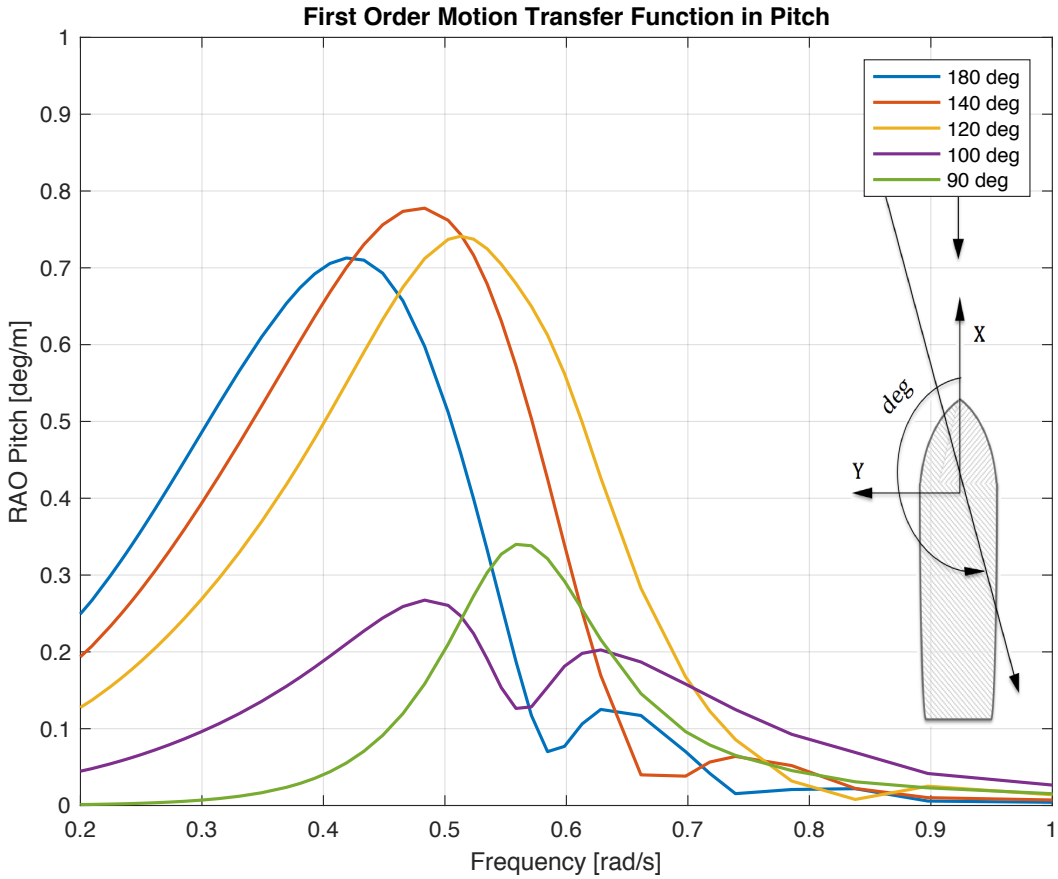

Figure 5.22: Motion RAOs in pitch for 0-50 degrees relative to the units bow

For the motion RAO in pitch, Figure 5.22, the sea state entering 40° relative to the bow, i.e. 140° in the SIMO definition, provides the highest amplification of the vessels rotation in pitch. At a frequency of ≈ 0.55 rad/s, resulting in a natural period of 11.4 s, this is in agreement with the natural period in pitch from Table 5.1 at 11.0 s.

As mentioned for the wave drift force coefficient in heave, the peaks correspond to the peaks for the motion RAOs in heave and pitch, seen from results this is true.

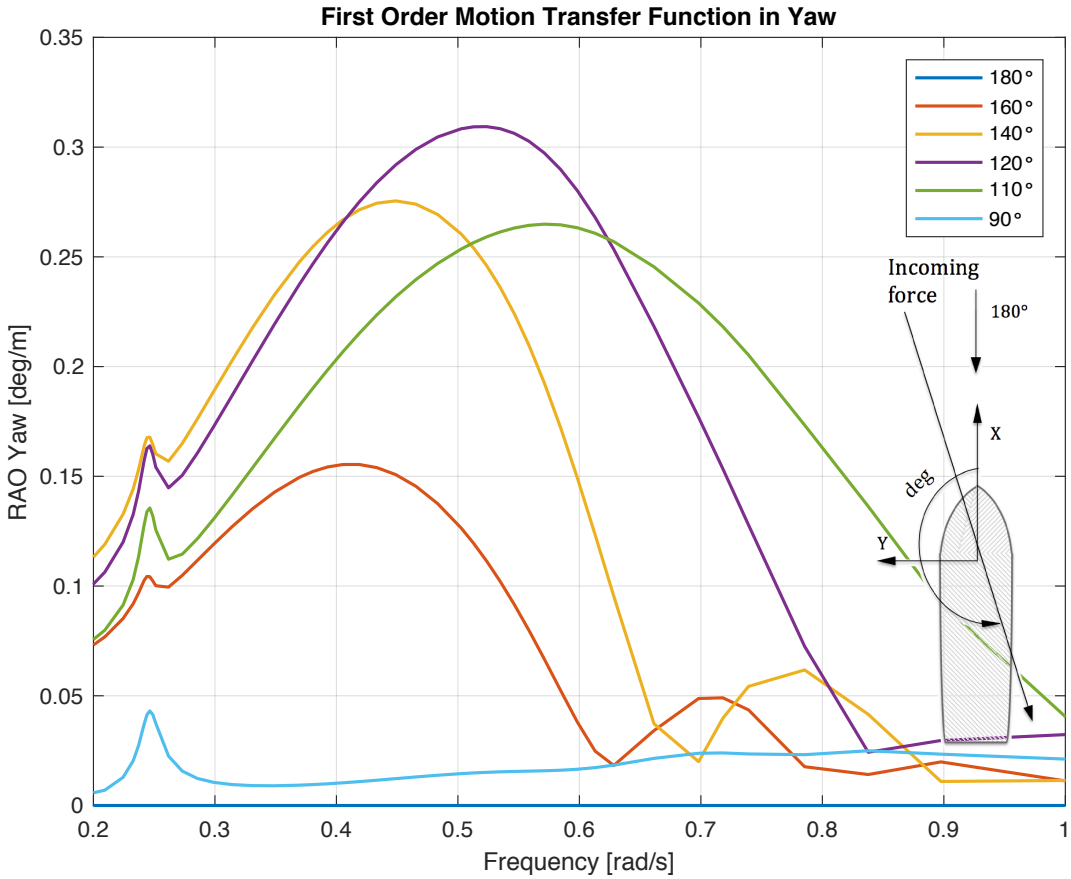

Figure 5.23: Motion RAOs in yaw for 0-50 degrees relative to the units bow

The yaw motion RAO is quite small, with the largest amplification at 0.3 deg/m seen from Figure 5.23. This implies that the motion of the sea state is larger than the motions of the vessel. The sea states coming in diagonally on the vessel's bow gives the highest motion RAO in yaw at periods between $10-15$s.

In total, the motion RAOs for the FPSO have reasonable values and are considered valid.

5.2.4 Free-Decay Test

A free-decay test provides information about the natural frequencies (or resonance periods), added mass and damping of the dynamic system. The parameters of interest are the natural period and damping. Before the test can be conducted, certain demands must be fulfilled; no other motions can be excited, the moorings must be slack and the ship should lie on an even

keel in prior to the test (Lund 2011). Slack tanks should not be present, but if they are, the free surface effect must be taken into account. In this way the measured motions are purely from the vessel's decay. If the test is performed in real life, additional requirements must be made.

In SIMO decay tests in surge and sway were executed in SIMO for the numerical model. The test itself was performed by disabling the mooring system, applying a known load on the vessel in one DOF at a time and releasing the vessel to measure the decay.

The displacement as a function of time in surge and sway are shown in Figure 5.24 and 5.25 respectively. The plot begins at the time when the force was removed. Visually, for both motions, the displacement decays smoothly, therefore the system is considered stable in surge and sway.

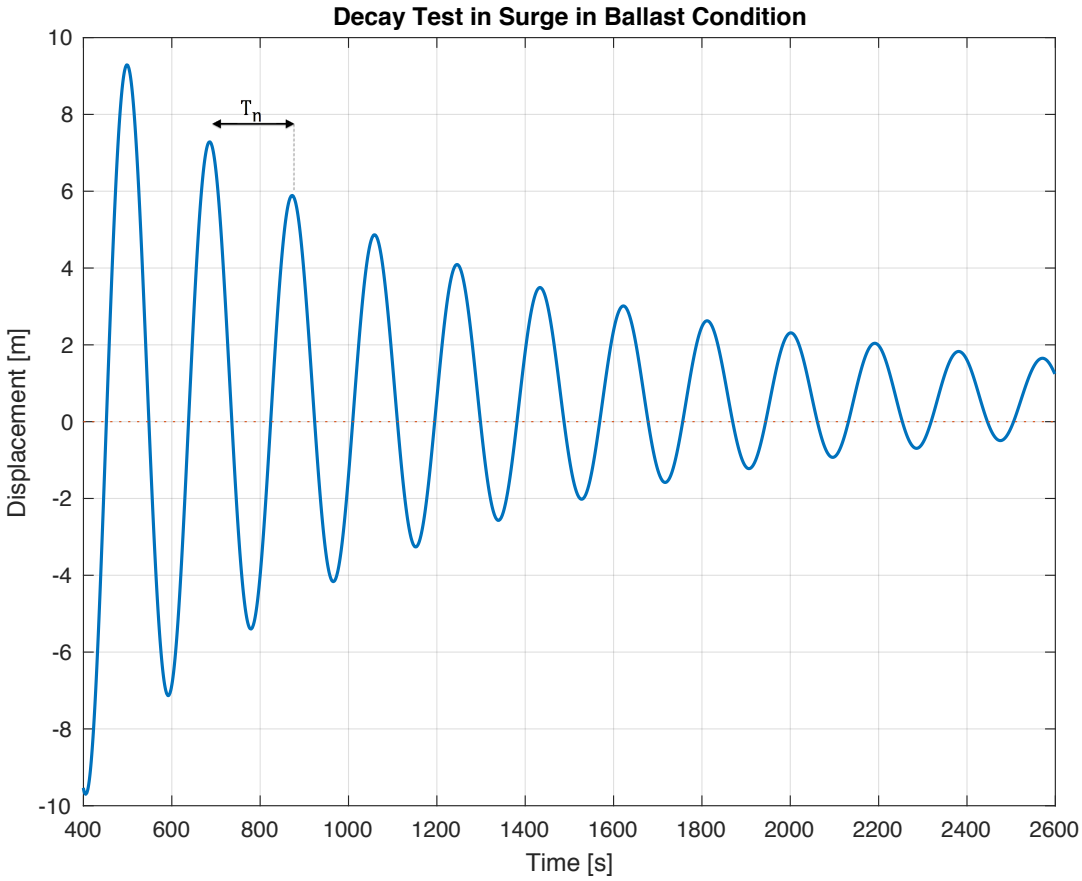

Figure 5.24: Free-decay test in surge in ballast condition

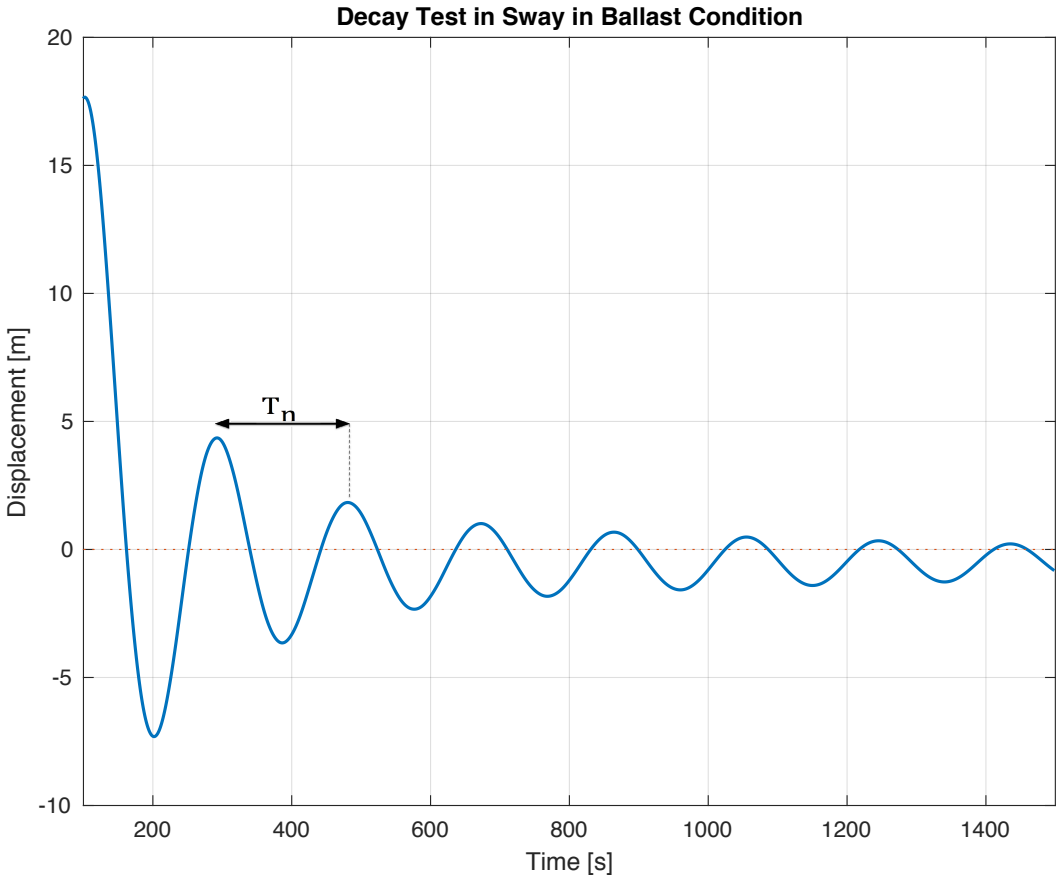

Figure 5.25: Free-decay test in sway in ballast condition

The time between every instance the ship returns to the starting position, or distance between two equivalent points on the decay graph, is the systems natural period, T_n. In this case, seen from Figure 5.24 and 5.25, the natural period is defined as the distance between two peaks. The critical damping of the system can be derived from the natural period by simple calculations, expressed as

$$c_{cr} = 2 \cdot m \cdot \omega_0 = 2 \cdot (M + A) \cdot \frac{1}{T_n} \tag{5.10}$$

where c_{cr} is the critical damping, m is the total mass, M is the structural mass of the vessel, A is the added mass in the DOF of interest, ω_0 is the eigenfrequency and T_n is the natural period.

The damping can be found from the decay curve and the critical damping. Based on the 10 first amplitudes, linearising the damping, and assuming that x_i and x_{i+1} are two succeeding

amplitudes, the logarithmic decrement is defined as (Steen 2014)

$$\Lambda = ln\frac{x_i}{x_{i+1}} \tag{5.11}$$

For low damping ratios, typically $\xi < 0.2$, the general relation between the logarithmic decrement and damping ratio can be approximated to

$$\Lambda \simeq 2\pi\xi \quad \Rightarrow \quad \xi = \frac{\Lambda}{2\pi} \tag{5.12}$$

It should be noted that this is only valid for the damping in surge, while the damping ratio in sway are too large for this approximation. Then the damping in surge can be found from the relation between the damping and critical damping

$$\xi = \frac{c}{c_{cr}} \quad \Rightarrow \quad c = c_{cr} \cdot \xi \tag{5.13}$$

The natural period, damping from SIMO, critical damping and damping ratio for surge and sway are listed in Table 5.7.

Table 5.7: Results from free-decay test in surge and sway

	Natural Damping	**Damping**	**Critical Damping**	**Damping Ratio**
	T_n [s]	$c\left[\frac{kNs}{m}\right]$	$c_{cr}\left[\frac{kNs}{m}\right]$	$\xi \cdot 100$ [%]
Surge	187.1	276	2406	11.5
Sway	190.6	-	-	-

The damping ratio should be around $10-40\%$ for the surge motion, hence the damping in surge is within reasonable values. By comparing Figure 5.24 and 5.25, the sway decays with a much steeper slope than the decay in surge.

The decay in sway, Figure 5.24, decays with a much steeper slope than the decay in surge, Figure 5.25.

The damping from the free-decay test will be extremely under-predicted since the risers and moorings are not present during the test. The slender system would, in addition to their weight, induce drag forces in the water when the vessel is excited. Furthermore, the decay test is per-

formed in quiet water which is another error source when finding the damping.

5.2.5 Static Pull-Out Test

A static pull-out test can be used to document the mooring system. The system restoring curves and line characteristics can be derived from the results. In addition, the slope of the tangent to the restoring curve is defined as the linear stiffness, hence the natural period can be calculated by use of the following equation found in Faltinsen (1990)

$$T_{n,i} = 2\pi\left(\frac{M_{ii} + A_{ii}}{C_{ii}}\right) \tag{5.14}$$

where M is the mass, A and C is the added mass and stiffness in the degree of freedom in question respectively.

The model was gradually displaced from the equilibrium position in the direction of interest, by steps of approximately 20m, and for each offset a static analysis was performed. In this way the restoring force curves for the mooring system were obtained for surge, sway and in-line direction. The total offset is ≈ 30% of L_{pp}, which equals 80m.

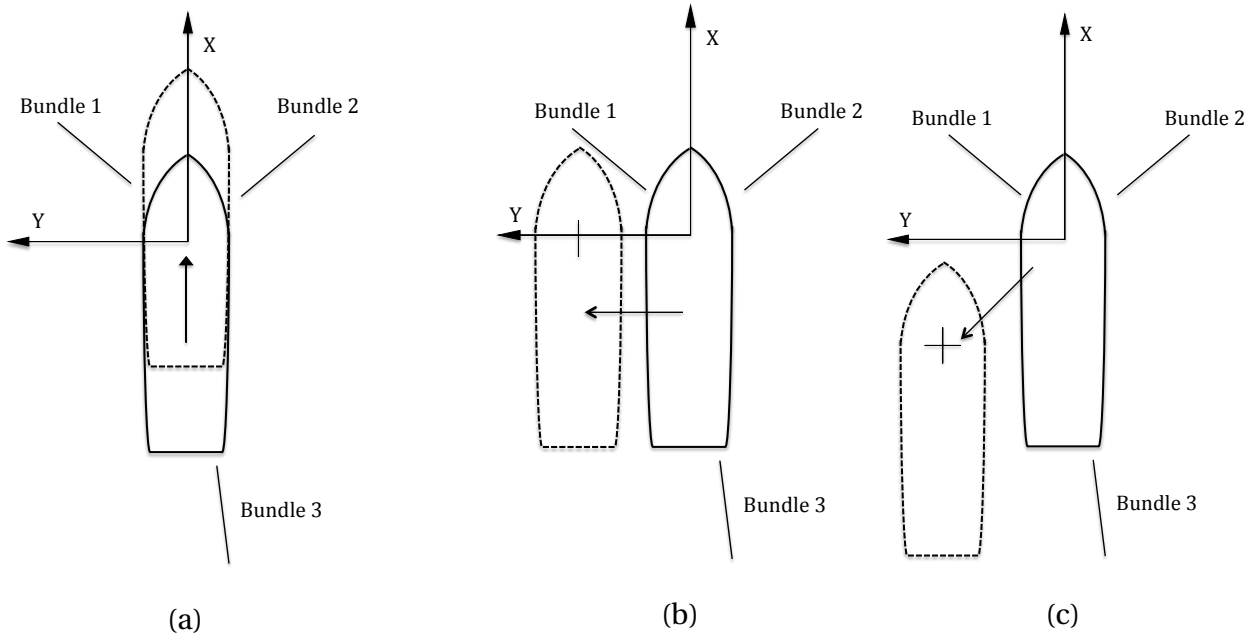

Figure 5.26: Illustration of the pullout direction in surge, sway and in-line denoted a), b) and c) respectively

The restoring curve in surge was obtained by moving the vessel in the positive x-direction, as seen from Figure 5.26 a). In sway, the restoring force was obtained by moving the vessel in the positive y-direction, illustrated in Figure 5.26 b). In addition, a pull-out test in the center of bundle 2 was conducted. This is directly in mooring line number 8, in order to obtain the inline restoring force of the system. As illustrated in Figure 5.26 c), the pull-out was performed in the negative x-direction and positive y-direction. The three restoring curves are presented in Figure 5.27.

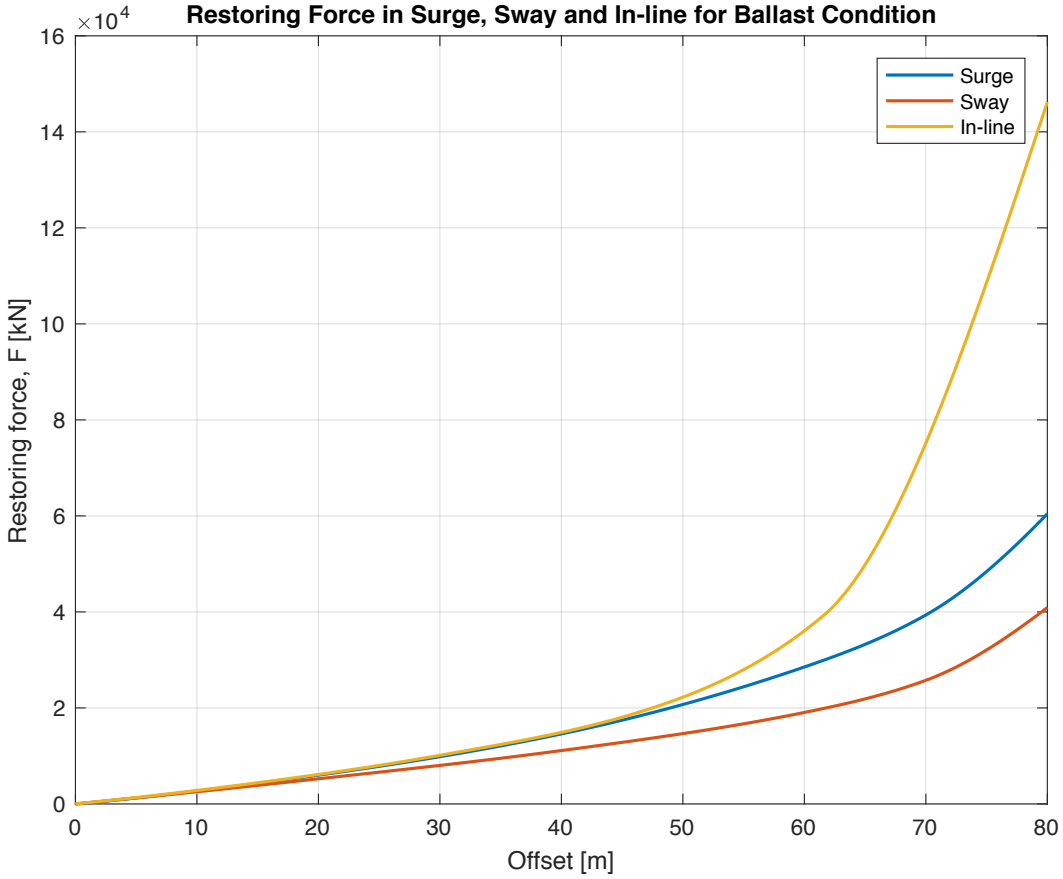

Figure 5.27: Comparison of the surge, sway and in-line restoring forces in ballast condition

Compared with the restoring curves in surge and sway, the inline restoring curve has a drastic increase after a displacement of 60m. Sway has clearly the smallest restoring force. In other words, the force required to move the vessel in sway is smaller then for the two other direction. Hence the sway direction is not as rigid compared to surge and in-line. The in-line restoring force is very rigid at an offset of 70-80m. Most likely, the FPSO will stay within an offset up to

50-60m.

The stiffness and natural period from the restoring curve in surge and sway were calculated in MatLab. The slope of the tangent to the restoring curve is defined as the linearised stiffness, C_{lin}, illustrated in Figure 5.28. From the restoring curves it's clear that the behaviour of the stiffness is highly non-linear for increasing offset, due to the non-linearities of the restoring curve. The natural period is calculated by Equation 5.14.

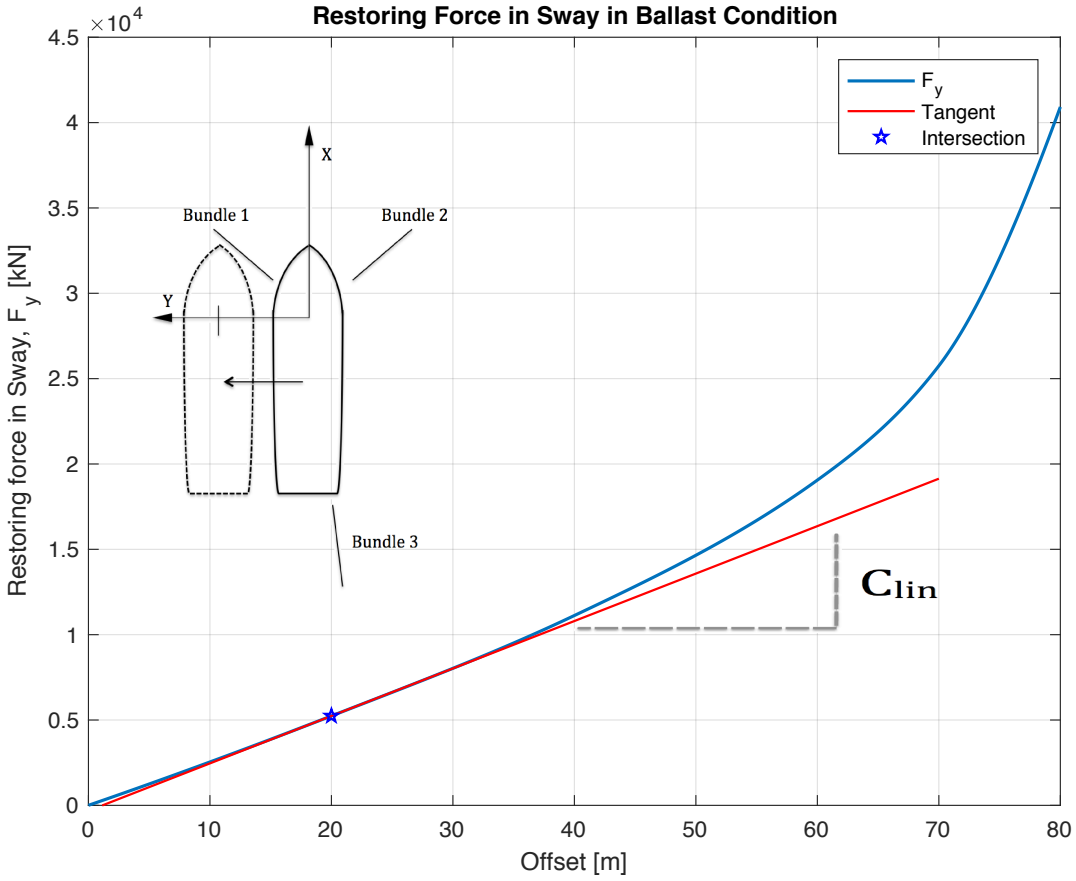

Figure 5.28: Restoring force in sway illustrating the tangent and linearized stiffness

In order to compare the natural periods calculated from restoring curves with the natural periods found from decay tests, the stiffness must be calculated from approximately the same offset as decay displacement. The decay displacement is approximately 10 m and 18 m in surge and sway respectively, hence the tangent intersection is approximately at these offsets. The calculated stiffness and natural period from the restoring curves for surge and sway are pre-

sented in Table 5.8. The natural periods from the free-decay test are 187s and 191s for surge and sway respectively, referring to Table 5.7. From this, the restoring natural periods are around 9% smaller in surge and 3% larger in sway, which means the results coincides quite well. Hence, the natural periods and linear stiffness are considered as reasonable.

Table 5.8: Natural period and stiffness in surge and sway

	Natural Period	**Stiffness**
	T_n [s]	C_{lin} [kN]
Surge	172	300
Sway	196	278

Line Characteristic

The line characteristic for mooring line 8 in bundle 2 is shown in Figure 5.29 and describes the flexibility, thus the relation between the tension in the top of the line and the offset of the system. Both the axial and horizontal tensions are plotted. The initial value of the axial tension is the axial pretension of the line, at 2209 kN.

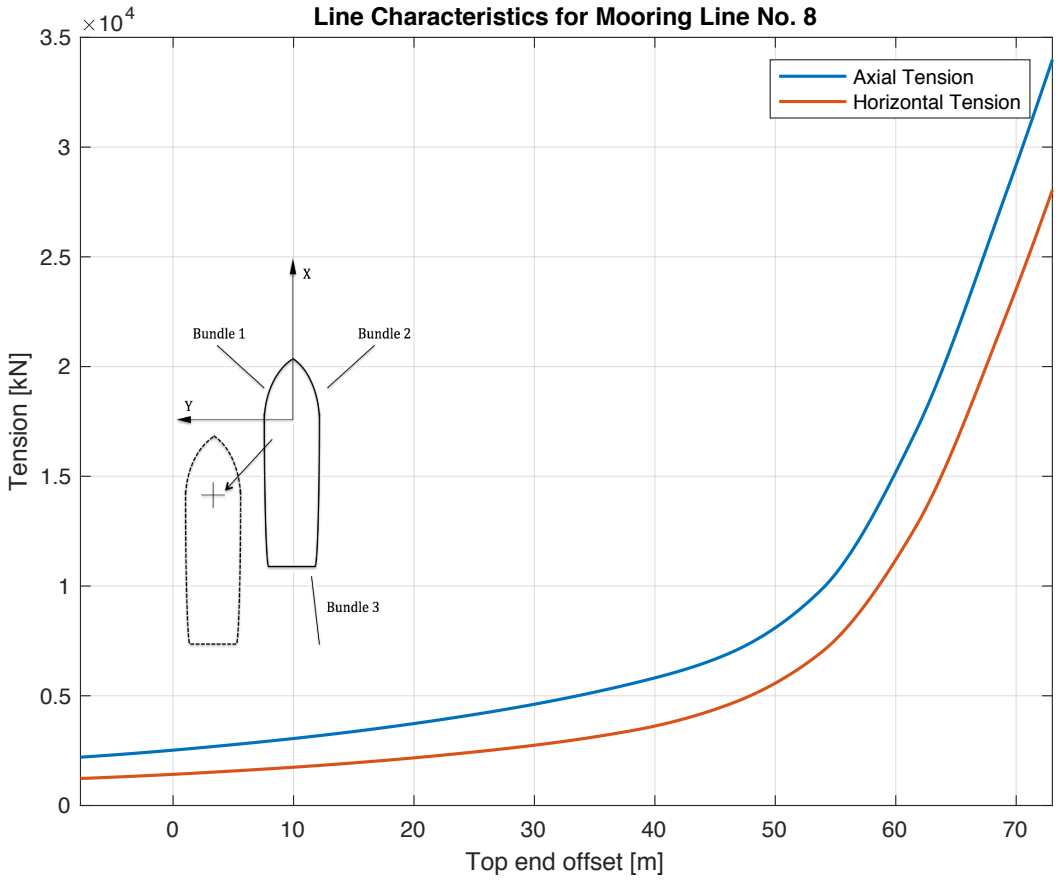

Figure 5.29: Line characteristics for mooring line number 8

Figure 5.30 illustrates how mooring line 8 behaves during the pull-out test at different offsets, where the upper and lower end represents the fairlead and the anchor point respectively. At the final step, step 5, the mooring line is almost fully stretched. The length of the free hanging line is now equal to the line length, hence the anchor is exposed to vertical loadings.

The restoring curves and values obtained from the different pull-out tests are within reasonable values, hence the performance of the system is therefore considered valid.

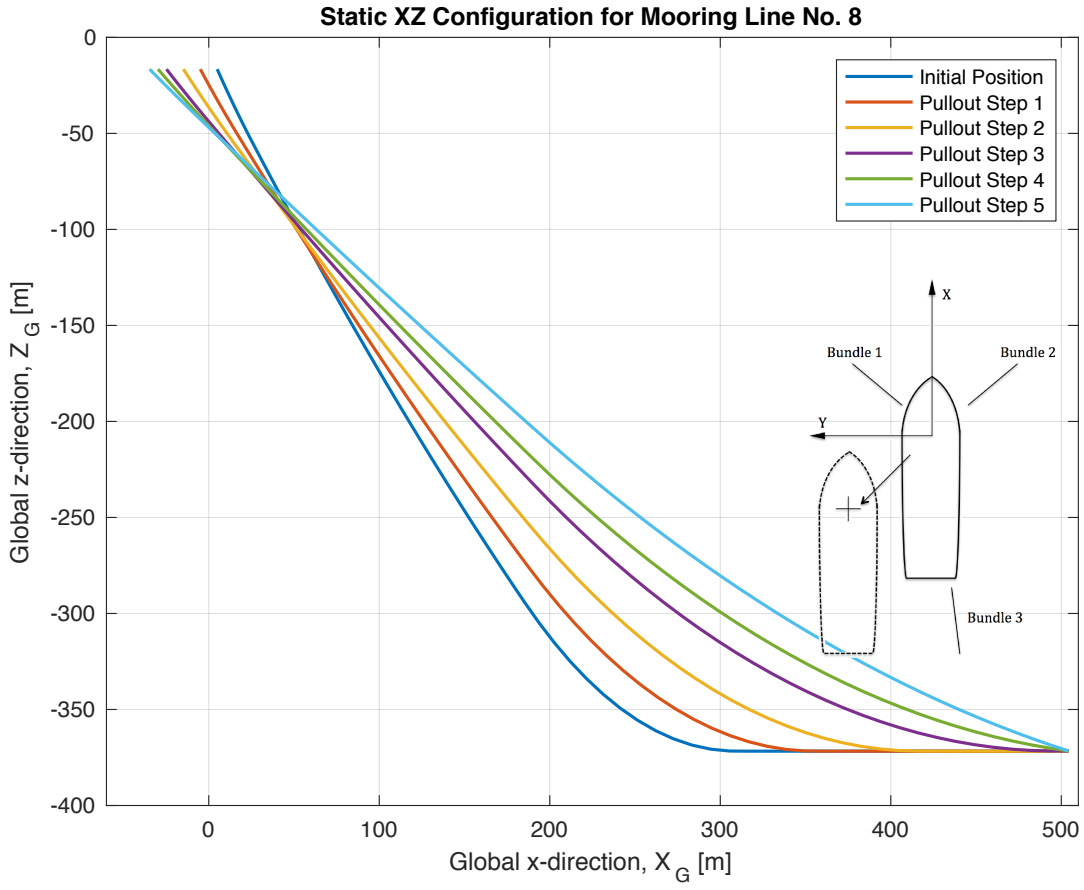

Figure 5.30: Vertical projection of mooring line 8 during pull-out

5.3 Environmental Conditions in the Barents Sea

5.3.1 Definition of Waves, Wind and Current

In order to gain a better insight in which sea states that are important for the mooring system of the FPSO, several weather conditions must be analysed. The environmental effects to be applied in mooring line response calculations for the ULS and ALS shall include the most unfavourable combination of wave, wind and current with a return period of at least 100 years for the combination (DNV GL 2015). Unfavourable conditions are those who leads to higher mooring loads. According to DNV GL (2015) it is usually acceptable in the Norwegian sector, and some other locations, to apply a combination of wind and waves with 100-year return periods together with current with a 10-year return period. This combination becomes less acceptable as load-effects

arising from current become more important.

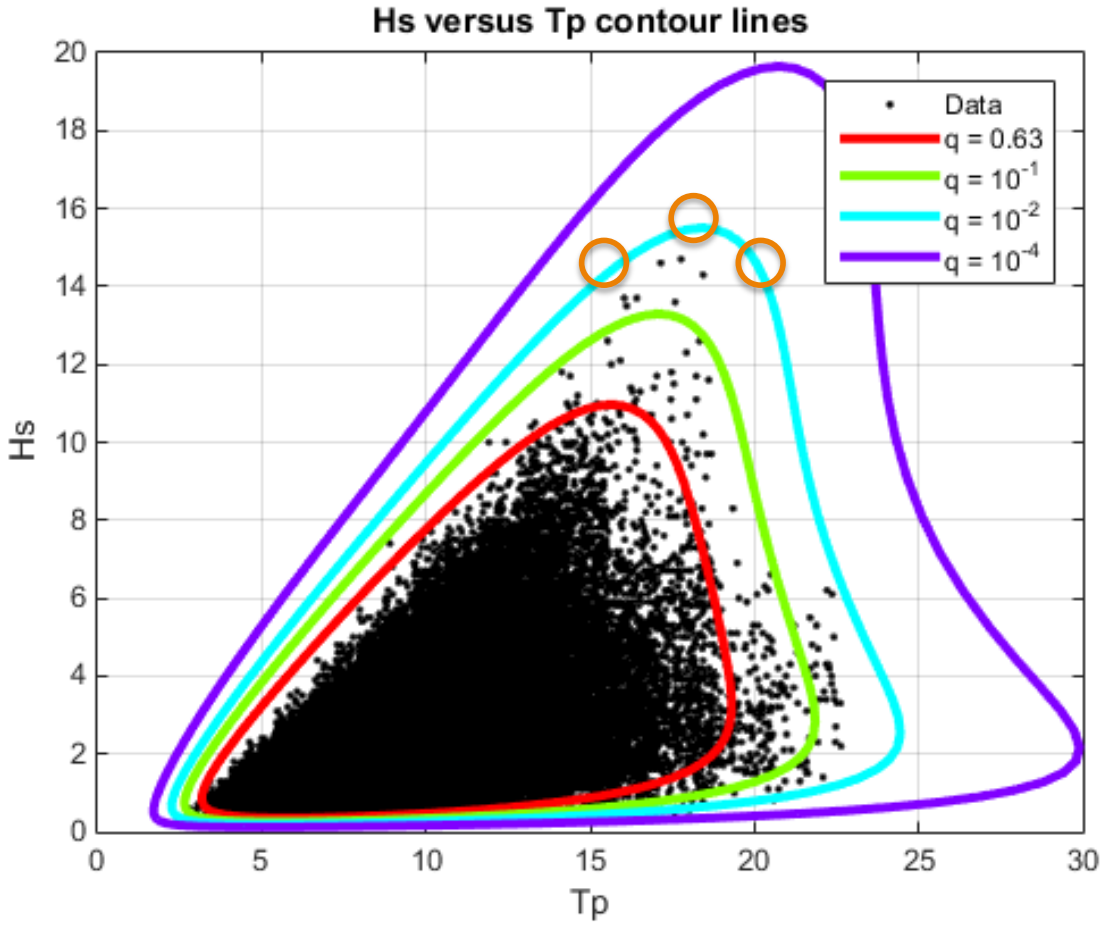

Figure 5.31: 1,100 and 10 000-year contour lines in the H_s-T_P plane for omnidirectional waves, (Dezecot & Eik 2016). Sea state duration of 3 hours.

The environmental conditions for the barents sea are based on the information given in *Metaocean Design Basis for the Barents Sea* written by Dezecot & Eik (2016). The 100-year contour line in Figure 5.31 is used to find the wave condition by examining the peak point on the contour line. In addition, the left and right side of the peak point are tested, as illustrated on the contour line. The wind and current are assumed to be constant in the three different wave states. The wind speed chosen is defined as omni-directional, for 1-hour wind speed 10m above the sea level at the barents sea field. The current speed is defined as omni-directional at 13m water depth at the barents sea field. The duration of extreme event is 10 minutes. Since the current velocity is very uncertain at the sea surface, and the ship has a draught at 17.1 m in ballast condition, the velocity at 13m water depth was chosen. In Appendix B the information for

waves, wind and current lies as attachments. The weather conditions are listed in Table 5.9.

Table 5.9: Definition of the 100-year conditions analysed in SIMO (Dezecot & Eik 2016)

	Waves (100 year)		**Wind Velocity**	**Current Velocity**
	H_S [m]	T_P [s]	**(100 year) [m/s]**	**(10 year) [m/s]**
Env 1	14.0	15.1		
Env 2	15.5	18.5	32.5	1.11
Env 3	14.0	20.4		

5.3.2 Direction of Waves, Wind and Current

There are two different ways of applying the loads if site specific data is not available (DNV GL 2015), which is the collinear and non-collinear environment. The *Collinear environment* is defined as when the wind, waves and current acts in the same direction. The *Non-collinear (spread) environment* is defined as waves coming directly towards the unit's bow (i.e. 0° relative to the unit's bow), wind incoming 30° relative to the waves and current 45° relative to the waves, as shown in Figure 5.32. This can be written as

$$\alpha_{wi} - \alpha_{wa} = 30^\circ \quad \text{and} \quad \alpha_{cu} - \alpha_{wa} = 45^\circ \tag{5.15}$$

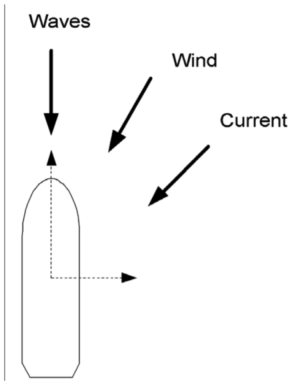

Figure 5.32: Directions of wind, waves and current for a non-collinear environment (DNV GL 2015)

There are in total seven weather parameters that must be defined for each environmental

condition; H_S, T_P, α_{wa}, V_{wi}, α_{wi}, V_{cu} and α_{cu}.

For all units both in-line and in-between directions shall be analysed according to DNV GL (2015). In this thesis three directional distributions are considered, one in-line and two in-between definitions.

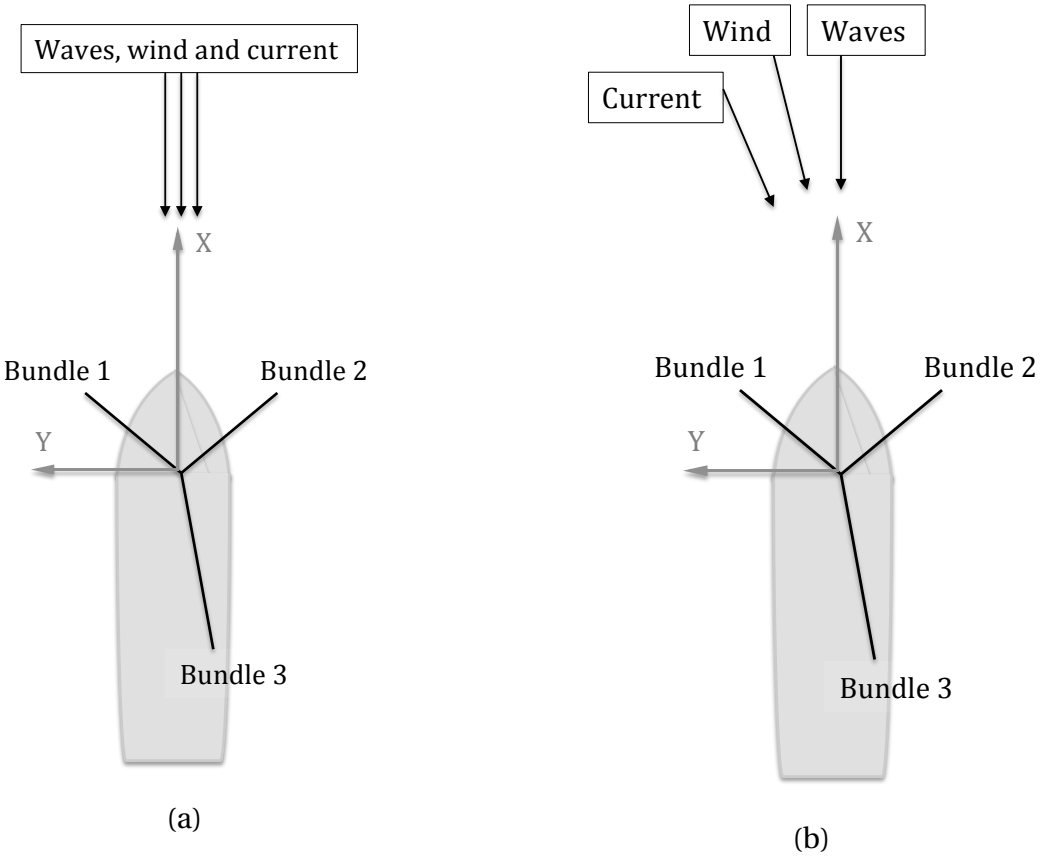

Figure 5.33: Definitions of in-between collinear and spread environment to the left (a) and right (b), respectively

The in-between direction is located between bundle 1 and bundle 2, as shown in Figure 5.33. It should be noted that this is directly towards a riser cluster. The DNV GL spread definition is used in Figure 5.33 (b).

The in-line directional distribution considered is applied with collinear environment traveling towards the centre of bundle 2. This is also the bundle with the smallest mooring line length.

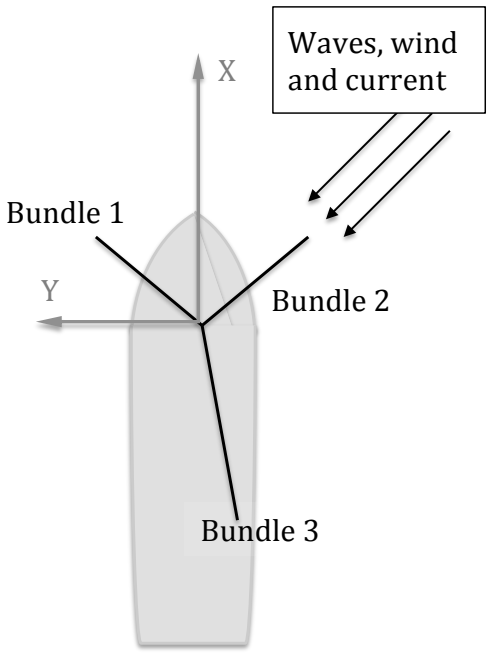

Figure 5.34: Illustration of in-line collinear environment

5.4 Riser Contribution

In SIMO, dynamic analyses for the FPSO with the riser system both present and disabled were performed for in-between collinear condition with three different environments. All simulations has the same wind and wave seeds, and a duration of 3 hours. When studying the mean and standard deviation of the responses it's representable to use only one simulation as comparison foundation. The extreme responses, on the other hand, are not representable with one simulation, then a number of simulations must be performed. This is not done for the riser considerations.

The main results and comparisons done in Excel are to be found in Appendix C.

5.4.1 Vessel Offset Motion

The offset is calculated as the square root of the x- and y-motions of the vessel. The mean offset with risers present is almost 15% larger for all environments for the system with risers compared to the system without risers, found from Table 5.10. This indicates that the system including

risers are located higher up on the restoring curve, hence the system is more rigid than the system without risers.

Table 5.10: Mean offset for the three environments for the in-between collinear condition

Mean offset	*Env 1*	*Env 2*	*Env 3*
Risers disabled	21.6	20.4	20.1
Risers included	25.1	24.0	23.6

In order to get a better insight in the motions, the contributions from wave- and low frequent motions are evaluated in Figure 5.35.

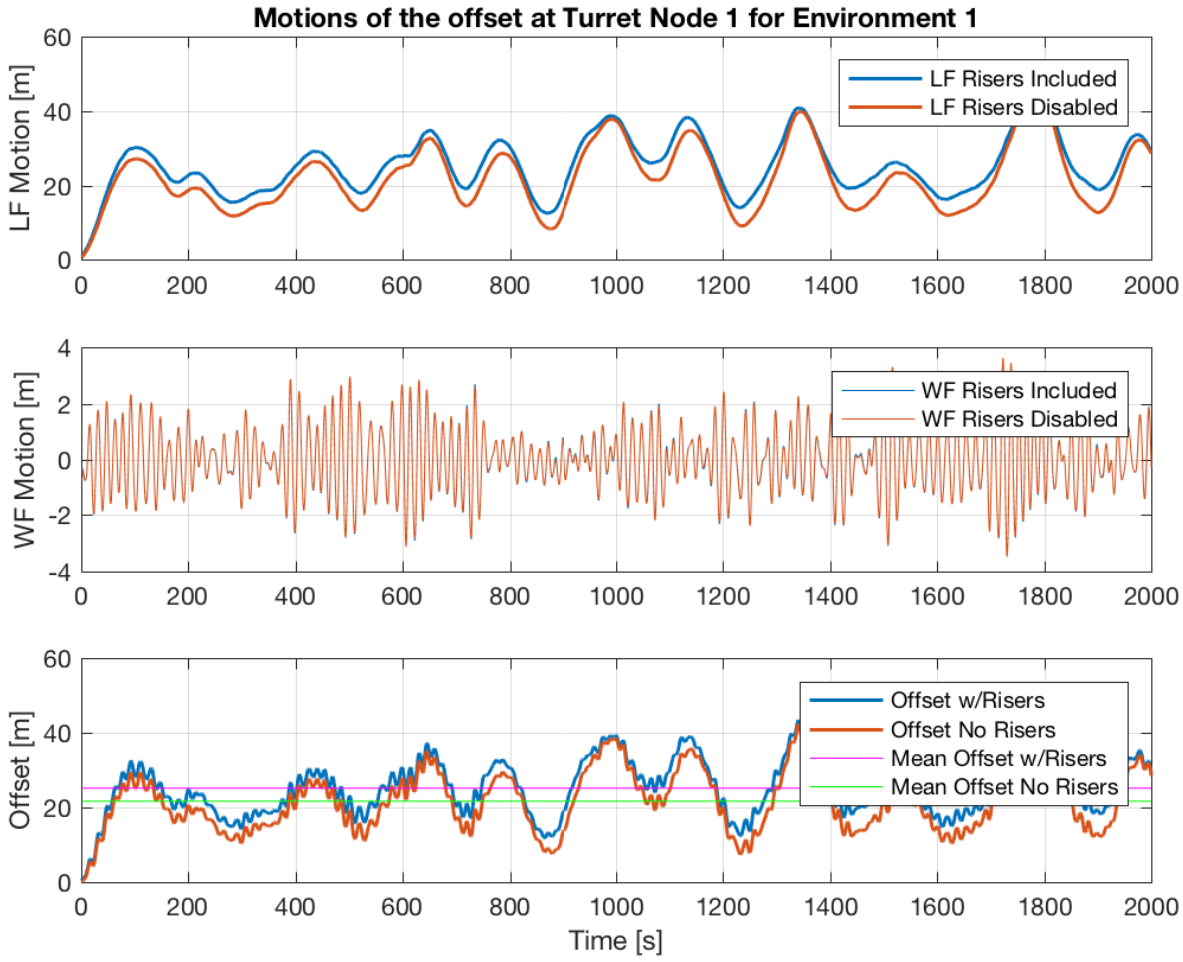

Figure 5.35: An excerption of the offset from the 3-hour time domain analysis for Env 1, comparing the LF and WF motions.

The WF and LF motions for environment 1 are derived by low-pass filtering and band-pass filtering in SIMO. From Figure 5.35 it can be seen that the WF motion for the system with and without risers are exactly the same, thus the WF motion is not affected by the risers. The LF motion on the other hand, has overall higher LF motions when the risers are included. By looking at the energy spectrum plotted in Figure 5.36, the WF motion energy spectrum for the two systems are naturally equal. While the LF motion for the system without risers has a higher energy spectrum compared with the system including risers. In other words this means that the risers induces a damping effect on the systems LF motions.

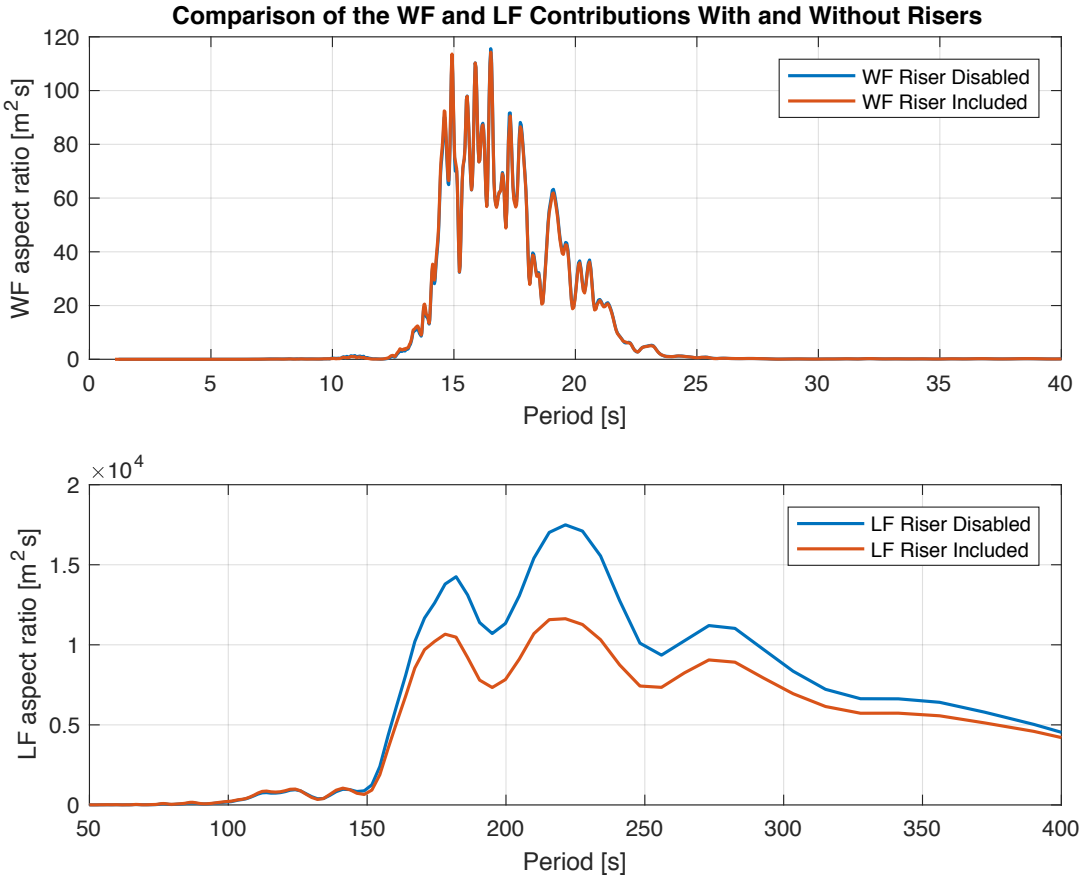

Figure 5.36: Sample density energy spectrum for LF and WF motions with and without risers present for 3-hour dynamic analysis for Environment 1.

Table 5.11: Offset total standard deviation for the three environments with or without risers

Offset total std	***Env 1***	***Env 2***	***Env 3***
Risers disabled	8.1	7.4	7.1
Risers included	7.3	6.6	6.4

When looking at the total offset standard deviation, presented in Table 5.11, it is around 10% larger for the system without risers compared with risers included. In Table 5.12 the WF and LF standard deviation for env 1 are listed. The WF std is exactly the same, which is expected since the energy spectrum is exactly the same for the two systems. On the contrary, the LF standard deviation for the system without risers is approximately 11% larger compared to the system including the risers, both for Env 1.

Table 5.12: WF and LF standard deviations from the energy spectrum for Env 1

Env 1	***WF std***	***LF std***
Risers disabled	1.3	7.9
Risers included	1.3	7.0

Considering the equation for the standard deviation for the LF motions, in case of small damping this can, according to Faltinsen (1990), be approximated to

$$\sigma_{X,LF} \simeq \sqrt{\frac{\pi \cdot S_{F,LF}(\omega_0, LF)}{2 \cdot B_{LF} C_{LF}}} \tag{5.16}$$

where $S_{F,LF}(\mu)$ is the spectral density of the low frequency part, B_{LF} and C_{LF} represents the low frequency damping and stiffness respectively. By small damping it is meant small relative to the critical damping, given in Eq. 5.10, which is confirmed small in the results from decay test.

By studying the formula for the standard deviation, it is evident that the standard deviation for the motion including the risers becomes smaller since the damping and stiffness term becomes larger. For the system without risers it's exactly opposite.

Overall, the system with risers has a larger mean offset but smaller LF motions than the system without risers, the WF motions are equal for the two systems. Looking at the total motion the two systems can provide the same maximum offset, only with different offset compositions.

The total offset can be expressed as

$$x_{TOT} = x_{max} = \overline{x} + max \begin{cases} x_{LF}^{max} + x_{WF}^{sig} \\ x_{LF}^{sig} + x_{WF}^{max} \end{cases} \tag{5.17}$$

where $\overline{x}$ is the mean offset, and the significant values are found by

$$x_{LF}^{sig} = 2 \cdot \sigma_{x,LF} \quad \text{and} \quad x_{WF}^{sig} = 2 \cdot \sigma_{x,WF} \tag{5.18}$$

where σ_x is the standard deviation of the response spectrum and is given from the area of the spectrum or as defined in Eq. 5.16 for the LF response.

Since only one simulation for the each of the three environments are performed, it is not a representative foundation to discuss the extreme value response as mentioned before. However, for the three environments the maximum offset for the systems with risers are found to be a 2-3% larger than without risers. This gives only an indication that the overall offset is quite similar, but to be certain several simulations must be performed.

It should be noted once again that the environment is applied directly into a riser cluster, with a collinear distribution. The incoming direction and spreading of the waves, wind and current may affect the importance of the risers. This is not considered in this thesis.

5.4.2 Top End Tension

The risers absorb environmental loads, in particular current, which affects the offset. Consequently, the leeward mooring lines experiences less loading when the risers are present compared to the system without risers. This can be seen from Figure 5.37 where the riser contribution for the mean axial tension for all mooring lines in environment 1 are compared.

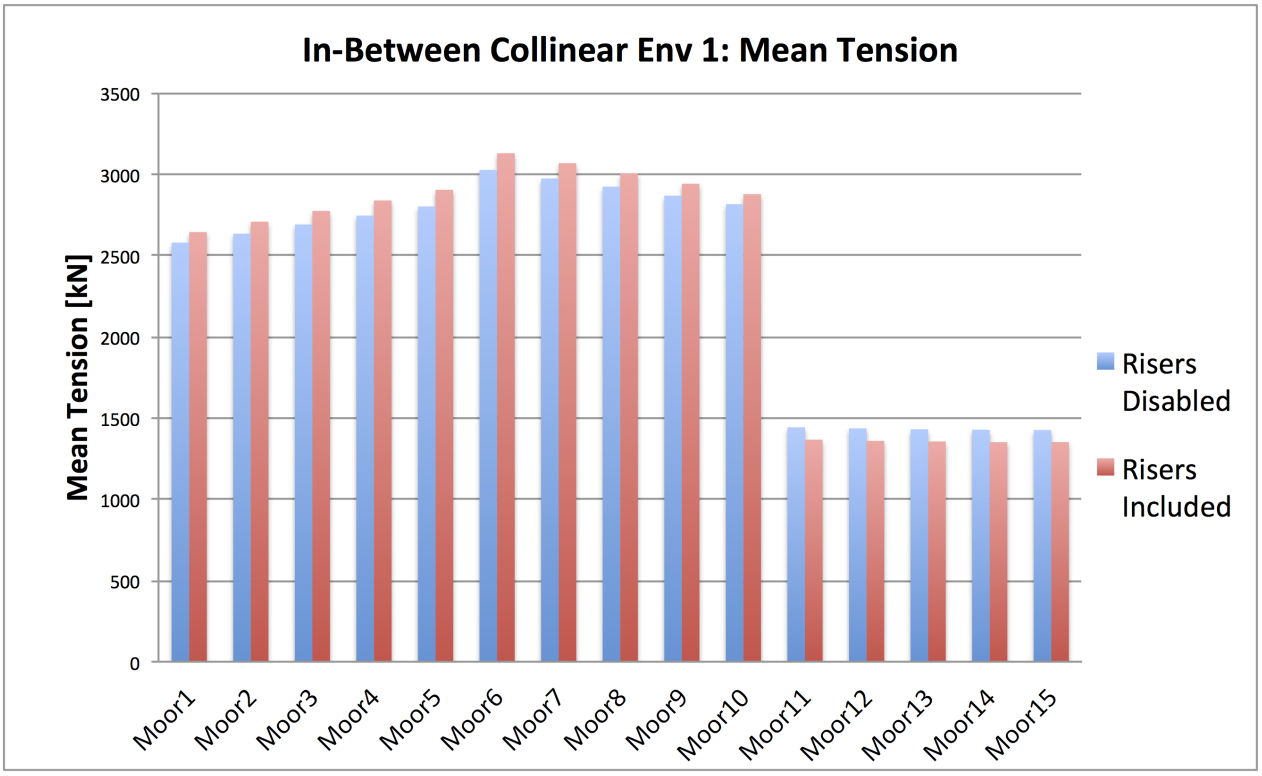

Figure 5.37: Comparison of the axial mean tension in env 1 for all mooring lines, with or without the riser system present. Bundle 1: Mooring 1 - 5, Bundle 2: Mooring 6 - 10, Bundle 3: Mooring 11 - 15.

It can be observed from the histogram that the risers provide a slightly higher mean tension for the moorings in bundle 1 and 2, while bundle 3 has a somewhat smaller mean tension. By calculation, the system with risers have 2-4% higher mean tension for bundle 1 and 2, which are the windward bundles for in-between collinear condition. Furthermore the mean tension in bundle 3, the leeward bundle, is $\approx 6\%$ smaller for the system including the risers.

5.4.3 Dynamic Turret Support Forces

The simplified vertical force at the bogies, F_Z^{BOG} found from Eq. 5.2, depends on the contribution from inertia and fairlead. The inertia term, $(M+A)\cdot\ddot{x}$, is practically unaffected by the risers. It's of interest to understand how much the risers contributes to the vertical force at fairlead F_Z^{CT}.

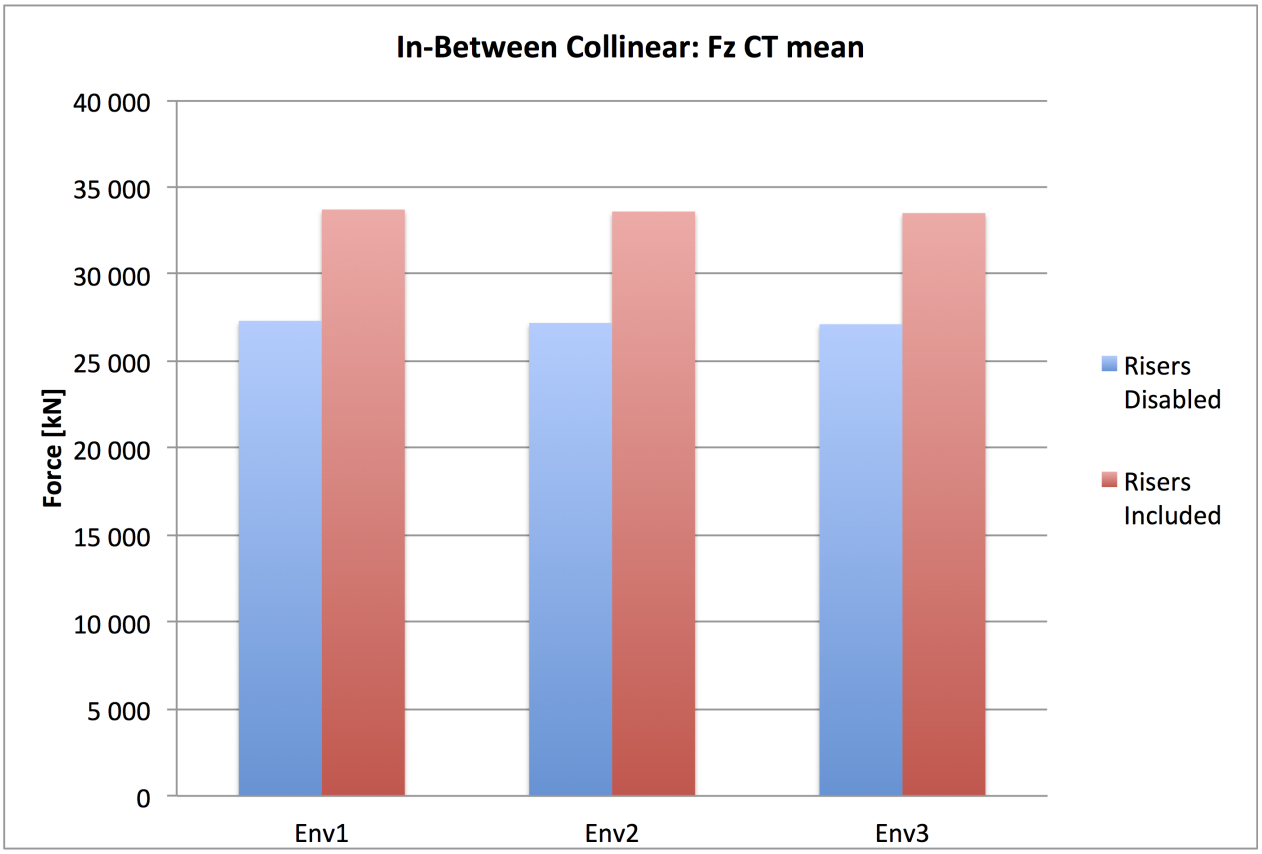

Figure 5.38: Comparison of the mean vertical force at fairlead with and without risers for the different environments

From Figure 5.38 it's clear that the system including risers have a higher vertical mean force at CT. Table 5.13 shows the results for the dynamic turret support forces in env 1. For the three environments the force is approximately 20 % larger for the system with risers compared to the system without risers. In addition, the standard deviation for the vertical mean force at fairlead is approximately 8% larger for the system including risers. Comparing the total force at bogies, F_Z^{BOG}, naturally also gives a deviation of around 20% since the inertia contribution is equal for the two cases. The standard deviation however, is $\approx$ 4% smaller for the system with risers compared to the system without risers. This can be explained as for the offset, that the risers induced higher damping and restoring terms to the system.

Table 5.13: The dynamic turret support forces for env 1 with and without risers

Env 1	$F^{RAD}_{X,mean}$ *[kN]*	$F^{BOG}_{Z,mean}$ *[kN]*	M^{BOG}_{mean} *[kNm]*
Risers disabled	3953	27316	126140
Risers included	4409	33714	160330

When comparing the horizontal force at the radial wheels, F^{RAD}_X, the risers has a contribution of approximately 11% for the mean force while the standard deviation is approximately the same compared to the system without risers. The mean moment at bogies, M^{BOG}, is about 22% larger when including the risers. Similarly to the radial force, the standard deviation is approximately the same for the two cases.

5.4.4 Riser Conclusion

In this study, the riser contribution to the mean vertical bogie force and mean offset is approximately 20% and 10% respectively. The mean axial tension at fairlead is however, not affected so much, 4% at max. It should be mentioned that riser impact on the extreme responses has not been examined. In conclusion, it is considered as valid to simplify the riser model by disabling the risers in this master thesis. This is due to the extra computational time discussed in the riser description and simplicity of the master thesis. If this was a dimensioning design case for the turret mooring system, the risers must have been included, it is only for simplicity that they are disregarded in the further analyses.

5.5 Number of Simulations

In total 40 simulations were performed for the in-between collinear condition in environment 1. All the simulations have different wind and wave seeds, in this way none of the simulations are equal. From this selection the Gumbel distribution can be used to describe the extreme responses. Then the probability density function (PDF) for the different responses of interest can be derived and plotted. The expectation, variance and 90% fractile for some of the extremes are plotted as a function of the number of simulations, N_{req}. When these variables converge

and have only a small deviation of around 5 – 7%, the number of required simulations in order to provide reliable results can be found.

Based on the equations in Section 4.4, the Gumbel PDF, variance and mean value relations can be calculated. Then, by using the response and its known values, the parameters μ and β can be derived. From the extreme response,x, the Gumbel parameters $Var(x)_{Gumbel}$ and $E(x)_{Gumbel}$ can be found as

$$Std(x) = \sqrt{Var(x)_{Gumbel}} \quad \Rightarrow \quad Var(x)_{Gumbel} = Std(x)^2 \tag{5.19}$$

$$E(x)_{Gumbel} = mean(x) \tag{5.20}$$

Using the Gumbel distribution formulas, and solving for β and μ

$$Var(x)_{Gumbel} = \frac{\pi^2}{6}\beta^2$$

$$\Rightarrow \beta = \sqrt{Var(x)_{Gumbel} \cdot \frac{6}{\pi^2}} = Var(x)_{Gumbel} \cdot \frac{\sqrt{6}}{\pi^2} \tag{5.21}$$

$$E(x)_{Gumbel} = \mu + \beta \cdot \gamma$$

$$\Rightarrow \mu = E(x)_{Gumbel} - \beta \cdot \gamma \tag{5.22}$$

The number of required simulations should be estimated for the response of interest in the analyses. The Gumbel distribution for estimating N_{req} was found from the dynamic turret support forces F_X^{RAD}, F_Z^{BOG} and M^{BOG}. In this case, the offset and the tension parameters could also be used to estimate N_{req}. The number of required simulations may be different by using the tension or other parameters, it is considered as unnecessary to calculate the number of required simulations for all parameters in this case, but the principle remains the same.

As an example, the PDF for the horizontal force at the radial wheels F_X^{RAD}, is shown in Figure 5.39. The rest of the PDFs for the dynamic turret support forces are to be found in Appendix D.

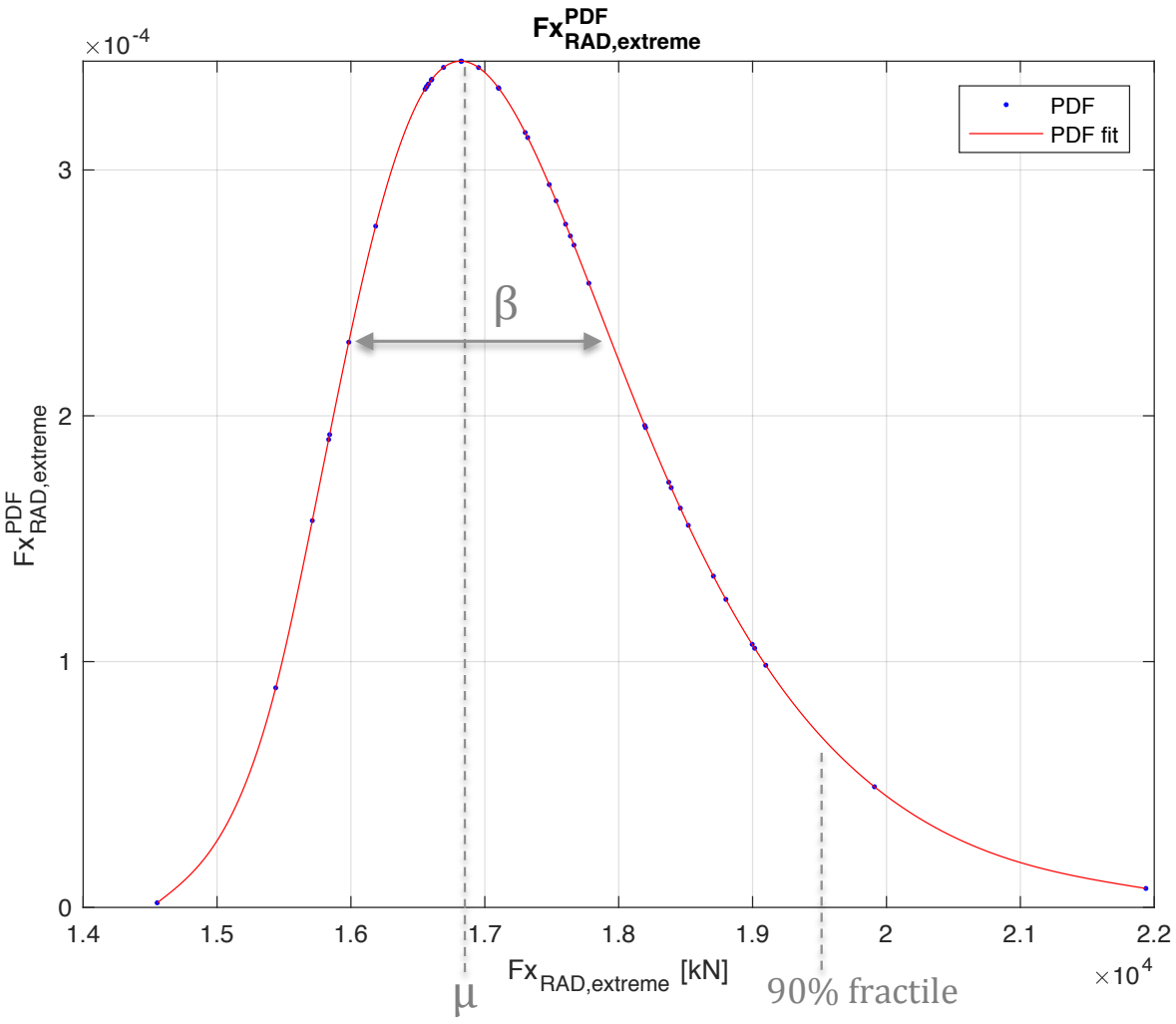

Figure 5.39: The probability density function for F_X^{RAD} based on 40 simulations.

In Figure 5.40 it can be observed that μ converges before β. This is due to that μ is directly associated with the expectation of the response, see Figure 5.39. This means that the mean of the response converges faster than β. Similarly, the 90% fractile is directly connected to the response, and converges quicker than β. Hence, β is the dimensioning parameter when deciding the number of required simulations.

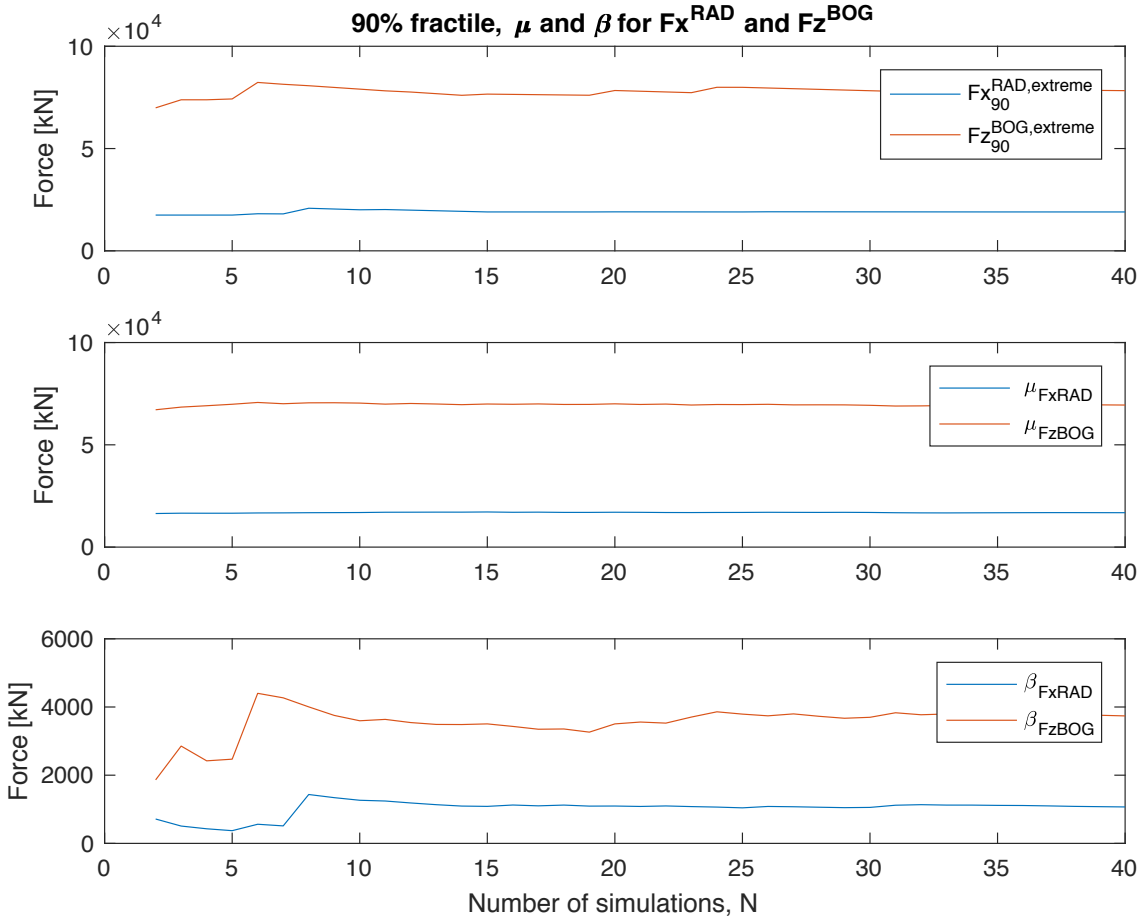

Figure 5.40: The 90% fractile, μ and β for F_X^{RAD} and F_Z^{BOG}

By visually examining Figure 5.40, the parameters have a smaller deviation after 10 simulations. In order to know exactly how large the discrepancies are, the deviation of the parameters are calculated. Setting different values of N_{req}, the deviations were below 5% at required number of simulations equal to 14, as presented in Table 5.14. A number of 14 simulations are therefore considered to give reliable results in the analyses to come.

Table 5.14: Parameter deviation for $N_{req} = 14$

	μ [%]	β [%]	90% fractile [%]
F_X^{RAD}	0.70	2.36	0.13
F_Z^{BOG}	0.40	4.81	1.40
M^{BOG}	0.8	4.70	0.70

5.6 Design Considerations and Requirements

This part is based on the references Larsen (2016) and ISO (2013).

There are several limit states for stationkeeping systems. The most common are

- Ultimate limit state (ULS): The structure is designed against overload for an intact mooring system in extreme weather conditions, usually with a 100-year return period. This means that the mooring lines shall be able to resist all known loads with a sufficient margin.
- Accidental limit state (ALS): The structure is designed against overload for a damaged system in extreme weather conditions, usually with a 100-year return period. This means that an accidental event shall not develop into a progressive collapse.
- Fatigue limit state (FLS): The structure is designed against fatigue failure taking all possible sea states into account. This means that the safety against failure shall be acceptable.

In this master thesis only the intact and accidental limit states are discussed further.

Characteristic Tension

The distribution for tension in a line gives the relation between the characteristic tension, T_{char}, and minimum breaking strength of the line, S_{MBS}. The safety factors for Class 3, which applies for the FPSO in question, is found in Table 5.15 from the International Standard ISO (2013).

Table 5.15: Safety factors for tension in mooring lines for permanent and mobile units on the Norwegian Continental Shelf (ISO 2013)

Limit state	**Permanent units**		**Mobile units**	
	100-year return period	*10-year return period*	*100-year return period*	*5-10-year return period*
Intact ULS	2.20	N/A	1.90	N/A
One line failure ALS^{1LB}	1.50	N/A	1.30	N/A
Two line failure ALS^{2LB}	N/A	1.50	N/A	N/A

The environmental conditions described in Section 5.3 is considered for ULS and ALS, but a larger range of environmental conditions must be provided for FLS. For ULS the requirement is applied as

$$T_{char}^{ULS} \cdot sf^{ULS} < S_{MBS} \tag{5.23}$$

For ALS, one line-break (1LB) correspond to 100-years weather conditions (100-year wave, 100-years wind and 10-years current forces) and two line-break (2LB) corresponds to 10-years weather conditions (10-years waves, 10-years wind and 1 year current force(s)). The requirements are mathematically formulated as

$$T_{char}^{1LB} \cdot sf^{1LB} < S_{MBS} \quad \text{and} \quad T_{char}^{2LB} \cdot sf^{2LB} < S_{MBS} \tag{5.24}$$

There are different ways of establishing the characteristic tension, T_{char}, and it differs from regulations and classes. When dimensioning a structure it is important to know if the characteristic tension is related as the most probable max (MPM) or for example the 90% fractile value. According to DNV GL (2015) the characteristic tension is defined as the MPM value.

Turret Dynamic Support Forces

When designing any steel structure, the regulations require that the structure is dimensioned by use of 90% fractile. The industry means that the regulations in some cases are not up to date. When dimensioning the vessel steel structure, which is not geo-stationary but weathervanes, the 90% fractile is an acceptable characteristic value. Regarding the turret steel structure, it's considered as industry consensus to use the MPM as the characteristic dimensioning value. This is because the turret is geo-stationary. This is illustrated in Figure 5.41.

When the local coordinate system of the vessel is aligned with the global coordinate system, then the position of point *A* equals point *B*. Otherwise, point *A* and *B* are different when referring to the turret or referring to the vessel.

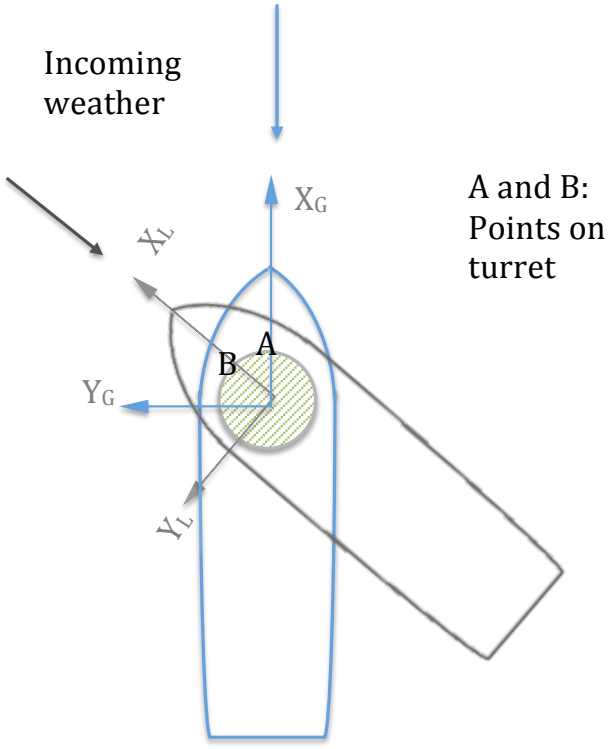

Figure 5.41: Illustration of geo-stationary turret and weathervaning vessel

5.6.1 Focus in Analyses

The numerical model is quite complex, therefore in this master thesis the model and the analyses are simplified to provide a more manageable model. For this reason, as described in this

chapter, three environmental conditions are to be examined, the risers system is disabled and the number of required simulations for reliable results are found to be 14.

Both ULS and ALS analyses are performed in SIMO. The parameters in focus are the tension in the mooring lines at fairlead, vessel offset and the dynamic turret support forces defined in Equation 5.1, 5.2 and 5.3. The characteristic value of the offset and tension are given as the most probable maximum, while the turret dynamic support forces are given by the 90% fractile value of the Gumbel distribution.

The mooring system design criteria for the freely weathervaning FPSO of interest is given in Table 5.16.

Table 5.16: Safety requirements for the FPSO, the safety factors are repeated from Table 5.15

	Safety factor for permanent unit in accordance with ISO (2013)	
Limit State	*Return period*	*Safety Factor*
ULS	100-year return period	2.20
ALS 1		1.50
ALS 2	10-year return period	1.50

In addition, Statoil has an internal requirement for the return period in ALS extreme condition, 10 000-year return period, with a safety factor equal to 1.1 In order to maintain the integrity of the risers, Statoil also has an internal offset requirement of 85m for the intact and one anchor line failure analyses.

Chapter 6

Results and Discussion

In this chapter the results from several coupled SIMO/RIFLEX analyses are presented and discussed. A number of ULS and ALS analyses are performed. Firstly all three environments are tested for the in-between collinear condition for the intact limit state. From these analyses, the most severe environment can be deduced. Secondly, the ULS analyses for in-between spread and in-bundle collinear cases are discussed. Then, three ALS conditions are analysed. These are one anchor line failure, two anchor lines failures and a 10 000 year condition, denoted as ALS 1LB, ALS 2LB and ALS extreme respectively. In all cases the vessel is in ballast condition. Finally, simple uplift calculations for the turret is presented.

As discussed in the previous chapter, the dimensioning value for the offset and tension is the most probable max (MPM) value, found from the Gumbel distribution. The tension in the mooring lines are obtained from the top of the line, at fairlead, where the maximum tension on the line is located. The 90% fractile for the Gumbel distribution is used as the dimensioning value for the dynamic turret support forces.

6.1 Ultimate Limit State Analyses

For the intact analyses, the main discussed results are presented in the text, the rest of the discussed results are given in Appendix E.

6.1.1 In-Between Collinear All Environments

The in-between collinear condition for all three environments are compared in order to conclude which environment that is considered as most severe. The analyses further are referred to as env 1, env 2 and env 3.

Vessel Offset

For the in-between collinear condition, the governing response will naturally be in the x-direction since the incoming environment is in the negative x-direction as explained in Section 5.3.

Table 6.1: The MPM and 90% value based on 14 seeds for the different environments

	Env 1	**Env 2**	**Env 3**
Offset MPM [m]	51.3	45.9	44.7
Offset 90% fractile [m]	62.3	54.8	52.6

Based on 14 seeds and comparing the design value MPM, presented in Table 6.1, env 1 has 10% and 13% larger maximum offset than env 2 and env 3 respectively. In addition, the 90% fractile offset for env 1 is on average 12% and 16% larger for than env 2 and env 3. In order to understand what motions the offset is divided into, the LF and WF contribution of the offset is filtered in the SIMO post-processor and presented in Figure 6.1.

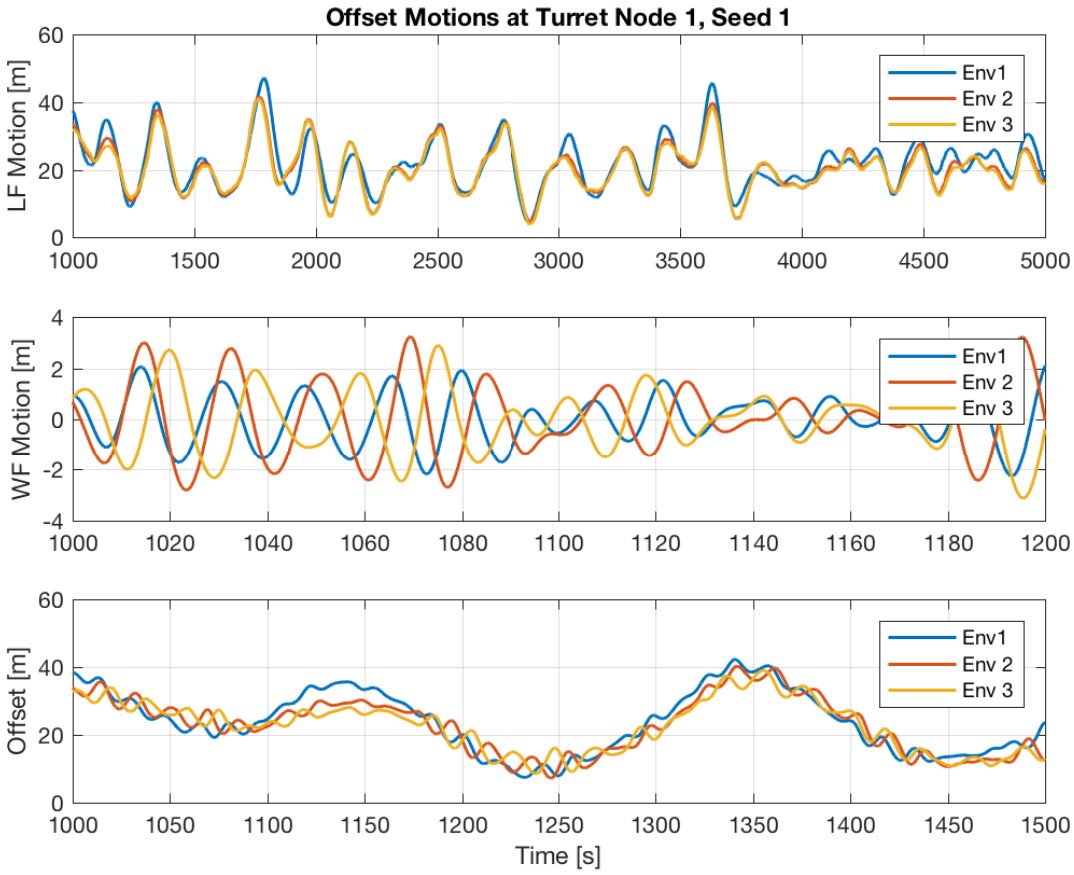

Figure 6.1: Sample time series of the LF, WF and total offset of turret node 1 for different environments, exemplified by seed 1, note that the time axis is not the same for all motions

Among the LF motions, env 1 clearly has larger amplitudes compared to the other environments. Some values are listed for comparison in Table 6.2. By only comparing the total maximum offset, env 1 is approximately 12% and 16% larger than the other environments. The mean offset on the other hand, has only small discrepancies.

Table 6.2: Mean and max offset of all simulations, in addition the standard deviation of the WF and LF motions for the time series are presented

Time series	**Env 1**	**Env 2**	**Env 3**
Mean offset of all 14 sim. [m]	22.0	20.9	20.5
Max offset of all 14 sim. [m]	64.7	56.8	54.6
WF std [m]	1.3	1.8	1.5
LF std [m]	7.9	7.0	6.8

The LF standard deviation for env 1 is larger than env 2 and 3, with 11% and 14 % respectively. The standard deviation for the WF motion for env 2 is 28% and 15 % larger than env 1 and 3 respectively.

The energy spectra as a function of period are also found from filtering the offset motions, plotted in Figure 6.2. The values for the LF energy spectrum are of much larger order of magnitude compared to the WF energy spectra.

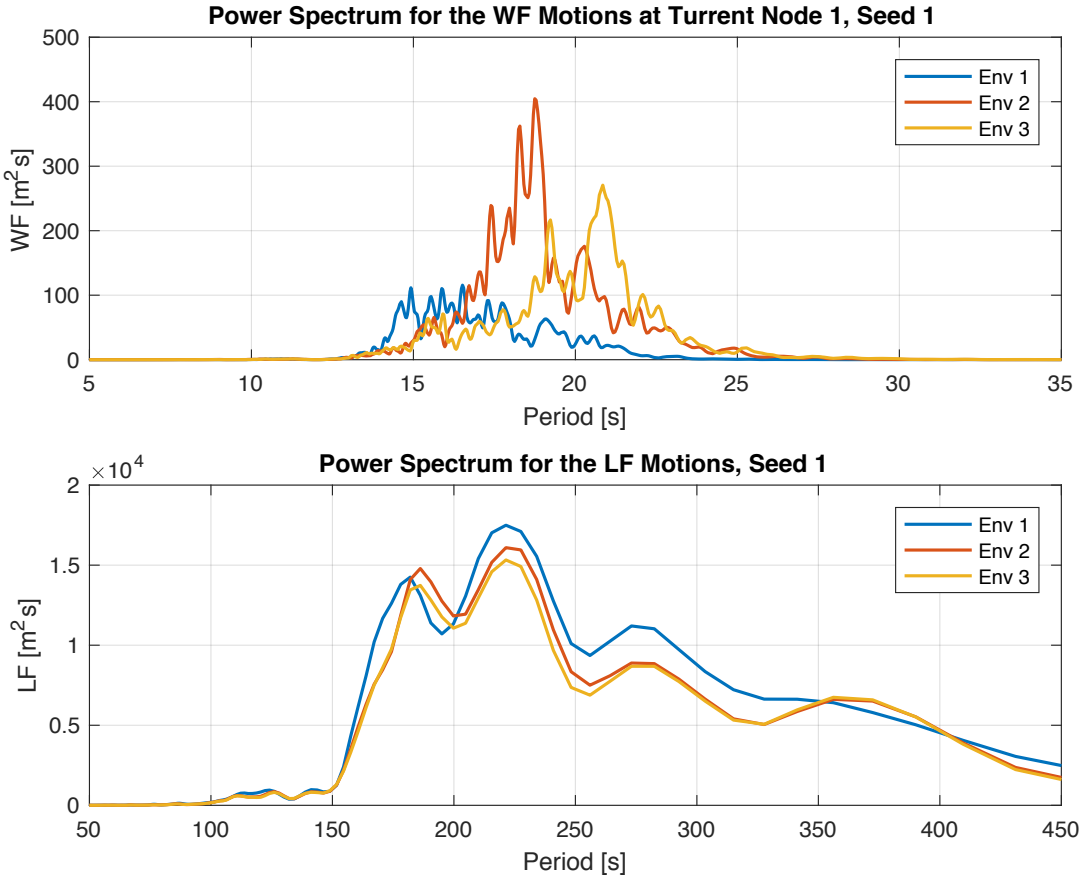

Figure 6.2: LF and WF power spectrum for turret node 1 for different environments, exemplified by seed 1

Looking at the energy spectra for the LF motions, env 1 has the largest energy. This is natural since env 1 is the sea state with the shortest period. When considering the WF motions, env 2 has the largest amplifications seen from the time series and hence the highest WF energy among the environments in the energy spectra. The peak of the WF spectrum is around a period of 18 s, which coincides with the specified peak period for env 2 at 18.5 s. The sample for the WF

spectrum for env 2 is also clearly larger than env 1, with a sample density around 20, i.e the peak period of the sea state. Env 1 on the other hand, has a large spread in the WF power spectrum, and with low energy.

Table 6.3: WF and LF standard deviation for the energy spectrum

Energy spectrum	**Env 1**	**Env 2**	**Env 3**
WF std [m]	30.5	75.3	51.0
LF std [m]	3800.9	3569.0	3380.2

The standard deviations for the LF and WF energy spectra are listed in Table 6.3. The discrepancies within the WF energy spectra for the different environments can be seen from the values for the WF standard deviation. Env 2 has 60% and 32% larger WF standard deviation than env 1 and 3. The differences between the LF standard deviation are not so large, with env 1 being 6% and 11% larger than env 2 and 3.

From an overall view, the results show that there are larger differences within the WF motions than for the LF motions. However, the impact from the WF motions does not affect the motion of the structure as much as the LF motions does. In other words, the energy in the LF motions are higher.

Top End Tension

The tension limit is expressed as a percentage of the minimum breaking strength (MBS) of the mooring component (API 2008). The MBS is defined by the mooring manufacturer, listed in Table 5.4 for the different line segments.

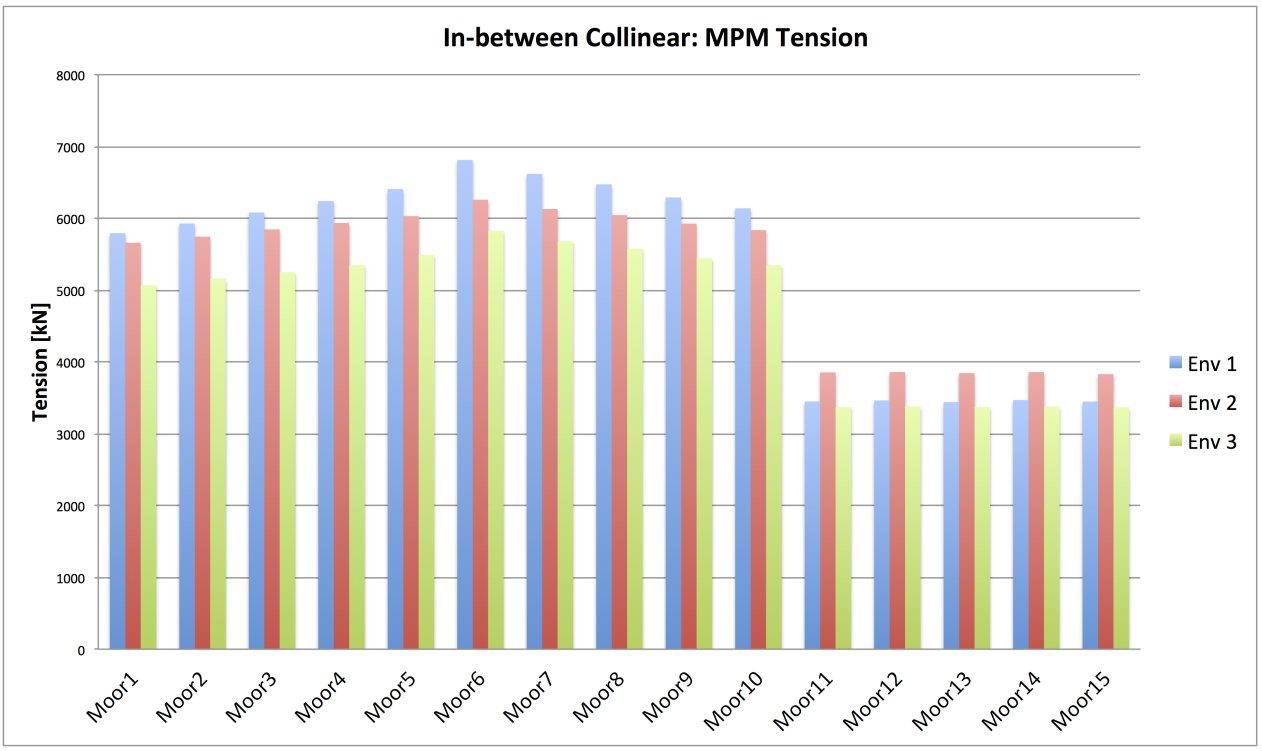

Figure 6.3: Comparison of the top end MPM tension for the different environments for the in-between collinear condition

The MPM tension in the mooring lines at fairlead for each environment is compared in Figure 6.3. Env 1 is somewhat larger than env 2, while quite larger than env 3 for the windward mooring lines in bundle 1 and 2. For bundle 3, env 1 has around 12 % smaller MPM tension compared to env 2, while approximately 3% larger than env 3. The most loaded line for all environments is mooring line 6, the MPM tensions with associated safety factors are listed in Table 6.4.

Table 6.4: The MPM tension value for the most loaded line for all environments, mooring line 6, and safety factor for segment 1

Mooring line 6	**Env 1**	**Env 2**	**Env 3**
MPM tension [kN]	6811	6258	5822
sf_{max} *[-]*	3.7	4.0	4.3
margin [-]	1.5	1.8	2.1

The MPM tension for the most loaded line for env 1 is 8% and 15% larger compared to env 2 and 3 respectively. The safety margin for Env 1, calculated with the maximum MPM values

from the results, is about 20 % less than for env 2. Therefore, env 1 is the critical environment considering the MPM top end tension in the mooring lines.

Dynamic Turret Support Forces

Some sample time series of the dynamic turret support forces are found in Figure 6.4. In addition to the total force, the contribution from inertia and chain table are included.

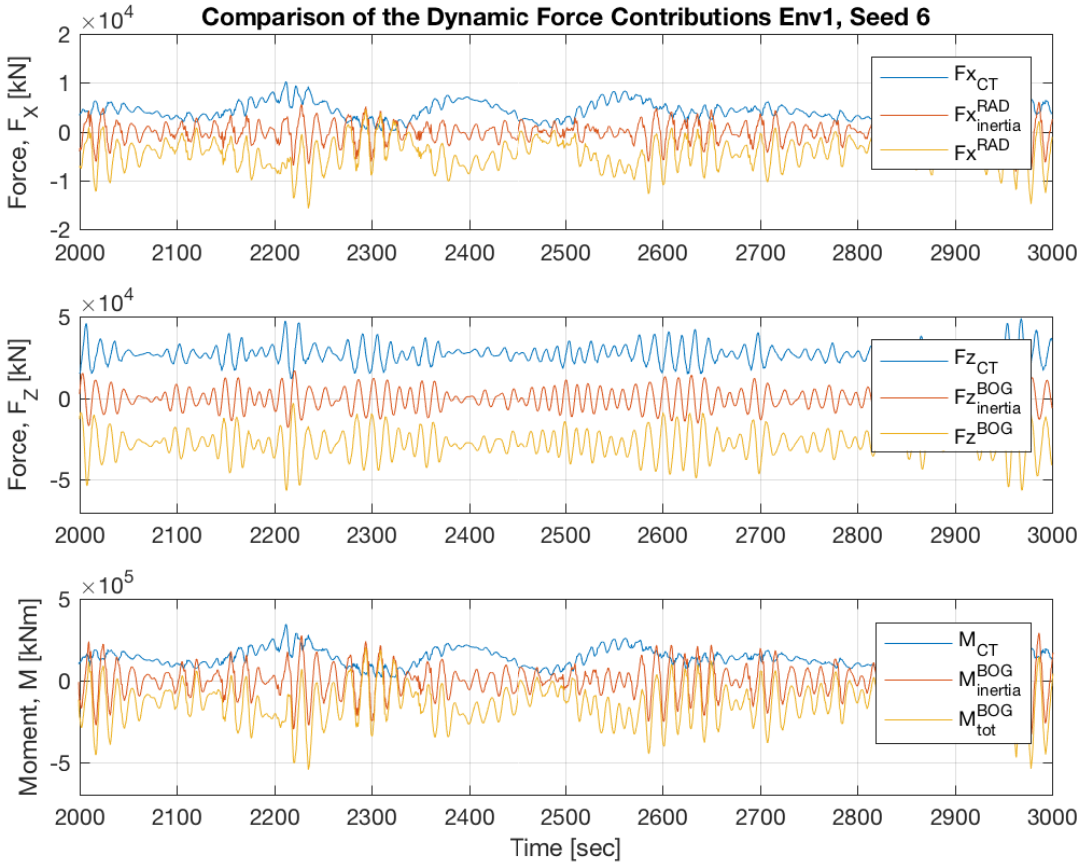

Figure 6.4: Sample time series of the dynamic turret support forces for in-between collinear condition for env 1

The time series shows that the F_X^{RAD} and M^{BOG} have a combination between WF and LF forces, while F_Z^{BOG} is a complete WF force. All inertia forces oscillates around zero, and are WF forces, hence the contribution from the inertia forces are very small for all dynamic turret support forces. The contribution from chain table, on the other hand, dominates. This means that the forces from mooring lines and risers gives the main contribution. The CT forces for

F_X^{RAD} and M^{BOG} have both WF and LF contributions. The CT force for the F_Z^{BOG} however, is a wave-frequent force.

The dynamic turret support forces are dimensioned by use of the 90% fractile, both MPM and 90% values are given in Table 6.5. Here, env 2 is somewhat larger than env 1 and env 3 still has the smallest dynamic forces.

Table 6.5: Comparison between the dynamic turret support forces for the different environments in the in-between collinear condition

	Env 1		**Env 2**		**Env 3**	
	MPM	*90 % fractile*	*MPM*	*90 % fractile*	*MPM*	*90 % fractile*
FXRAD [kN]	17088	19308	17136	20072	15695	17689
FZBOG [kN]	69629	76030	69318	77836	61646	69368
MBOG [kNm]	628270	672120	620440	707180	555640	624440

It is a very small deviation between env 1 and env 2 when comparing the MPM values of the dynamic forces, while env 3 is clearly the environment with the smallest forces. This can be seen from Table 6.6. This indicates that the turret dynamic forces are more sensitive toward WF motions, i.e. env 2, compared to the LF motion dominated env 1.

Env 2 has the highest dynamic turret support forces, but there is no requirement that the dynamic turret support forces needs to maintain. Hence, from an overall view, the two first sea states are approximately equally "bad" when considering the dynamic turret support forces.

Table 6.6: Deviation between the dynamic turret support forces for the different environments in the in-between collinear condition

	Env 2		**Env 3**	
Env 1	*MPM*	*90% fractile*	*MPM*	*90% fractile*
F_X^{RAD} *[%]*	-0.3	-4.0	8.2	8.4
F_Z^{BOG} *[%]*	0.4	-2.4	11.5	8.8
M^{BOG} *[%]*	1.2	-5.2	11.6	7.1

Critical Sea State

Summing up, env 1 is generally dominated by the low frequent motions, while env 2 has a large contribution from the wave frequent motions. Env 3 has approximately the same LF motions as env 2, but less WF energy.

If the purpose of the simulations are to exploit fatigue and fracture problems, then an environment giving rapid motions hence many cycles may be the worst environment. In this case that is env 2. In this thesis the focus lies in the following responses; MPM offset, MPM top end tension and 90% fractile value of the dynamic turret support forces. With this in mind, env 1 provides the overall largest offset and top end tension. The dynamic turret support forces are slightly higher for env2, but these forces are not subjected to any requirement. Hence env 1 is considered as the most fatal sea state. This is because ship-shaped units are sensitive to LF motion, and therefore the sea state with the shortest period is the most critical one. Env 1 is further investigated for the in-between spread and in-bundle collinear condition.

6.1.2 In-Between Collinear vs. In-Between Spread

The in-between spread condition is compared with the in-between collinear condition, both analysed for the worst sea state. The difference between these conditions are the spreading of the applied environment.

Vessel Offset

The offset obtained in the two analyses are displayed in Table 6.7. There are barely a difference between the MPM or the 90% fractile comparing the two analyses. This implies that the spreading, at least the DNV GL spread definition, has only a minor contribution to the offset MPM and 90% fractile considering the in-between contribution. The implication may be different for an other directional distribution.

Concerning the offset requirement of 85m, due to the flexibility of the risers, both conditions are well within the criteria for the MPM and 90% fractile value. Hence, the integrity of the risers are maintained for both conditions.

Table 6.7: Offset for in-between collinear and spread ballast conditions for Environment 1

	Offset	
Environment 1	*MPM [m]*	*90% fractile [m]*
In-between Collinear Condition	51.3	62.3
In-between Spread Condition	51.6	63.3

Top End Tension

The heading of the vessel for the in-between collinear and spread are respectively 2.6° and 17.3°, hence the tension distribution of the mooring lines will be somewhat different. The tension for the mooring lines are compared in Figure 6.5. The in-between spread condition has a more evenly tension distribution compared to the in-between collinear condition. For bundle 1, the tension for the mooring lines are roughly 7-9% larger for the spread condition in comparison with the collinear condition. Bundle 2 on the other hand, has approximately the same top end tension for both cases. The leeward lines in Bundle 3 are more prone to tension for the spread condition, with a difference of 4-10% compared to the in-between collinear case.

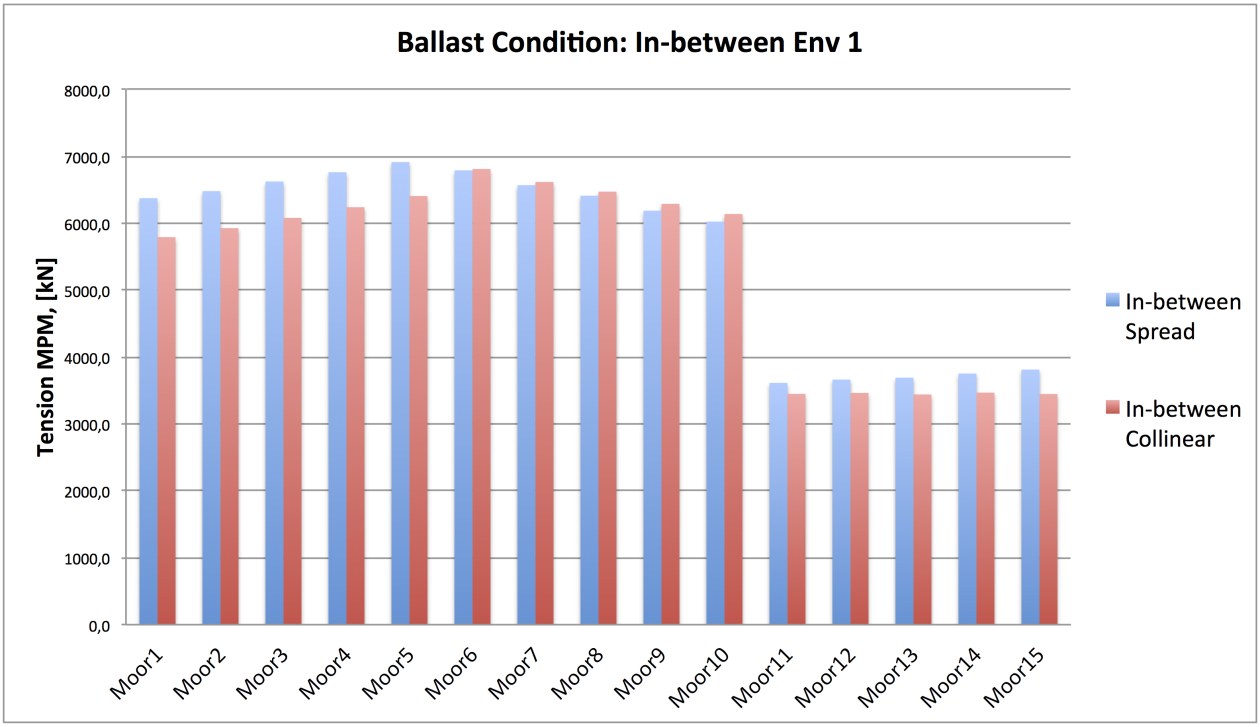

Figure 6.5: MPM tension for all mooring lines in the in-between collinear and spread conditions

The safety factor for the mooring line with the maximum tension for both cases can be found in Table 6.8. The tension discussed in the results are located at the fairlead, thus at the upper point of segment 1. Segment 2 and 3 have a smaller minimum breaking load than segment 1. The loading on the mooring lines at the lower segments are not known, but by using the fairlead tension, a conservative estimation of the safety factor can be conducted. If the lower segments can endure the fairlead tension, then they can withstand the actual force on the specific location as well. It should be noted that this is only an estimation, and that the safety factor for segment 1 is the only representative safety factor.

All of the segments are within the ULS safety factor for permanent moorings on the Norwegian Continental Shelf at 2.2, found in Table 5.16. The upper segment has a margin of 1.44 and 1.50 for the spread and collinear condition respectively. This implies that the mooring line can manage much higher tensions, and if this was the maximum tension to occur in all analyses, one could reduce the mooring line cost by downsizing the mooring line to achieve a smaller safety factor margin. It is desirable, from a economical design point of view, to satisfy the safety factor the unit is subjected to, but not with a very large margin. Since this requires stronger material, which usually results in a more expensive structure.

Table 6.8: Safety factor with associated margin for all segments in env 1

		In-between Collinear		**In-between Spread**	
	MBL [kN]	sf_{MPM}^{max}	*margin*	sf_{MPM}^{max}	*margin*
Segment 1 *(top chain)*	25173	3.70	1.50	3.64	1.44
Segment 2 *(mid-wire rope)*	22000	3.23	1.03	3.18	0.98
Segment 3 *(bottom chain)*	22876	3.36	1.16	3.31	1.11

Dynamic Turret Support Forces

The three dynamic forces F_X^{RAD}, F_Z^{BOG} and M^{BOG} are not affected much by changing the spread of the environment. The MPM and 90% fractile for the different forces are presented in Table

6.12. The spread condition is nearly 5% larger compared to the collinear condition for all dynamic turret support forces. In addition the 90% fractile in spread condition are 1%, 7% and 4% larger compared to the collinear F_X^{RAD}, F_Z^{BOG} and M^{BOG} respectively. The standard deviation is quite larger for the collinear condition for F_X^{RAD} and M^{BOG}, respectively 19% and 27% larger compared to the spread condition. The standard deviation for F_Z^{BOG} is almost the same for the spread and collinear condition, but with a 3% reduction comparing the collinear condition with the spread. Since F_Z^{BOG} is primarily affected by the WF motions, this indicates that the WF contribution is not so affected by the spreading change.

Table 6.9: Dynamic turret support force results for the in-between collinear and spread condition

	In-between Collinear			**In-between Spread**		
	MPM	*90 % fractile*	*Stdev*	*MPM*	*90 % fractile*	*Stdev*
F_X^{RAD} *[kN]*	17088	19308	1134	17896	19444	1403
F_Z^{BOG} *[kN]*	69629	76030	4606	73153	82016	4470
M^{BOG} *[kNm]*	628270	672120	28180	663920	702580	38517

6.1.3 In-Between Collinear vs. In-Line Collinear

The in-line collinear condition is compared to the in-between collinear condition, both analysed for the worst sea state.

Vessel Offset

The offset for the in-line collinear condition is much smaller than for the in-between collinear condition. As discussed earlier, the in-line restoring force plotted in Figure 5.27, illustrates that the system requires a larger force to move the vessel and moorings for higher offsets. This agrees well with the results, which implies that the in-line condition is more rigid than the in-between collinear condition considering the offset. Both conditions are loaded with env 1 in a collinear directional distribution, providing the same force on the vessel.

The most probable maximum offset for the in-between collinear condition is approximately 24% larger compared to the in-line collinear condition, found in Table 6.10. In addition the

90% fractile offset is almost 30% larger for the in-between compared to the in-line collinear condition. Both the MPM and 90% fractile for the two conditions satisfy the requirement of 85m.

Table 6.10: Offset for in-between collinear and in-line collinear ballast conditions for Environment 1

	Offset	
Environment 1	*MPM*	*90% fractile*
In-between Collinear	51.27	62.32
In-line Collinear	39.24	44.36

Top End Tension

The MPM tension for the two collinear conditions for all mooring lines are presented in Figure 6.6. By changing the location of the incoming weather, the tension distribution has changed quite much. Now, bundle 1 and 3 consist of leeward mooring lines, while only bundle 2 consist of windward mooring lines. In contrast to the in-between condition, where bundle 1 and 2 include windward moorings and the leeward mooring lines are located in bundle 3.

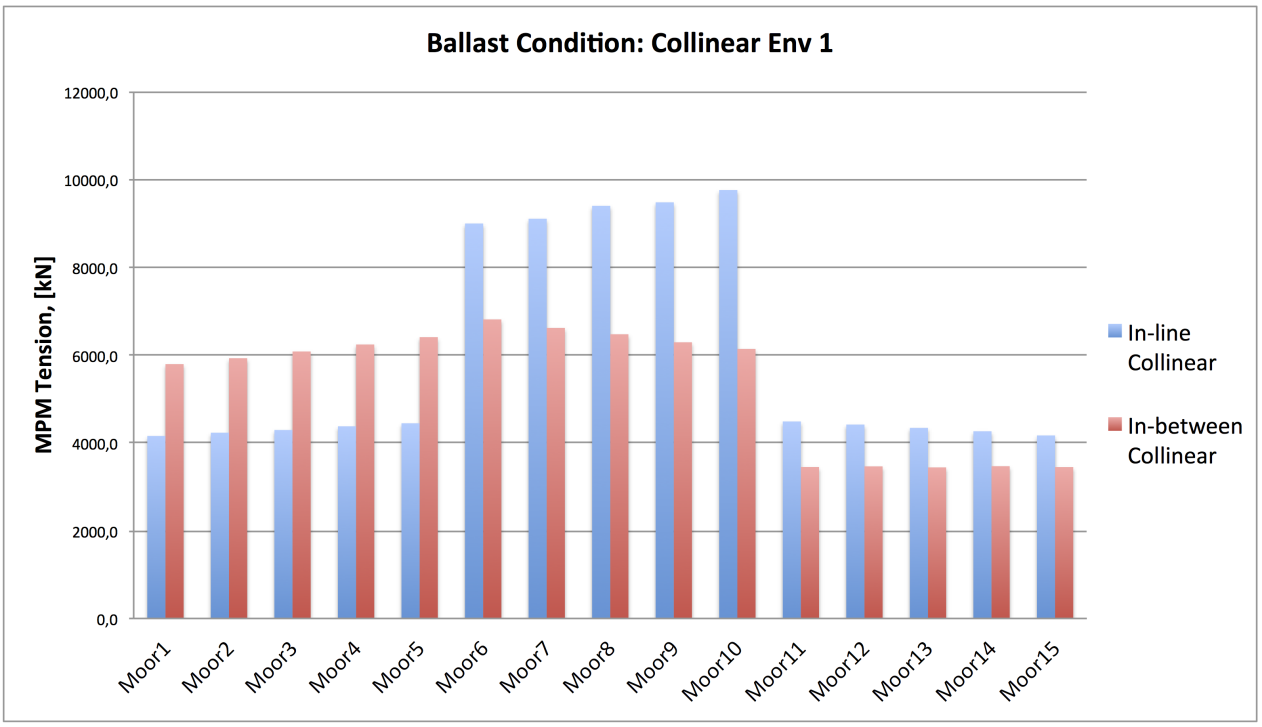

Figure 6.6: MPM tension for all mooring lines in the in-between collinear condition compared to in-line collinear condition

The MPM tensions are therefore much less in bundle 1 and 3 compared to bundle 2 for the in-line condition. In-between bundle 1 has approximately 30% higher tension compared to bundle 1 in the in-line condition. Bundle 2 on the other hand are prone to much higher tensions for the in-line case, with a span of 25-38% larger tension in comparison to the in-between case. The tension in the mooring lines in bundle 3 have an increase of about 20% for the in-line condition compared to the in-between condition, i.e. the lines are less slack.

The safety factors for all segments are presented in Table 6.11. The dimensioning tension is found in mooring line 10, at 9757 kN. Segment 2 is clearly the dimensioning parameter, especially if the 90% fractile value was used. The safety factors for segment 2 and 3 are conservative since they are based on the top end tension, the tension along the line on the lower segments will most probably be smaller, or in worst case, equal to the maximum tension found at fairlead.

Hence, the in-line collinear condition is the dimensioning parameter. For the representative segment, i.e. segment 1, this condition has a margin of 0.38.

Table 6.11: Safety factor with associated margin for all segments in Environment 1 for the in-between and in-line collinear condition

		In-between Collinear		**In-line Collinear**	
	MBL [kN]	sf_{MPM}^{max}	*margin*	sf_{MPM}^{max}	*margin*
Segment 1 *(top chain)*	25173	3.70	1.50	2.58	0.38
Segment 2 *(mid-wire rope)*	22000	3.23	1.03	2.25	0.05
Segment 3 *(bottom chain)*	22876	3.36	1.16	2.34	0.14

Dynamic Turret Support Forces

There are almost no change in the F_Z^{BOG} MPM and 90% fractile value comparing the in-line and in-between collinear condition. The MPM values on the other hand, for F_X^{RAD} and M^{BOG}, are approximately 8% larger and 14% larger for the 90% fractile value for the in-line compared to the in-between collinear condition.

As discussed before, env 1 is LF dominated, while F_Z^{BOG} consist of WF motions, hence changes in this force are small.

Table 6.12: Dynamic turret support force results for the in-between collinear and spread condition

	In-between Collinear			**In-line Collinear**		
	MPM	*90 % fractile*	*Stdev*	*MPM*	*90 % fractile*	*Stdev*
F_X^{RAD} *[kN]*	17088	19308	1134	18652	22158	1867
F_Z^{BOG} *[kN]*	69629	76030	4606	68592	76662	5078
M^{BOG} *[kNm]*	628270	672120	28180	675990	794780	56582

Critical Directional Distribution

The offset for the in-between collinear and spread condition are almost equal. The offset for the in-line collinear condition on the other hand, is 24% smaller compared to the in-between

collinear condition. The vessel offsets are all well within the requirement provided by Statoil. Hence, this parameter is not considered as critical for any of the cases.

The tension of the moorings are subjected to the DNV GL safety factor of 2.2 for intact condition, from Table 5.16. Table 6.13 represents the safety factor for segment 1 for the in-between collinear, in-between spread and in-line collinear condition. Comparing the different cases, the safety factor and margin is by far smallest for the in-line collinear condition, but within the acceptance criteria.

Table 6.13: Safety factor with associated margin for the dimensioning segment for all directional distributions

		In-between Collinear		**In-between Spread**		**In-line Collinear**	
	MBL [kN]	sf_{MPM}^{max}	*margin*	sf_{MPM}^{max}	*margin*	sf_{MPM}^{max}	*margin*
Segment 1 *(top chain)*	25173	3.70	1.50	3.64	1.44	2.58	0.38

The dynamic turret support forces does not have any requirement, but the in-line collinear condition obtains the highest forces. All the dynamic turret support forces are within reasonable values. Therefore, seen from an overall perspective, the top end tension is the dimensioning parameter, thus the in-line collinear condition should be further investigated for the ALS conditions.

6.2 Accidental Limit State Analyses

In addition to intact analyses, it is interesting to investigate the mooring systems ability to resist accidental loads and maintain the integrity and system performance due to anchor line failure and extreme weather conditions. The FPSO is a permanent mooring system, and on the Norwegian Continental Shelf it is required to perform both one and two line failures analyses. Therefore both one and two anchor lines are assumed to have failed, denoted as ALS 1LB and ALS 2LB. In addition an extreme weather condition is analysed, this is done by applying a 10 000-year condition. This is not demanded by the regulations, but is an internal Statoil procedure.

It's of interest to to test the top end tension on the moorings in their worst case. The condition leading to the worst line tensions in the ULS analyses are further examined for the ALS analyses. Hence the in-line collinear condition with env 1 is used in the ALS analyses.

Some of the results are presented in the text, the rest of the discussed results are given in Appendix F.

ALS Environments

The environmental conditions for ALS 1LB is the same as for the intact condition, thus 100-year return period for the waves and wind, while 10-year return period for the current. When performing a two line break analysis, 10-10-1-year return period is used for the waves, wind and current respectively. The environment to the left of the peak in the contour lines are used, hence the environment with the shortest peak period, as for the 100 year condition.

In NORSOK Standard (2007) the combinations of the environmental actions for the ALS extreme 10 000-year condition is defined in three ways, with 10 000-year return period for either waves, wind or current. It is the worst case scenario that should be picked, in this case the current will not lead to the worst case. It's not evident if the wind or waves will provide more vessel response. For a structure with a large topside, such as a semi-submersible, has a large non-submerged reaction area that absorbs wind loads. For ship-shaped units, the waves often provides larger loads on the unit. In order to know for sure, two cases of the ALS extreme are tested, with a 10 000-year return period for the waves and wind for each condition. The resulting return period for the wind/waves and current are an annual probability of exceedance at 100- and 10-years respectively.

The environmental definitions for all ALS analyses are found in Table 6.14

Table 6.14: The different environmental definitions for ALS analyses

		ALS 1LB	**ALS 2LB**	**ALS Extreme**	
				Waves	***Wind***
Return period (waves-wind-current)		*(100-100-10)*	*(10-10-1)*	*(10 000-100-10)*	*(100-10 000-10)*
Waves	*Hs [m]*	14.0	13.0	18.0	14.0
	Tp [s]	15.1	15.8	17.1	15.1
Wind	*[m/s]*	32.5	29.5	32.5	37.0
Current	*[m/s]*	1.11	0.97	1.11	1.11

6.2.1 ALS 1LB

One mooring line is assumed to fail, hence a one anchor line failure analysis for the mooring system is performed. The mooring response analysis is carried out as for the ULS in-line collinear condition, but now with one line missing. According to DNV GL (2015) the characteristic tension is the same as for the ULS, i.e. the MPM tension value is used. In order to test the integrity of the mooring system for the worst possible case in ballast condition, the second most loaded mooring line is broken. Seen from the results plotted in the histogram in Figure 6.6, mooring line 9 is the second most loaded line, hence this mooring line is disabled from the analysis.

Vessel Offset

The offset MPM value for one line failure is 46.5m, seen from Table 6.15. Compared to the intact condition, the offset of the vessel has increased with approximately 7m for the one anchor line failure. In other words, this means that the offset in ALS 1LB is almost 16% larger than the ULS. The offset requirement of 85m also applies for the one line failure, hence this criteria is fulfilled with a large margin.

Table 6.15: Intact and one line failure offset comparison

	ULS		**ALS 1LB**	
	MPM	*90% fractile*	*MPM*	*90% fractile*
offset [m]	39.2	44.4	46.5	51.4

Top End Tension

All MPM tensions for the mooring lines for both the intact and one line failure are compared in Figure 6.7. The MPM tension in the mooring lines for ALS 1LB for bundle 1 and 3 are on average 6% and 4% smaller compared to the intact condition. Bundle 2 on the other hand, now with only four mooring lines, have an increase of around 21% in comparison to the intact condition. The maximum tension is found to be in mooring line 10 at 12563 kN. Compared to the intact condition at 9757 kN, this is an increase of around 22%. Mooring line 10 is therefore still the governing line when considering the safety factor.

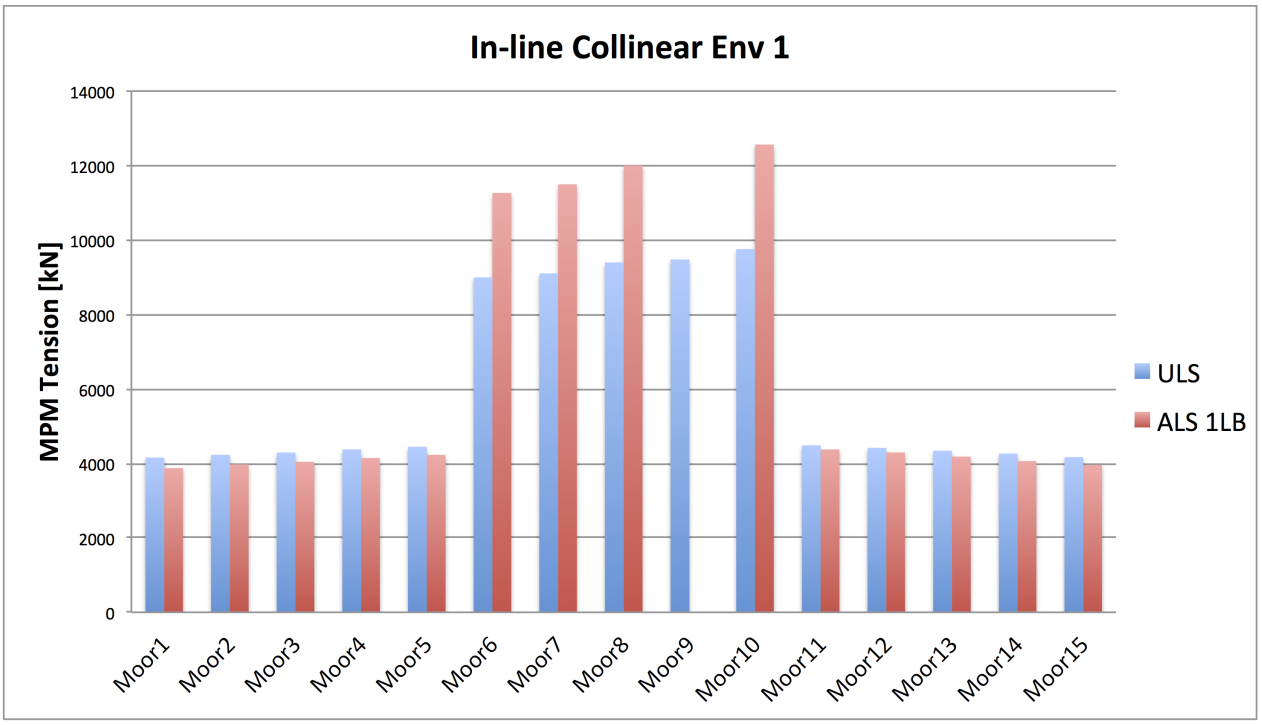

Figure 6.7: Comparison of the mooring line tension for the intact and ALS 1LB in-line collinear condition

The safety factor for the different segments are provided in Table 6.16. The MPM tension for the one line failure adheres the DNV GL requirement with a margin of 0.50 for the upper segment. The conservative estimation for segment 2 and 3 are also within the requirement considering the MPM values. If the characteristic tension was put to be the 90% fractile, the tension would not satisfy the criteria. The 90% fractile is 40% larger than the MPM value, hence a characteristic tension within these two values will provide less margin or not comply with the

regulations.

Table 6.16: Safety factor for mooring line 10 with associated margin for all segments for one anchor line failure

	In-line ALS 1LB				
	MBL [kN]	sf_{MPM}^{max}	*margin*	$sf_{90\%}^{max}$	*margin*
Segment 1 *(top chain)*	25173	2.00	0.50	1.23	-0.27
Segment 2 *(mid-wire rope)*	22000	1.75	0.25	1.07	-0.43
Segment 3 *(bottom chain)*	22876	1.82	0.32	1.11	-0.39

Dynamic Turret Support Forces

The dynamic forces and moment, F_X^{RAD}, F_Z^{BOG} and M^{BOG}, decreases when the system has less mooring lines. The dynamic forces are governed by the contribution from chain table, which means the contributions from moorings (and risers if included). The average tension over the lines are higher after the line is broken, but the contribution from weight from all active mooring lines are smaller. Compared to the intact condition, F_X^{RAD}, F_Z^{BOG} and M^{BOG} are 0.5%, 7% and 1% smaller for ALS 1LB respectively. The standard deviation also decreases for all forces when a line is broken. This indicates that the vertical force at bogies are more sensitive towards mooring line failure than the two other dynamic turret support forces. The smaller the dynamic turret support forces becomes, the turret is less exposed towards uplift.

Table 6.17: Dynamic turret support force results for the in-line collinear intact and one anchor line failure

	In-line Collinear: Intact			**In-line Collinear: ALS 1LB**		
	MPM	*90 % fractile*	*Stdev*	*MPM*	*90 % fractile*	*Stdev*
F_X^{RAD} *[kN]*	18652	22158	1867	18560	22010	1810
F_Z^{BOG} *[kN]*	68592	76662	5078	64291	71440	4634
M^{BOG} *[kNm]*	675990	794780	56582	669130	788060	55440

6.2.2 ALS 2LB

In addition to the mooring line broken in ALS 1LB, the second most loaded line is removed providing the ALS 2LB analysis. From the results the second most loaded line is mooring line 8 and mooring line 10 is still the most loaded line, seen from Figure 6.7. Hence mooring line 8 and 9 are broken. Now, a 10-year environmental condition is applied, but the safety factor for the tension at fairlead is still the same.

Offset

The MPM and 90% fractile values for the offset are presented in Table 6.18. The MPM value from the probability density function for the offset in the two line failure system is approximately 48 m. This is almost 4% more compared to one line failure and almost 20% more than the intact condition. The increase from one to two line failures is not so drastic. There is no requirement for the offset in the two line failure state, however the offset is well within the criteria provided by Statoil for intact and ALS 1LB.

Table 6.18: Intact and one line failure offset comparison

	ULS		**ALS 2LB**	
	MPM	*90% fractile*	*MPM*	*90% fractile*
offset [m]	39.2	44.4	48.2	53.6

Top End Tension

The mooring line MPM tensions for all mooring lines in the intact, one and two line failures are illustrated in Figure 6.8. From the results, now with 13 active mooring lines and only three lines in bundle 2, mooring line 10 is still the most loaded line, now with a MPM tension of 14253 kN. This is approximately 32% and 12% increase compared to the one anchor line failure and intact system.

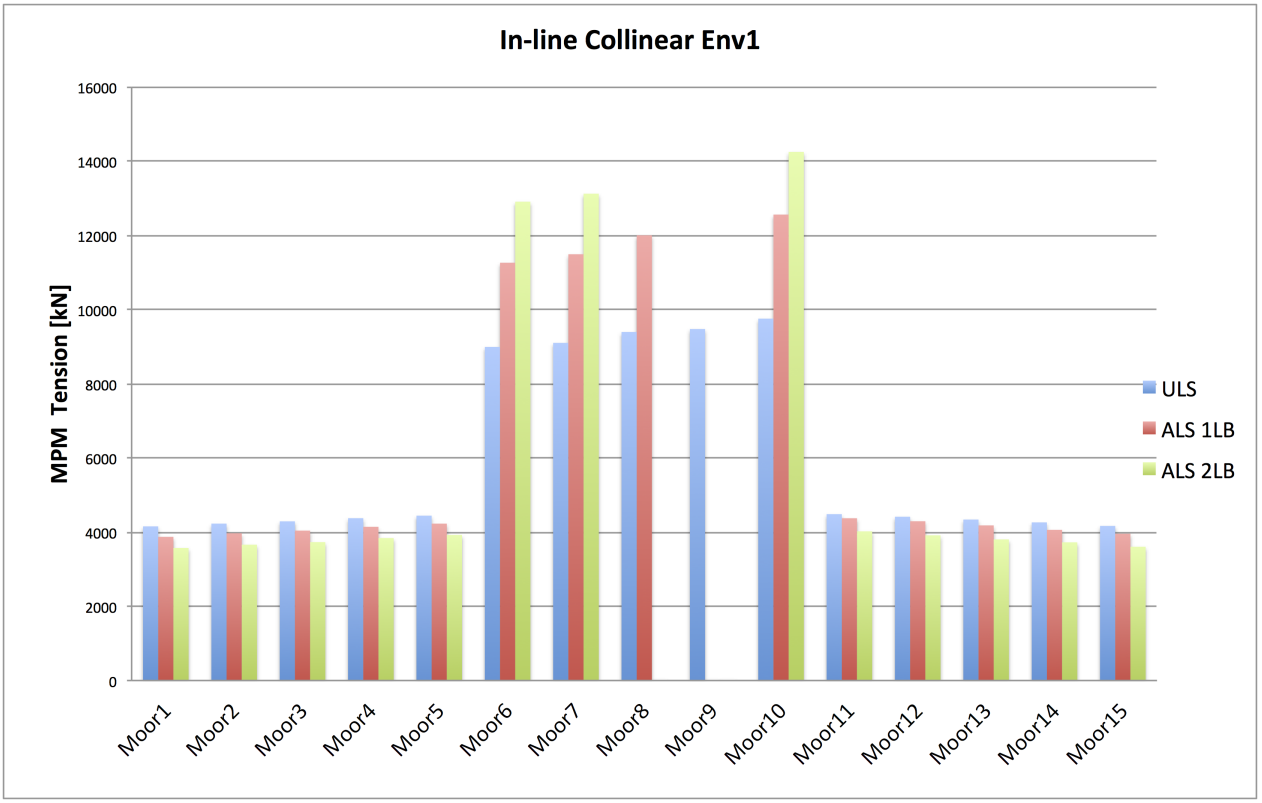

Figure 6.8: Comparison of the mooring line tension for the intact, ALS 1LB and ALS 2LB in-line collinear condition

The critical safety factor margin to the safety factor is therefore smaller for two anchor line failures than one anchor line failure. Similarly as for ALS 1LB, the 90% fractile for ALS 2LB does not satisfy the safety factor at 1.5.

Table 6.19: Safety factor for mooring line 10 with associated margin for all segments for two anchor line failure

	In-line ALS 2LB				
	MBL [kN]	sf_{MPM}^{max}	*margin*	$sf_{90\%}^{max}$	*margin*
Segment 1 *(top chain)*	25173	1.77	0.27	1.26	-0.24
Segment 2 *(mid-wire rope)*	22000	1.54	0.04	1.10	-0.40
Segment 3 *(bottom chain)*	22876	1.60	0.10	1.14	-0.36

An interesting observation is that there is only a slight difference between one and two line failure 90% fractile values, with almost 3% deviation. In Figure 6.9 the intact, one and two mooring line failure PDF for mooring line 10 is compared. From intact to one line failure the whole PDF is staggered to the right, thus higher tensions, with a lower probability and higher MPM value of the distribution. From one to two line failure the PDF is staggered to the right, but going towards the same maximum value, which means that the distribution becomes more narrow-banded. In addition the probability of the peak point increases a bit. From this one can see that the MPM value of the PDF increases as one and two lines are removed from the simulations.

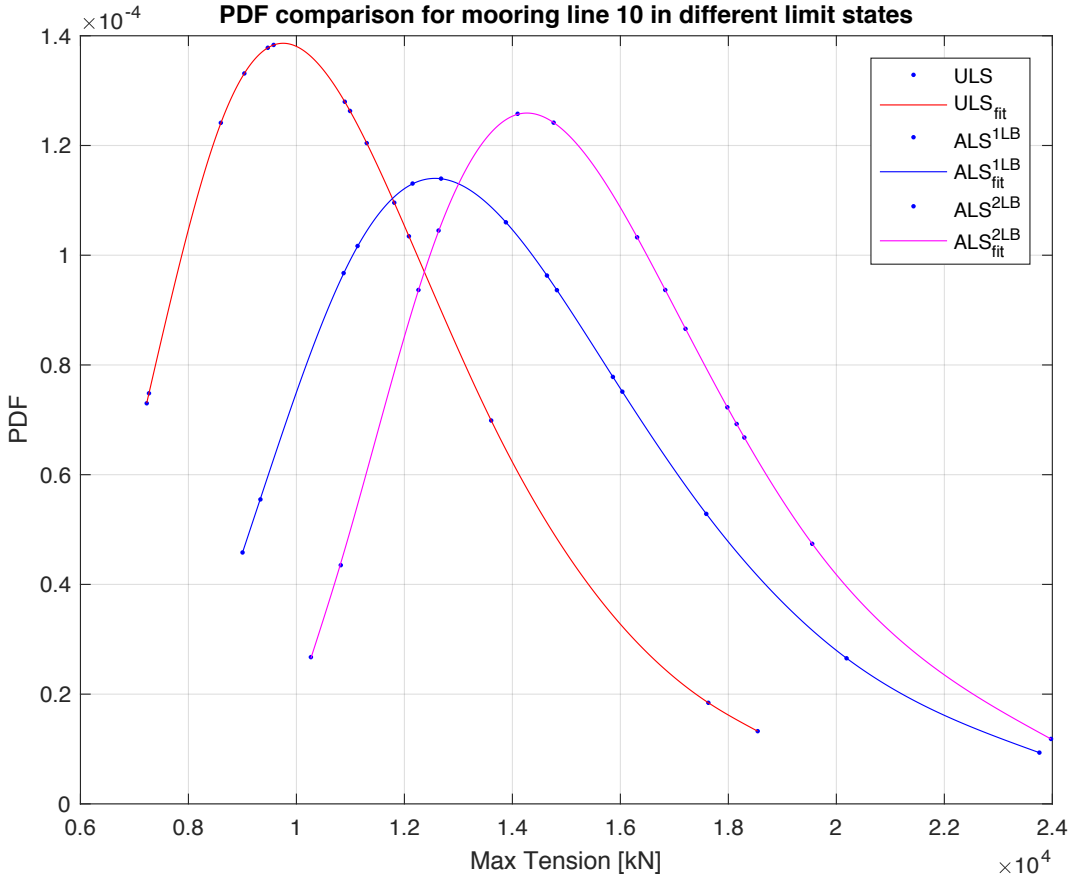

Figure 6.9: PDF for intact, one and two mooring line failure for mooring line 10

Dynamic Turret Support Forces

Similarly as in ALS 1LB, the dynamic forces and moment, F_X^{RAD}, F_Z^{BOG} and M^{BOG}, decreases when the system looses one extra mooring line. The results for dynamic turret support forces

intact and 2LB is presented in Table 6.23. The MPM value of the F_X^{RAD}, F_Z^{BOG} and M^{BOG} are respectively 19%, 25% and 19% smaller for two line failure compared to the intact condition. The difference relative to each other are approximately the same for the one and two line failure conditions, with F_Z^{BOG} as the force with largest reduction at around 6% smaller than F_X^{RAD} and M^{BOG}. The danger of uplift is an even smaller problem in this case, as the dynamic forces are smaller.

Table 6.20: Dynamic turret support force results for the in-line collinear intact and two anchor lines failures

	In-line Collinear: Intact			**In-line Collinear: ALS 2LB**		
	MPM	*90 % fractile*	*Stdev*	*MPM*	*90 % fractile*	*Stdev*
F_X^{RAD} *[kN]*	18652	22158	1867	15651	19740	1546
F_Z^{BOG} *[kN]*	68592	76662	5078	54875	62460	3877
M^{BOG} *[kNm]*	675990	794780	56582	568000	695360	52023

The inertia forces of the dynamic turret support forces are practically the same for the intact and accidental limit states. The chain table forces on the other hand, changes when a line is broken. Figure 6.10 shows that the CT forces are significantly smaller for the ALS 2LB compared to the intact condition. For the F_Z^{CT} force, there is no superimposing LF contribution, as for the F_X^{CT} force. Therefore, F_Z^{BOG} experiences a larger reduction than the combined WF and LF forces, F_X^{RAD} and M^{BOG}. This also applies for the ALS 1LB.

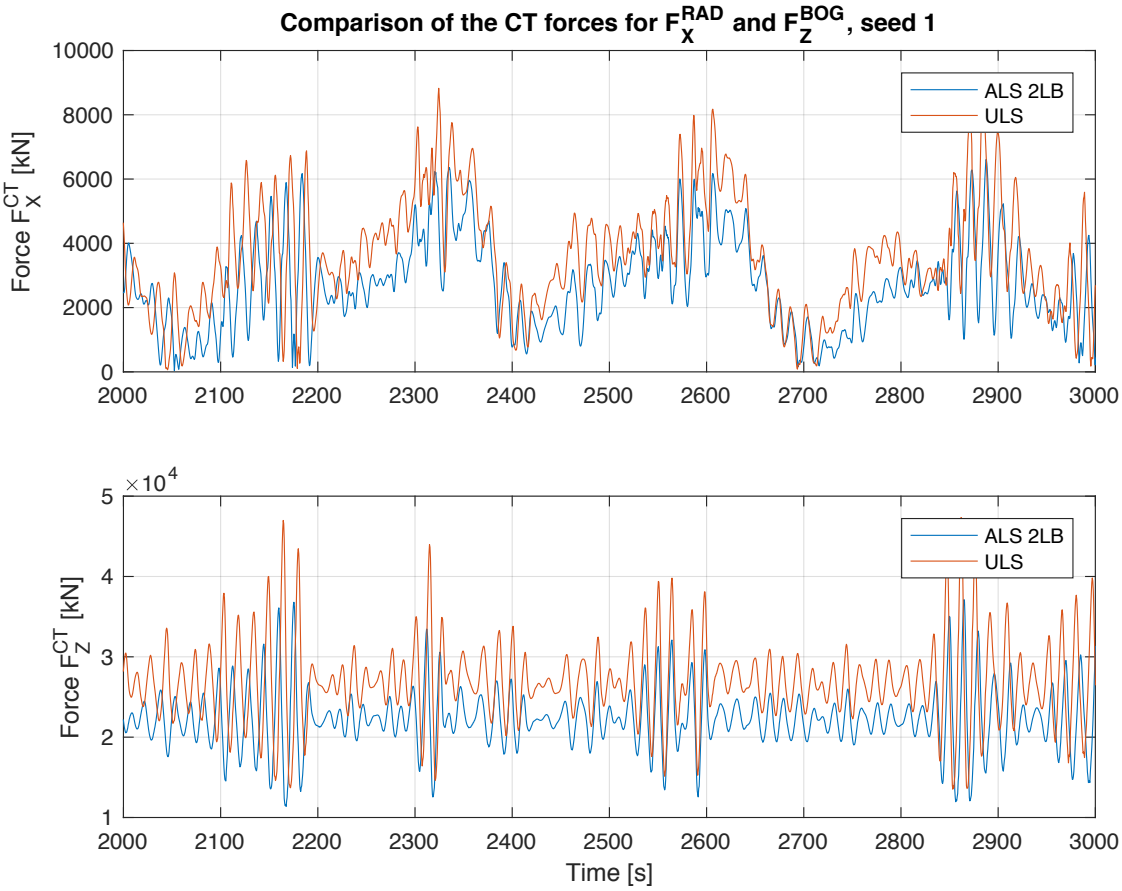

Figure 6.10: Comparison of the CT forces for F_X^{RAD} and F_Z^{BOG}, exemplified by seed 1

6.2.3 ALS Extreme

Both the wave and wind extreme definitions are presented and discussed. The extreme conditions are compared towards each other and concluded which is the dimensioning limit state for the FPSO. This condition is further discussed up against the other ULS and ALS cases for the in-line collinear condition.

Extreme Waves vs. Wind

Considering the offset of the two extreme limit state analyses, the extreme waves are slightly larger than the wind for both the MPM and 90% value. Table 6.21 displays the offset results. The difference for both values are around 1m which constitutes in a 1% or 2 % deviation. Hence, the wave and wind extreme definitions results in nearly equal vessel offset.

Table 6.21: Offsets for extreme waves and wind

	ALS Extreme			
	MPM	*90% fractile*	*MPM*	*90% fractile*
offset [m]	41.4	47.6	42.1	48.1

The tension in the mooring lines for the two cases are more interesting. Figure 6.11 displays the MPM tension for all mooring lines for the 10 000 year waves and wind definition. It is clear that the extreme waves results in a system which has higher loaded mooring lines compared to the extreme wind. This is especially true for the leeward moorings located in bundle 1 and 3, where the tension is 25% larger for the waves compared to the wind. The windward bundle on the other hand, has a smaller deviation, where the MPM tension for the moorings are approximately 6% larger for the waves.

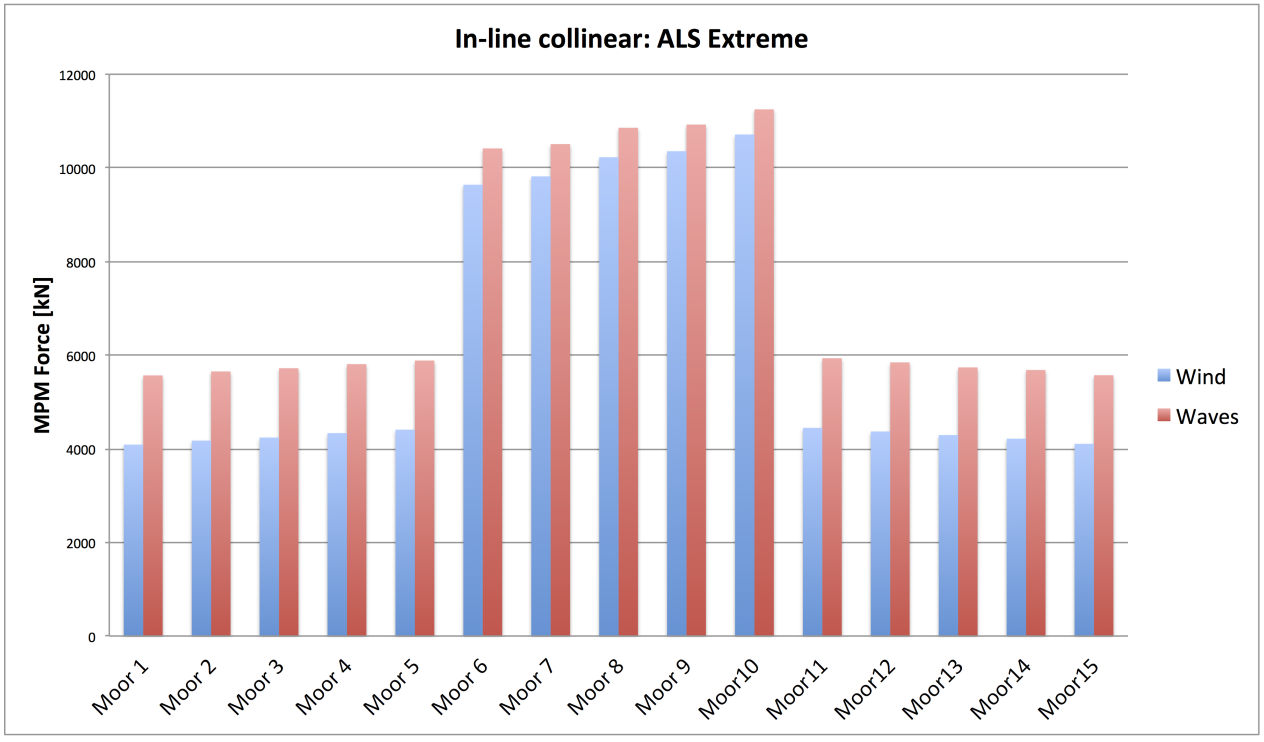

Figure 6.11: Comparison of the MPM tension for the mooring lines in the waves and wind ALS extreme definitions

Looking at the 90% fractile value of the tension gives a more complex picture. Here, the tensions in bundle 1 and 3 for the extreme waves are on average 27% and 20% larger compared

to the extreme wind weather. However, the most loaded bundle, i.e. the windward bundle 2, has approximately 7% larger tension compared to the extreme waves for the 90% fractile.

In Table 6.22 the safety factors for the MPM and 90% fractile values for the most loaded mooring line are compared for the upper line segment for the two ALS extreme conditions. All conditions fulfils the required safety factor provided by Statoil. The results implies that the extreme waves are dimensioning for the MPM values, while the extreme wind is dimensioning with respect to the 90% fractile value. As explained earlier, the MPM value should be used as the characteristic tension, hence the waves are considered as the worst extreme case regarding the tensions in the moorings.

Table 6.22: Comparison of the extreme waves and wind safety factors for mooring line 10 at segment 1

	Segment 1				
	MBL	*MPM*		*90% fractile*	
ALS Extreme	$[kN]$	sf_{max}	*margin*	sf_{max}	*margin*
Waves	25173	2.24	1.14	1.42	0.32
Wind	25173	2.35	1.25	1.33	0.23

The deviation of the dynamic turret support forces for the extreme weather are provided in Table 6.24. The results shows that the extreme waves have a much larger impact on the dynamic turret support forces than the extreme wind has. The 90% fractile is used for dimensioning the turret forces, and in this case the extreme wave condition has on average 34% larger forces than the extreme wind.

Table 6.23: Dynamic turret support force results for the in-line collinear intact and two anchor lines failures

	ALS Extreme: Waves			**ALS Extreme: Wind**		
	MPM	*90 % fractile*	*Stdev*	*MPM*	*90 % fractile*	*Stdev*
F_X^{RAD} *[kN]*	22709	26443	1955	19269	17672	1926
F_Z^{BOG} *[kN]*	86718	10340	7944	69006	66133	5056
M^{BOG} *[kNm]*	815120	951380	64910	692950	644380	56556

Comparing the magnitude of the deviations, the difference for the MPM is almost half of the difference of the 90% fractile. In other words, the PDF shape for the extreme waves and wind are quite different, i.e. the waves have much broader spectrum. This gives large differences when dimensioning the steel of the turret.

Table 6.24: Deviation between the dynamic turret support forces for the two extreme limit states

		Extreme Wind	
		MPM [%]	*90% fractile [%]*
Extreme Waves	F_X^{RAD}	15	33
	F_Z^{BOG}	20	36
	M^{BOG}	15	32

In conclusion, the environmental condition for the ALS extreme waves are definitely more critical compared to the extreme wind for the ship-shaped FPSO. This fits well with the expectation. Therefore the ALS extreme waves are further discussed compared to the ULS and other ALS cases.

6.2.4 Comparison of ALS extreme waves, ULS and ALS 1LB and 2LB

Vessel Offset

The MPM offset for the extreme waves condition is approximately 42m, which is nearly 3m and 8% larger than the intact condition. There is not an offset requirement for the extreme condition, nevertheless, the offset is well within the ULS criteria.

The probability density functions for the different limit states are compared in Figure 6.12. It can be seen that the MPM offset increases in the following order; intact, ALS extreme, ALS 1LB and 2LB. The width of the spectra are quite similar, this means that the spectra moves to the right, hence distributed over a higher range of maximum offsets.

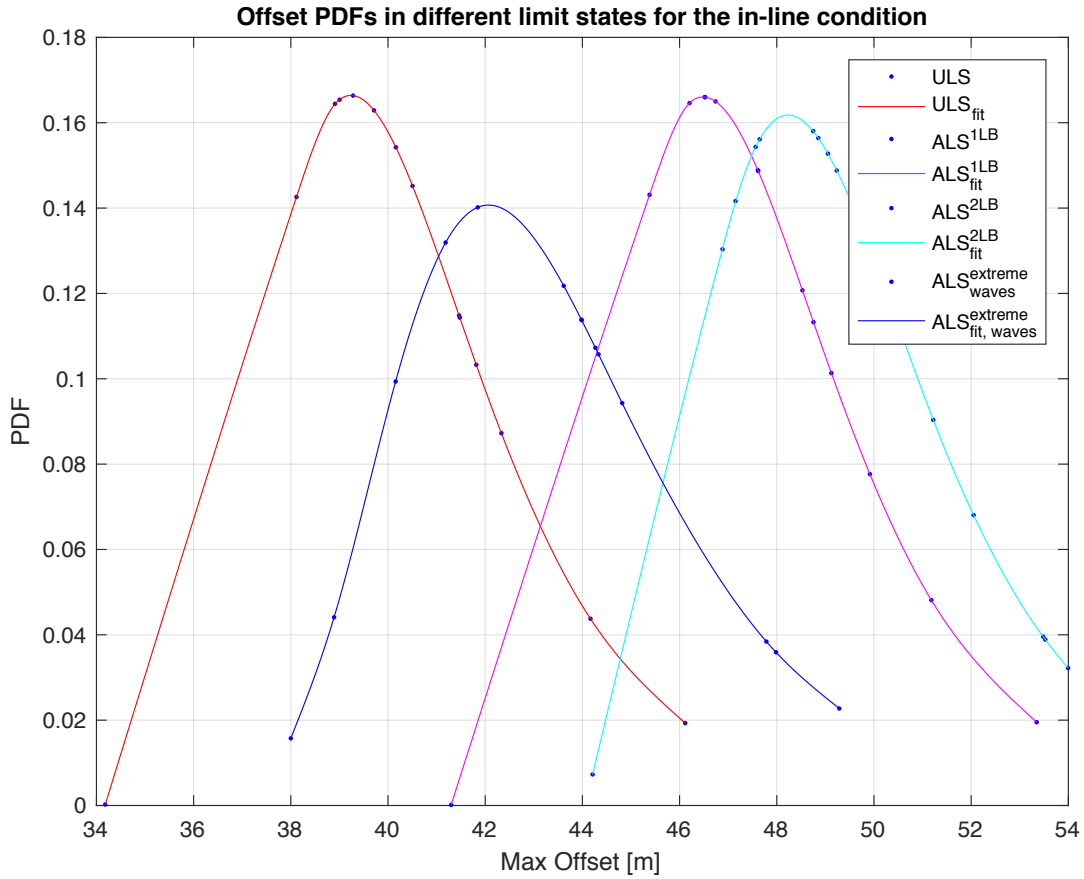

Figure 6.12: The probability density function for the different limit states for the in-line collinear condition

Comparing all the offsets values, both MPM and 90% fractile for the Gumbel distribution, implies that the offset requirement of 85m is not dimensioning considering in-line collinear condition. Table 6.25 displays the MPM and 90% fractile values for all limit states.

Table 6.25: Offset comparison for the in-line collinear condition in different limit states

Offset	**ULS**	**ALS 1LB**	**ALS 2LB**	**ALS extreme waves**
MPM [m]	39.2	46.5	48.2	42.1
90% fractile [m]	44.4	51.4	53.6	48.1

Top End Tension

All the mooring lines are active in the analysis for the ALS extreme waves. Bundle 1 and 2, which are the leeward mooring lines, have approximately 25% higher tension than the intact condition. Bundle 1 on the other hand, has only a 13% increase compared to the intact condition. The mean tension of all lines has increased from ≈ 6000kN to 7420kN going from intact to extreme condition, in other words the average tension has increased by 20%.

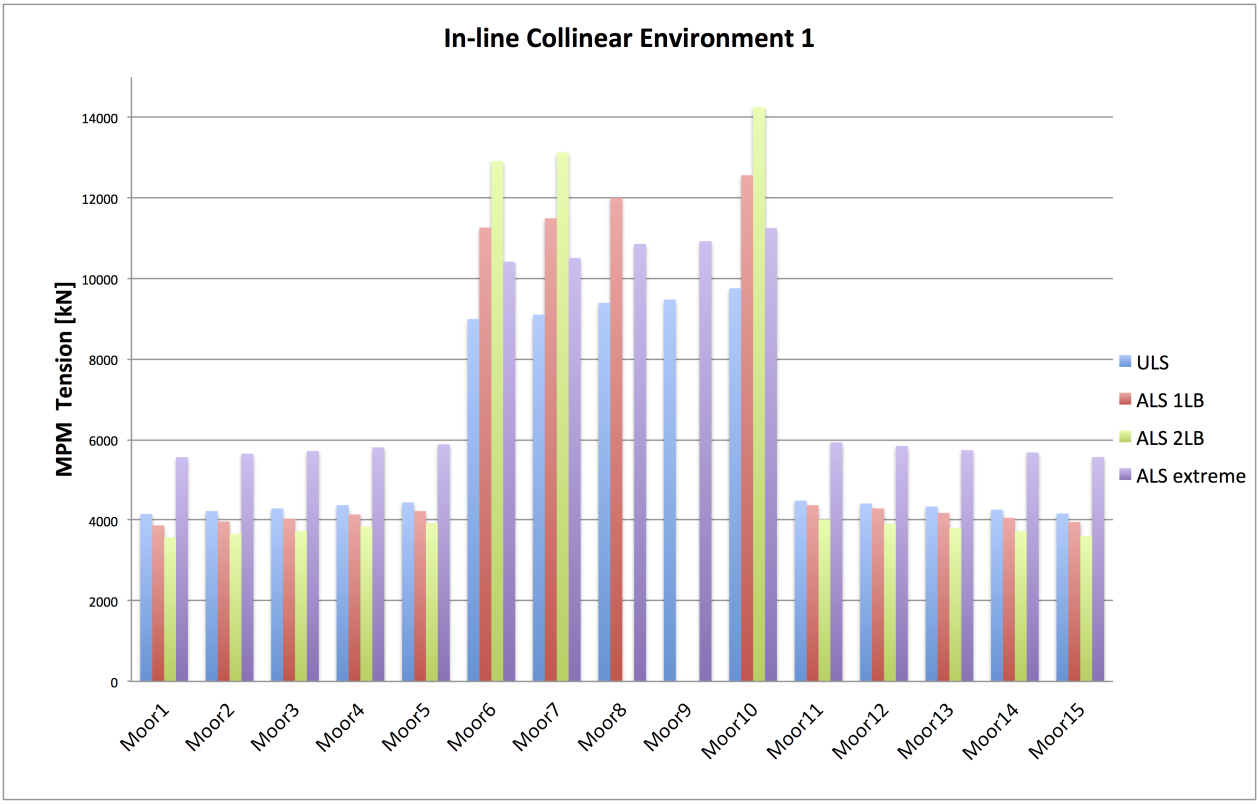

Figure 6.13: Comparison of MPM tension for the different limit states for the in-line collinear condition

All line tensions for the in-line collinear ULS and ALS cases are compared in Figure 6.13. From the results, there is a clear trend that the leeward lines, which are the slack lines, experiences less tension when a line is broken.

The windward lines experiences a severe increase, with mooring line 10 as the most loaded line for all limit states. The overall tension per mooring line for ALS extreme has approximately 20% higher tension than the intact condition. The safety factor for the most loaded line is within the internal criteria 1.1. This applies for both the MPM and 90% values, and all segments on the

line. The MPM safety factor margin for segment 1 was found to be 1.14, which is quite large compared to the other limit states. From Table 6.26 the dimensioning parameter is the safety factor from the two line failure analyses, with a margin of 0.27.

Table 6.26: Comparison of the safety factors for mooring line 10 at the fairlead, segment 1

	Segment 1			
	ULS	*ALS 1LB*	*ALS 2LB*	*ALS Extreme*
Requirement [-]	2.2	1.5	1.5	1.1
Safety factor [-]	2.58	2.00	1.77	2.24
Margin [-]	0.38	0.50	0.27	1.14

Dynamic Turret Support Forces

The extreme sea state with a return period of 10 000-years for the waves is approximately 17% larger for F_X^{RAD} and M^{BOG}, and 20% larger for F_Z^{BOG} compared to the intact condition, based on the MPM values.

The F_X^{RAD} probability density functions for the different limit states are compared in Figure 6.14. The results show that the 90% fractile for the two line break is close to the MPM value for one line break and intact conditions. Similarly, the intact and one line break condition 90% values are lower than the MPM value for the extreme ALS condition. The PDFs for F_Z^{BOG} and M^{BOG} have the same trend.

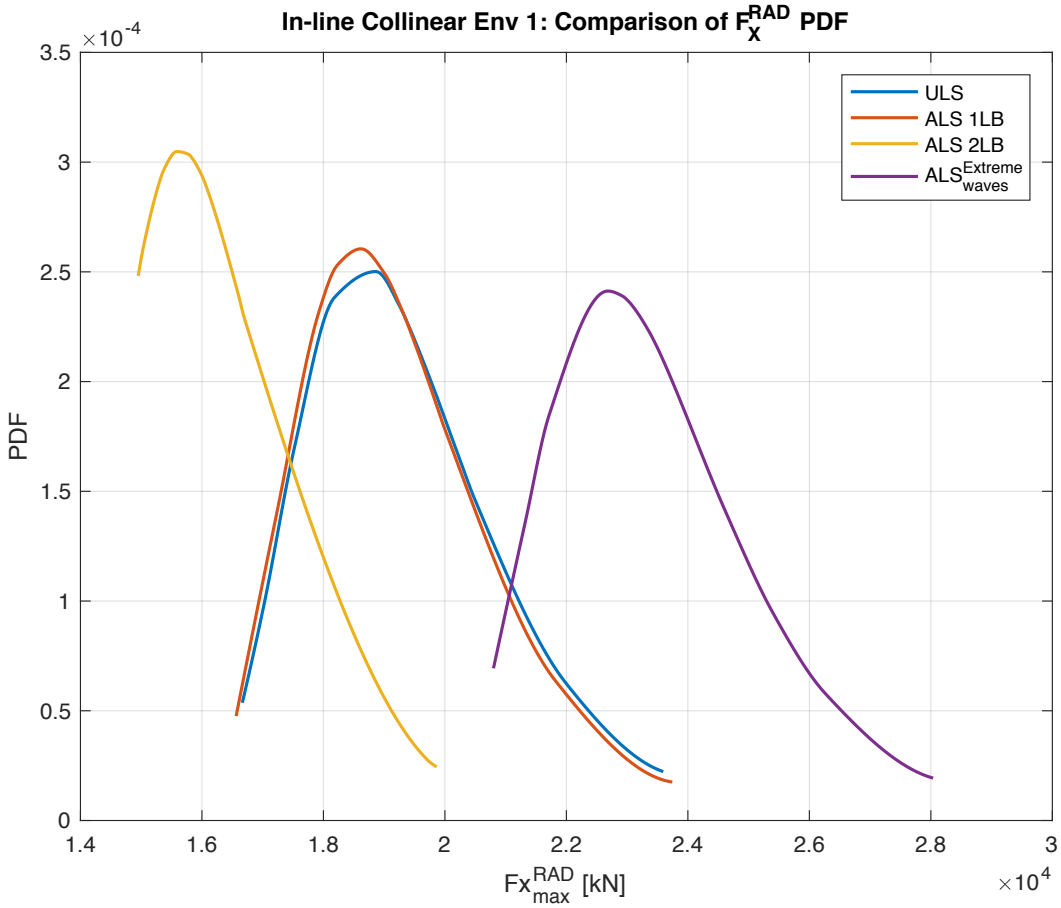

Figure 6.14: PDFs for F_X^{RAD} in different limit states for in-line collinear condition

Since the dynamic turret forces decreased when removing the mooring lines, the extreme condition has even larger dynamic support forces compared to these cases. This also implies that the uplift phenomena will be more critical in this sea state. Calculation of the uplift is performed in the next section.

6.3 Turret Uplift Estimation

The uplift is calculated for the in-line collinear intact condition and the case where the phenomena is most likely to occur, hence the ALS extreme waves in-line collinear condition is further examined. The principle calculating the turret support forces at the bogies are explained in Section 5.1.2. Based on the simple model described as alternative 1, assuming that all the dynamic support forces are accounted for in the end of the beam, an estimate of the net weight of the

turret can be quantified.

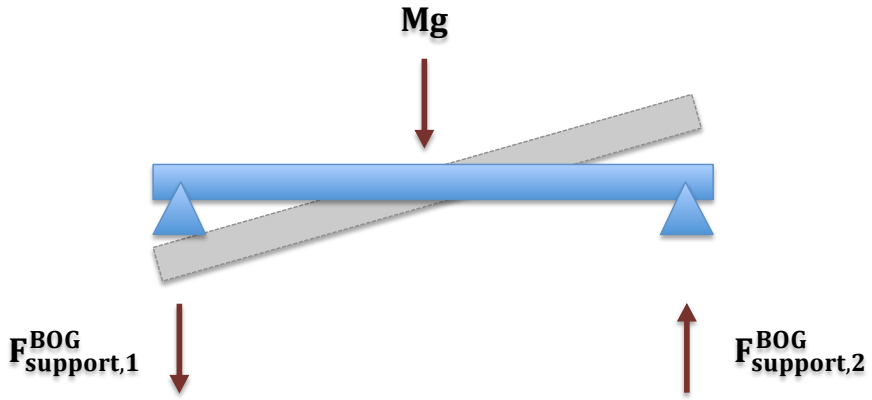

Figure 6.15: Principle sketch of how the turret mass can be estimated

The bogie support forces are found by using the equations given in Eq. 5.4. By neglecting the influence from buoyancy, since this is unknown, the turret weight can be found by applying beam theory for the principle sketch found in Figure 6.15.

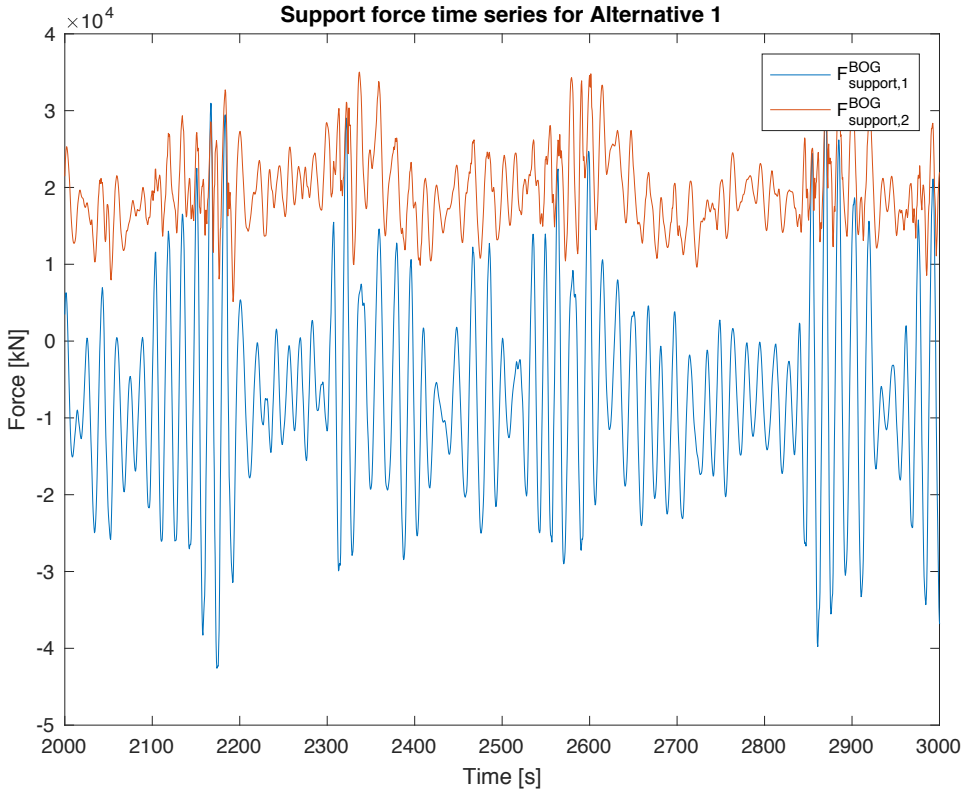

Figure 6.16: Sample time series of the support forces at bogies, seed 1

A sample of the time series for the support forces in seed 1 are plotted in Figure 6.16. This shows that the support force in end 1, $F^{BOG}_{support,1}$, is the critical force with respect to uplift. Hence, from moment equilibrium about beam end 2, the estimated net turret weight can be found as

$$M_{req} = -\frac{2}{g} \cdot max\left(F^{BOG}_{support,1}\right) \tag{6.1}$$

where g is the earth gravity, $max(F^{BOG}_{support,1})$ is the maximum negative force found from all 14 simulations and M_{req} is therefore the required turret weight in order to prevent uplift for all values found in the time series.

From calculations in MatLab the required turret mass is 12646 tonnes for the ALS extreme waves condition, which is over twice as much as the weight used in the turret model in SIMO, at 6100 tonnes from Table 5.6. The required turret mass for the intact condition were found to be 9411 tonnes, which is 35% larger than the given turret weight.

The results are expected to be somewhat conservative since, in addition to be a simplified 2D model, the buoyancy in water is not included, and that the dynamic turret support forces used in calculation of the turret bogie support force are based on the model with a weight of 6100 tonnes. An iteration process could be used to find a more accurate estimate, using the mass as input in the calculation of the turret dynamic support forces.

However, alternative 1 gives a rough estimate of what the turret weight should be. This approach is conservative, but considering the simplifications made, the results are of the right order of magnitude.

Chapter 7

Summary, Conclusions and Recommendations for Further Work

7.1 Summary and Conclusions

The main categories of station keeping are pure mooring systems, such as spread and single-point moorings, dynamic positioning systems and thruster-assisted mooring systems. Typical arrangements are taut, semi-taut and catenary systems. Mooring lines can be divided into several segments, with different material and buoyancy elements along the line. Mooring lines are often made of chain, synthetic fibre rope, wire rope or a combination of them. Two limit states are described and analysed, these are the intact and accidental limit state.

In order to design a mooring system, the top end motion must be calculated. The FPSO has several pipelines, and is therefore sensitive towards heave motions and offset in the horizontal direction. The equations of motion is solved in all six degrees of freedom to determine the responses, as the top end tension in the mooring lines. The motions of a mooring system is divided into static and dynamic motions. The static forces have contributions from the mean forces from waves, wind and current. The dynamic forces on the other hand, are defined by the low-frequent (LF) and wave-frequent (WF) motions from the waves and wind. For a moored vessel the surge, sway and yaw motions are excited by WF, LF and mean wave drift forces. Roll, heave and pitch responses are mainly caused by WF loads. The mooring system creates stiffness, hence a mooring system can be seen as the interaction between the elastic and geometrical stiff-

ness.

The software SIMO is used to perform simple intact and accidental limit state analyses in the time domain of the coupled SIMO-RIFLEX model. For simplicity the numerical model and the tested conditions are constrained. The contour line method was used to find the environments of interest, the directional distribution of the environments are shortened to three; in-between collinear and spread, and in-line collinear condition. The risers contribute around 20% to the total vertical force at bogies, due to the extra computational time and limitations in this thesis, the riser model is simplified by disabling the risers in the analyses. The number of required simulations, found from the Gumbel distributions for the dynamic turret support forces, are 14. The energy spectra of the offset motion shows that the risers induces a damping effect on the systems LF motions.

The following conclusions can be deduced:

- The three environments are compared for the in-between collinear condition in order to define the most severe environment. The results show that *environment 1*, located to the left of the contour line peak, is the most critical sea state considering the extreme responses as offset, top end tension and dynamic turret support forces. This is because ship-shaped units are sensitive to low-frequency motion, and therefore the sea state with the shortest wave period is the most critical one.

- By filtering the wave- and low-frequency motions, the energy spectra for these contributions are plotted. The results show that the LF motions provides a larger impact on the structure responses compared to the WF motions.

- The intact analyses consist of three different directional spreadings of environment 1, compared to each other. With respect to the vessel offset, the in-between collinear condition was most severe, with a MPM offset of 51.6 m. Considering the top end tension in the lines, the heaviest loaded line is found for the in-line collinear condition, with a safety factor of 0.38. The dynamic turret support forces are not subjected to any requirements, but the largest dynamic forces obtained among the three different directional distributions were in the in-line collinear condition.

- All mooring lines fulfils the intact and accidental requirements given by DNV GL (2015) for permanent units on the Norwegian Continental Shelf. In addition the vessel offset and ALS extreme condition are within the requirements provided by Statoil. The dimensioning parameter for the FPSO is the tension in the heaviest loaded line in the two anchor line failure analysis, with a margin of 0.27.

- The ALS extreme condition can be defined in three ways, with a 10 000year return period for the waves, wind or current. In this case only the two first are of importance when defining the most severe case. From the results the waves provided the highest responses of the vessel and mooring system. This is because the unit is ship-shaped, in other words streamlined, and do not have a dominating topside that provides much resistance in the case of extreme wind.

- The inertia terms of the dynamic turret support forces are very small in comparison to the mooring forces at fairlead for the FPSO. The forces F_X^{RAD} and M^{BOG} consist of both WF and LF forces, where the LF forces dominates, in contrast to F_Z^{BOG} which consist of WF motions.

- Among the analyses tested, the largest dynamic turret support forces are situated in the ALS extreme in-line collinear condition, hence this case is most prone to uplift. By use of a simplified turret model, described as alternative 1, the required weight to prevent uplift for the intact and ALS extreme in-line collinear condition were found to be 9411 tonnes and 12646 tonnes respectively. This is only a rough estimate, but the results are within reasonable values.

7.2 Recommendations for Further Work

The focus in this thesis has been to develop a foundation of the principles and the methodology of the design of mooring systems, and for a permanent system in particular. Therefore the subject has only been touched in the surface, not fully immersed into all areas.

Recommendations for further work are as follows:

- A couple of analyses in the time domain were performed. It would be interesting to get a more complete view of the system, and perform frequency domain analyses in addition and compare the results. This can be done by use of the software MIMOSA, which is a tailor made anchor line analysis program provided by DNV GL. By comparing the response, the importance of non-linear effects can be investigated.

- An interesting aspect might be to modify the composition of the mooring lines. This can be done by several measures; changing the number of lines, the dimensions in form of diameter and strength on one or several line segments, and/or the formation of the mooring system (e.g. having 4 clusters of lines connected to the turret). Then evaluation of the response for the different cases can be compared.

- In the simplified model of the FPSO, the risers are disconnected. This induces loss of confidence in the results. Hence, for a design analysis the risers must be included.

- The riser formation can also be investigated. Some examples are; smaller clusters, even spreading of the riser all around the turret or adding future risers.

- For marine constructions in general, the fatigue damage of a mooring system is an important design aspect. Within this theme, there are many paths to focus on. Some exemplifying suggestions are; which sea state contributes to highest fatigue loads or which segment is most prone to fatigue damage.

- The turret is only modelled as a beam in SIMO, the weight and dynamic turret support forces are then post-processed, these are large simplifications. A suggestion to gain a more holistic picture of the turret can be made by creating a 3D model of the turret including steel weight and entrapped water, providing turret support forces and a calculation of the uplift.

- A number of different sea states, spreading and distributions to find and understand the dimensioning parameters can be performed. Some exemplifying suggestions are; applying spread direction on the in-line condition to see how the tension distribution becomes, explore different in-line and in-between conditions (all bundles are unique, hence they

will provide different dimensioning parameters). In order to check the worst cases of the offset, a sensitivity study of the in-between condition should be tested.

References

Aas, K. (2017), Johan Castberg mooring design - Half way through FEED, where are we?, Statoil ASA, Tekna, DP and Mooring of offshore installations 2017.

API (2008), *Design and Analysis of Stationkeeping Systems for Floating Structures*, api recommended practice 2sk third edition, october 2005. addendum, may 2008. edn, American Petrolium Institute (API).

Barltrop, N., ed. (1998), *Floating Structures: a guide for design and analysis*, Vol. Two, The Centre for marine and Petroleum Technology (CPTM).

de Boom, W. (1989), The Development of Turret Mooring Systems for Floating Production Units, *in* 'OTC 5978', Single Buoy Moorings Inc., Offshore Technology Conferance (OTC), pp. 201–212.

Dezecot, C. & Eik, K. J. (2016), Metaocen Design Basis for the Barents Sea, $DocumentNo.: RE-SKR_$00001 Revision 6 (Final), Statoil ASA, Metaocean: Caroline Dezecot. Air temperatures, snow, icing, sea ice and icebergs: Kenneth J. Eik.

DNV GL (2015), *DNVGL-OS-E301: Position Mooring*, Det Norske Veritas Germanicher Lloyd (DNV GL).

Faltinsen, O. M. (1990), *Sea loads on ships and offshore structures*, Cambridge ocean technology series, Cambridge University Press, Cambridge.

Fylling, I. J. (1980), Analyses of Anchoring Systems, Report, The Ship Research Institute of Norway.

ISO (2013), *ISO 19901-7: Petroleum and natural gas industries - Specific requirements for offshore structures: Stationkeeping systems for floating offshore structures and mobile offshore units*, 2nd edn, International Organization for Standardization (ISO), Geneva, CH.

Kvitrud, A. (2014), Anchor Line Failures - Norwegian Continental Shelf 2010-2014, Technical report, Petroliumstilsynet (PTIL).

Larsen, C. M. (2014), *TMR 4182 Marine dynamics*, Akademika Forlag.

Larsen, K. (2015), Static equilibrium of a mooring line, Technical report, NTNU.

Larsen, K. (2016), TMR4225 Marine Operations Lecture Notes # 8 – Station keeping and mooring systems, Lecture, Norwegian University of Science and Technology (NTNU).

Larsen, K. (2017), Mail from Kjell Larsen. Recieved Thursday April 27th.

Lund, A. (2011), *Skipsteknikk*, number ISBN 978 – 82 – 7674 – 647 – 1, 5th edn, Fagbokforlaget Vigmostad og Bjørke AS.

MARINTEK (2016*a*), *RIFLEX 4.8.2 Theory Manual*.

MARINTEK (2016*b*), *SIMO 4.8.2 Theory Manual*.

MARINTEK (2016*c*), *SIMO 4.8.2 User Manual*.

Myrhaug, D. & Lian, W. (2009), *Marine Dynamics: Lecture Notes*, NTNU.

Naciri, M., Jamet, C., Daran, R., Vedeld, S., Drijver, P. & Visser, V. (2011), 'The Skarv FPSO turret mooring system: A 5.000 -ton challenge'.
URL: *http://www.offshore-mag.com/articles/print/volume-71/issue-1/drilling-__completion/the-skarv-fpso-turret-mooring-system-a-5000-ton-challenge.html*

Naess, A. & Gaidai, O. (2008), 'Estimation of extreme values from sampled time series', *Elsevier, Structural Safety 31 (2009) 325-334* .

NORSOK Standard (2007), *NORSOK N-003: Actions and action effects*, 2 edn, NORSOK Standard, Strandveien 18, P.O. Box 242 N-1326 Lysaker NORWAY.

Ormberg, H. & Larsen, K. (1998), 'Coupled analysis of floater motion and mooring dynamics for a turret-moored ship', *Elsevier Science Ltd: Applied Ocean Research* (20), 55–67.

Paik, J. K. & Thayamballi, A. K. (2007), *Ship-Shaped Offshore Installations*, Cambridge University Press.

SBM Offshore (2012), *SBM Offshore | Turret Solutions* , SBM Offshore.

Statoil (2016), Characteristic value of «Design Limit». Classification: Internal.

Statoil (n.d.), Model Description. Model Description in SIMA.

Steen, S. (2014), *Lecture Notes TMR7: Experimental Methods in Marine Hydrodynamics*, Akademika Forlag, Marine Technology Centre Trondheim, Norway.

Svalastog, Å. K. D. (2016), Design of Mooring Systems with Focus on Frequency Domain Analysis of a Turret Moored FPSO, Project Thesis, Norwegian University of Science and Technology (NTNU).

Appendix A

Simplified Dynamic Equilibrium of the Turret

The simplified, global dynamic turret model is used to find the three responses of interest when designing the turret

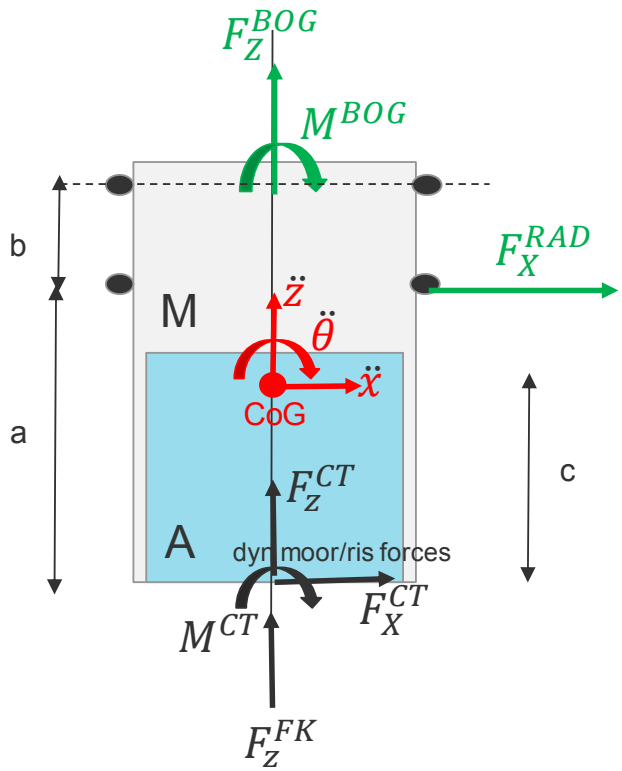

Figure A.1: Simplified dynamic equilibrium of turret (Larsen 2017)

Figure A.1 gives:

Equilibrium in horizontal direction

$$\sum F_X = (M+A)\cdot \ddot{x}$$

$$\Rightarrow F_X^{CT} + F_X^{RAD} = (M+A)\cdot \ddot{x}$$

$$\Rightarrow F_X^{RAD} = (M+A)\cdot \ddot{x} - F_X^{CT} \tag{A.1}$$

Equilibrium in vertical direction

$$\sum F_Z = (M+A)\cdot \ddot{z}$$

$$\Rightarrow F_Z^{FK} + F_Z^{CT} + F_Z^{BOG} = (M+A)\cdot \ddot{z}$$

$$\Rightarrow F_Z^{BOG} = (M+A)\cdot \ddot{z} - F_Z^{CT} - F_Z^{FK} \tag{A.2}$$

Moment equilibrium at turret COG

$$\sum M^{COG} = I^{COG}\cdot \ddot{\Theta}$$

$$\Rightarrow M^{CT} - F_X^{CT}\cdot(a+b+c) - F_X^{RAD}\cdot(b+c) + M^{BOG} = I^{COG}\cdot\ddot{\Theta}$$

$$\Rightarrow M^{BOG} = I^{COG}\cdot\ddot{\Theta} - M^{CT} + F_X^{CT}\cdot(a+b+c) + F_X^{RAD}\cdot(b+c)$$

$$\Rightarrow M^{BOG} = I^{COG}\cdot\ddot{\Theta} - M^{CT} - F_X^{CT}\cdot a + (M+A)\cdot\ddot{x}\cdot(b+c) \tag{A.3}$$

The three main equations are Equation A.1, A.2 and A.3.

Appendix B

Environmental Conditions in the Barents Sea

The data used in the metaocean design basis written by Dezecot & Eik (2016) lies as an attachment.

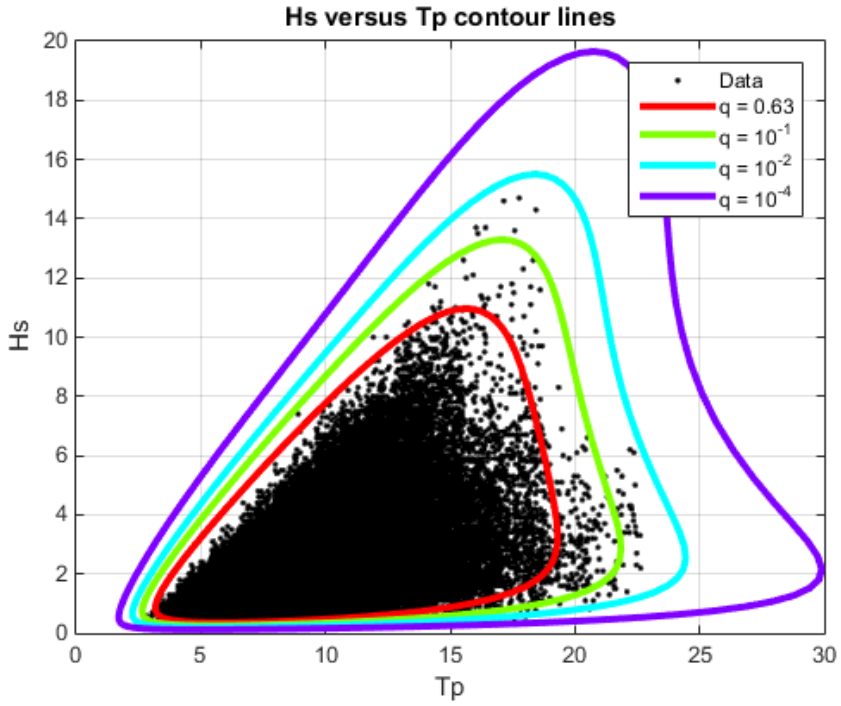

Figure 3-9 **q – probability contour lines of H_S – T_p for q = 0.63, 10^{-1}, 10^{-2} and 10^{-4} for omni-directional waves at the [redacted] Field. Duration of sea state is 3 hours.**

Table 3-13 **q – probability contour values of H_S – T_p for q = 0.63, 10^{-1}, 10^{-2} and 10^{-4} for omni-directional waves at the [redacted] Field. Duration of sea state is 3 hours. T_{pL} and T_{pH} are lower and higher limits of T_p, respectively.**

Annual probability of exceedance											
0.63			10^{-1}			10^{-2}			10^{-4}		
H_S [m]	T_{pL} [s]	T_{pH} [s]	H_S [m]	T_{pL} [s]	T_{pH} [s]	H_S [m]	T_{pL} [s]	T_{pH} [s]	H_S [m]	T_{pL} [s]	T_{pH} [s]
10.9	15.7	15.7	13.3	17.2	17.2	15.5	18.5	18.5	19.8	20.9	20.9
10.0	13.0	17.3	13.0	15.8	18.1	15.0	16.6	19.7	19.0	18.6	22.3
9.0	11.6	17.8	12.0	14.0	19.0	14.0	15.1	20.4	18.0	17.1	23.0
8.0	10.3	18.2	11.0	12.7	19.4	13.0	13.8	20.7	17.0	15.9	23.3
7.0	9.1	18.5	10.0	11.5	19.7	12.0	12.7	21.0	16.0	14.9	23.5
6.0	7.9	18.8	9.0	10.3	19.9	11.0	11.6	21.2	15.0	13.9	23.6
5.0	6.8	19.0	8.0	9.3	20.2	10.0	10.5	21.4	14.0	13.0	23.7
4.0	5.8	19.2	7.0	8.2	20.5	9.0	9.5	21.7	13.0	12.0	23.8
3.0	4.8	19.2	6.0	7.1	20.9	8.0	8.5	22.0	12.0	11.1	23.9
2.0	3.9	18.7	5.0	6.1	21.2	7.0	7.5	22.4	11.0	10.2	24.1
1.0	3.0	17.0	4.0	5.2	21.6	6.0	6.5	22.8	10.0	9.3	24.3
			3.0	4.2	21.8	5.0	5.6	23.3	9.0	8.4	24.7
			2.0	3.4	21.5	4.0	4.7	23.9	8.0	7.4	25.1
			1.0	2.5	19.9	3.0	3.8	24.3	7.0	6.5	25.7
						2.0	3.0	24.2	6.0	5.6	26.5

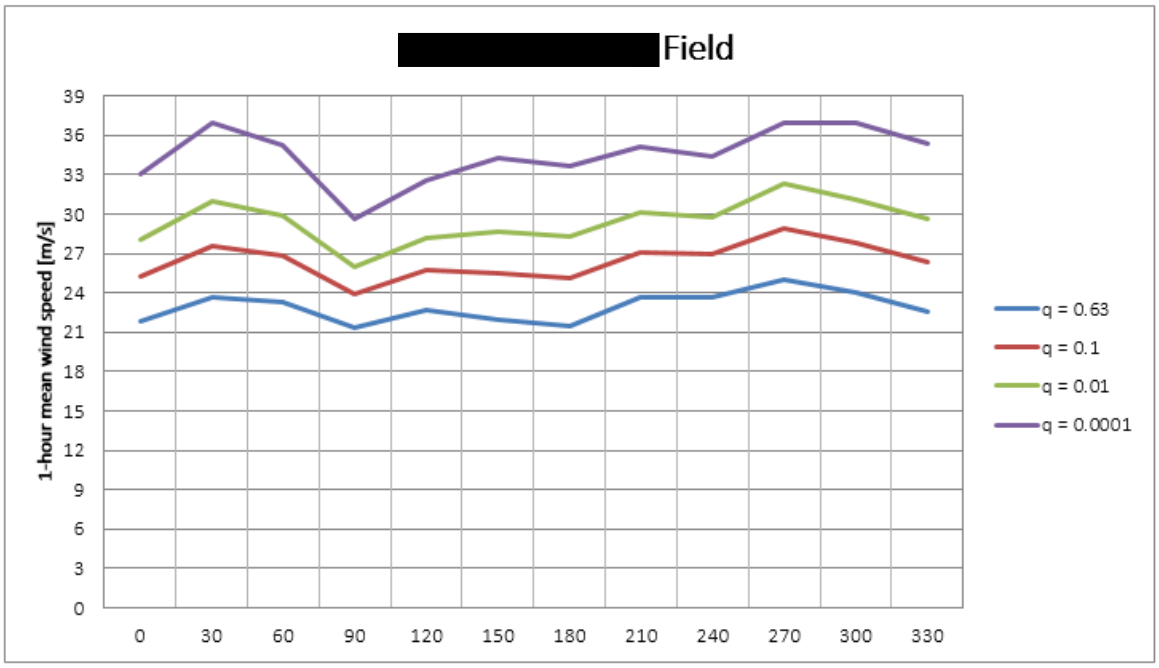

Figure 2-5 **Directional extreme values of 1-hour mean wind speed of annual probability of exceedance of 0.63, 10^{-1}, 10^{-2} and 10^{-4} 10 m above sea level at the [redacted] Field.**

Table 2-6 **Directional and omni-directional Weibull parameters and corresponding extreme values for 1-hour mean wind speed 10 m above sea level at the [redacted] Field. Duration of event is 1 hour.**

Direction	Sector prob.	Weibull parameters			Annual probability of exceedance			
		Shape	Scale	Location	0.63	10^{-1}	10^{-2}	10^{-4}
-	[%]	-	[m/s]	[m/s]	[m/s]	[m/s]	[m/s]	[m/s]
0°	7.73	2.129	9.03	0.04	22.0	25.0	28.0	33.0
30°	8.51	1.926	8.64	0.67	23.5	27.5	31.0	37.0
60°	9.56	2.023	8.75	0.82	23.5	27.0	30.0	35.0
90°	11.81	2.706	10.82	-0.71	21.5	24.0	26.0	29.5
120°	9.91	2.436	10.59	-0.48	22.5	25.5	28.0	32.5
150°	6.67	1.961	8.30	0.53	22.0	25.5	28.5	34.0
180°	6.01	1.988	8.40	0.35	21.5	25.0	28.5	33.5
210°	7.92	2.268	10.52	-0.38	23.5	27.0	30.0	35.0
240°	8.60	2.375	10.94	-0.57	23.5	27.0	29.5	34.5
270°	8.38	2.056	9.96	0.10	25.0	29.0	32.5	37.0*
300°	8.04	2.003	9.20	0.43	24.0	28.0	31.0	37.0
330°	6.87	1.933	8.43	0.45	22.5	26.5	29.5	35.5
0° - 360°	**100.00**	**2.140**	**9.45**	**0.18**	**26.5**	**29.5**	**32.5**	**37.0**

** Indicates when the directional extreme doesn't correspond to the Weibull parameters as adjusted to the omnidirectional extreme value.*

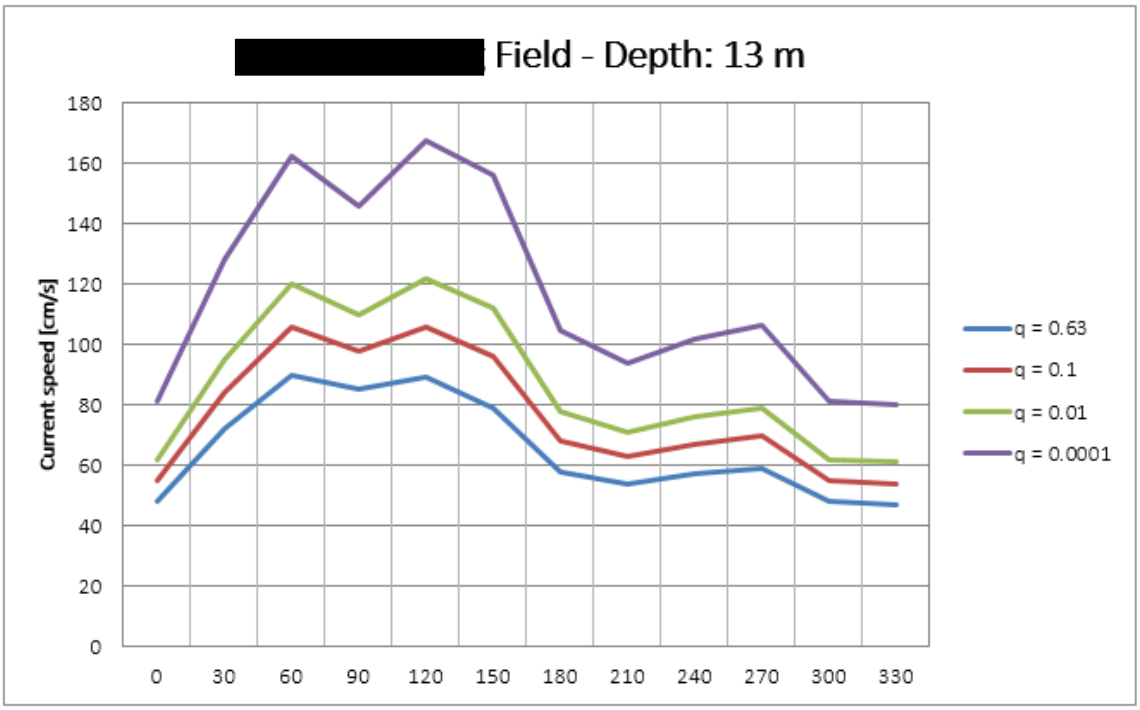

Figure 4-12 **Direction variation of current speed of annual probability of exceedance of 0.63, 10^{-1} and 10^{-2} at 13 m depth at the [redacted] Field.**

Table 4-14 **Weibull parameters and corresponding extreme values for the sector and omni-directional distributions of current speed at 13 m depth at the [redacted] Field. Duration of extreme event is 10 minutes.**

Direction sector	Sector prob.	Weibull parameters			Annual probability of exceedance			
		Shape	Scale	Location	0.63	10^{-1}	10^{-2}	10^{-4}
[°]	[%]	-	[cm/s]	[cm/s]	[cm/s]	[cm/s]	[cm/s]	[cm/s]
0	5.40	1.804	15.22	0.06	48	55	62	81
30	8.62	1.499	16.87	1.84	72	84	95	128
60	15.30	1.395	17.95	3.72	90	106	120	162
90	18.16	1.543	19.60	2.99	85	98	110	146
120	12.49	1.280	15.42	4.75	89	106	122	167
150	7.61	1.233	13.61	3.34	79	96	112	156
180	5.78	1.527	14.51	1.38	58	68	78	104
210	5.72	1.666	15.40	0.23	54	63	71	94
240	5.56	1.580	15.09	1.06	57	67	76	102
270	5.89	1.541	14.98	1.44	59	70	79	106
300	4.82	1.760	14.78	-0.02	48	55	62	81
330	4.65	1.775	14.72	0.08	47	54	61	80
0 – 360	**100.00**	**1.324**	**15.47**	**3.02**	**97**	**111**	**125**	**167**

Appendix C

Riser Consideration

Some of the main comparisons done in Excel is included here to support the discussion about the importance of including risers in the analyses.

No risers	**Risers**	**Deviation**
Mean Offset	Mean Offset	NoRiser/Riser
m	m	%
21,61	25,10	13,90
20,42	24,03	15,02
20,06	23,59	14,96

No risers	**Risers**	**Deviation**	
Std Offset	Std Offset	NoRiser/Rise	NoRiser/Riser
m	m	%	%
8,12	7,26	-11,83	10,58
7,37	6,63	-11,21	10,08
7,15	6,42	-11,23	10,10

Figure C.1: Comparison of mean and standard deviation for the offsets

	MEAN TENSION (COLLINEAR INBETWEEN)											
	No risers:				With risers:					No riser		
		Tmean Env1 [kN]	Tmean Env2 [kN]	Tmean Env3 [kN]		Tmean Env1 [kN]	Tmean Env2 [kN]	Tmean Env3 [kN]		Tmean Env1 %	Tmean Env2 %	Tmean Env3 %
Bundle 1 (windward)	Moor1	2578,30	2548,70	2540,40	Moor1	2643,00	2614,30	2604,60	With riser	2,45	2,51	2,46
	Moor2	2633,20	2600,50	2591,40	Moor2	2707,10	2675,00	2663,60		2,73	2,79	2,71
	Moor3	2689,90	2653,40	2642,30	Moor3	2773,30	2737,60	2724,30		3,01	3,08	3,01
	Moor4	2744,50	2704,80	2692,40	Moor4	2837,80	2798,60	2783,30		3,29	3,35	3,27
	Moor5	2800,60	2756,60	2742,90	Moor5	2903,20	2860,40	2843,50		3,53	3,63	3,54
Bundle 2 (windward)	Moor6	3025,60	2982,10	2952,60	Moor6	3128,00	3088,60	3054,80		3,27	3,45	3,35
	Moor7	2972,70	2933,80	2905,40	Moor7	3067,20	3032,40	2999,90		3,08	3,25	3,15
	Moor8	2922,50	2887,70	2860,60	Moor8	3004,40	2973,40	2942,80		2,73	2,88	2,79
	Moor9	2867,00	2836,50	2810,90	Moor9	2940,70	2914,20	2885,10		2,51	2,67	2,57
	Moor10	2814,60	2788,20	2763,60	Moor10	2876,40	2853,40	2826,00		2,15	2,28	2,21
Bundle 3 (leeward)	Moor11	1442,10	1466,10	1481,30	Moor11	1366,20	1386,60	1402,80		-5,56	-5,73	-5,60
	Moor12	1435,70	1459,50	1475,00	Moor12	1358,60	1378,50	1395,30		-5,67	-5,88	-5,71
	Moor13	1430,20	1453,60	1469,60	Moor13	1355,00	1374,70	1391,80		-5,55	-5,74	-5,59
	Moor14	1427,30	1450,30	1466,50	Moor14	1350,70	1370,00	1387,40		-5,67	-5,86	-5,70
	Moor15	1425,50	1448,40	1464,70	Moor15	1351,20	1370,50	1388,00		-5,50	-5,68	-5,53

Figure C.2: Mean axial tension for the systems with and without risers present

	STANDARS DEVIATION TENSION (COLLINEAR INBETWEEN)								Deviation	No riser		
	No risers	Tstd Env1 [kN]	Tstd Env2 [kN]	Tstd Env3 [kN]	Risers	Tstd Env1 [kN]	Tstd Env2 [kN]	Tstd Env3 [kN]		Tmean Env1 %	Tmean Env2 %	Tmean Env3 %
Bundle 1 (windward)	Moor1	508,41	480,84	407,84	Moor1	517,16	489,32	414,33	**With riser**	1,69	1,73	1,57
	Moor2	515,85	483,59	413,25	Moor2	525,20	492,62	420,02		1,78	1,83	1,61
	Moor3	528,84	491,38	423,08	Moor3	538,05	500,58	429,82		1,71	1,84	1,57
	Moor4	537,76	495,57	429,98	Moor4	546,57	504,22	436,55		1,61	1,72	1,50
	Moor5	553,46	506,06	442,36	Moor5	562,18	514,98	448,82		1,55	1,73	1,44
Bundle 2 (windward)	Moor6	564,50	508,06	457,43	Moor6	559,41	504,89	452,99		-0,91	-0,63	-0,98
	Moor7	541,93	489,94	438,62	Moor7	536,52	486,01	433,78		-1,01	-0,81	-1,12
	Moor8	530,64	482,26	428,53	Moor8	526,96	479,94	424,96		-0,70	-0,48	-0,84
	Moor9	510,80	466,81	411,98	Moor9	506,98	463,81	408,13		-0,75	-0,65	-0,94
	Moor10	501,44	461,10	403,60	Moor10	499,11	459,62	401,01		-0,47	-0,32	-0,65
Bundle 3 (leeward)	Moor11	393,34	421,37	359,14	Moor11	354,40	381,34	324,75		-10,99	-10,50	-10,59
	Moor12	394,16	422,36	360,46	Moor12	355,25	382,39	325,89		-10,95	-10,45	-10,61
	Moor13	390,08	418,48	357,33	Moor13	351,35	378,46	322,98		-11,02	-10,57	-10,64
	Moor14	392,54	421,39	359,79	Moor14	354,36	381,70	325,56		-10,77	-10,40	-10,51
	Moor15	389,59	418,30	357,47	Moor15	351,50	378,73	323,13		-10,84	-10,45	-10,63

Figure C.3: Axial tension standard deviation for the systems with and without risers present

RISER CONTRIBUTION
In-between collinear

Sensitivity study for the vertical loads at fairlead

MEAN

	No Risers FzBOG Inerti [kN]	**With risers** FzBOG Inerti [kN]	Deviation [%]
Env1	4952,80	4950,20	-0,05
Env2	4612,10	4605,50	-0,14
Env3	4182,30	4175,20	-0,17

The inertia forces are practicly the same with and without risers

	No Risers Fz CT mean [kN]	**With risers** Fz CT mean [kN]	Deviation [%]
Env1	27314,00	33712,00	18,98
Env2	27193,00	33597,00	19,06
Env3	27118,00	33508,00	19,07

The vertical chain table force for the different cases is approx
19% larger for the system with risers vs the system without risers

STD

	No Risers Inertia_FzBO [kN]	**With risers** Inertia_FzBO [kN]	Deviation [%]
Env1	3637,90	3632,70	-0,14
Env2	3376,40	3368,40	-0,24
Env3	3070,10	3063,90	-0,20

	No Risers Fz_CT_std [kN]	**With Risers** Fz_CT_std [kN]	Deviation [%]
Env 1	5144,20	5596,40	8,08
Env 2	5062,90	5458,80	7,25
Env 3	4269,00	4619,80	7,59

Std for Fz CT is 7-8% larger for the system with risers vs no risers

Figure C.4: Sensitivity study for the vertical loads at fairlead

DYNAMIC TURRET SUPPORT FORCES			
No risers			
	Env1	Env2	Env3
FxRAD_mean	3952,60	3733,60	3662,50
FzBOG_mean	27316,00	27196,00	27121,00
MBOG_mean	126140,00	119690,00	117090,00
FxRAD_std	3088,70	3471,10	3008,40
FzBOG_std	8113,10	7875,00	6805,20
MBOG_std	119900,00	126970,00	110220,00

With risers			
	Env1	Env2	Env3
FxRAD_mear	4408,60	4197,30	4123,40
FzBOG_mear	33714,00	33600,00	33511,00
MBOG_mear	160330,00	154240,00	151450,00
FxRAD_std	3061,80	3447,00	2985,60
FzBOG_std	7826,60	7624,80	6538,70
MBOG_std	121250,00	127220,00	110660,00

Figure C.5: Mean and standard deviation for the dynamic turret support forces

		No Risers		
		Deviation env 1 [%]	Deviation env 2 [%]	Deviation env 3 [%]
With Risers	FxRAD_mea	10,34	11,05	11,18
	FzBOG_mea	18,98	19,06	19,07
	MBOG_mea	21,32	22,40	22,69
	FxRAD_std	-0,88	-0,70	-0,76
	FzBOG_std	-3,66	-3,28	-4,08
	MBOG_std	1,11	0,20	0,40

Figure C.6: Dynamic contribution comparison in percent between system with and without risers

Appendix D

Number of Required Simulations

The rest of the PDFs and Gumbel parameters which are used as a foundation when deciding the number of required simulations, N_{req}.

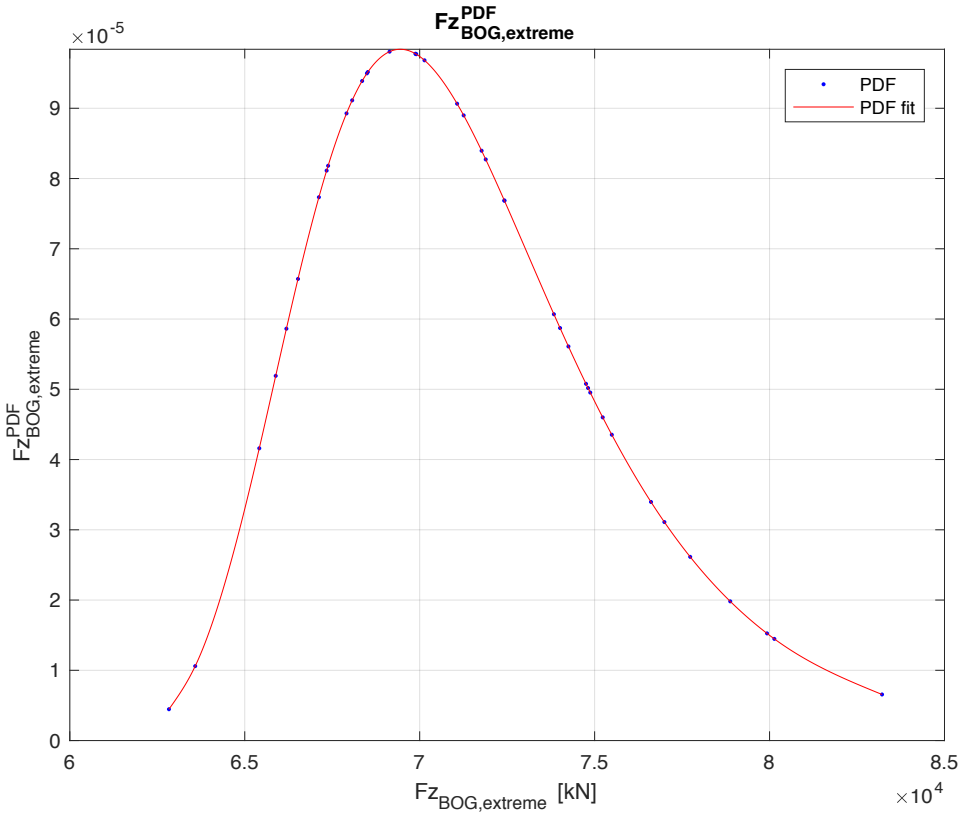

Figure D.1: Probability density function for the vertical force at bogies, F_Z^{BOG} based on 40 simulations

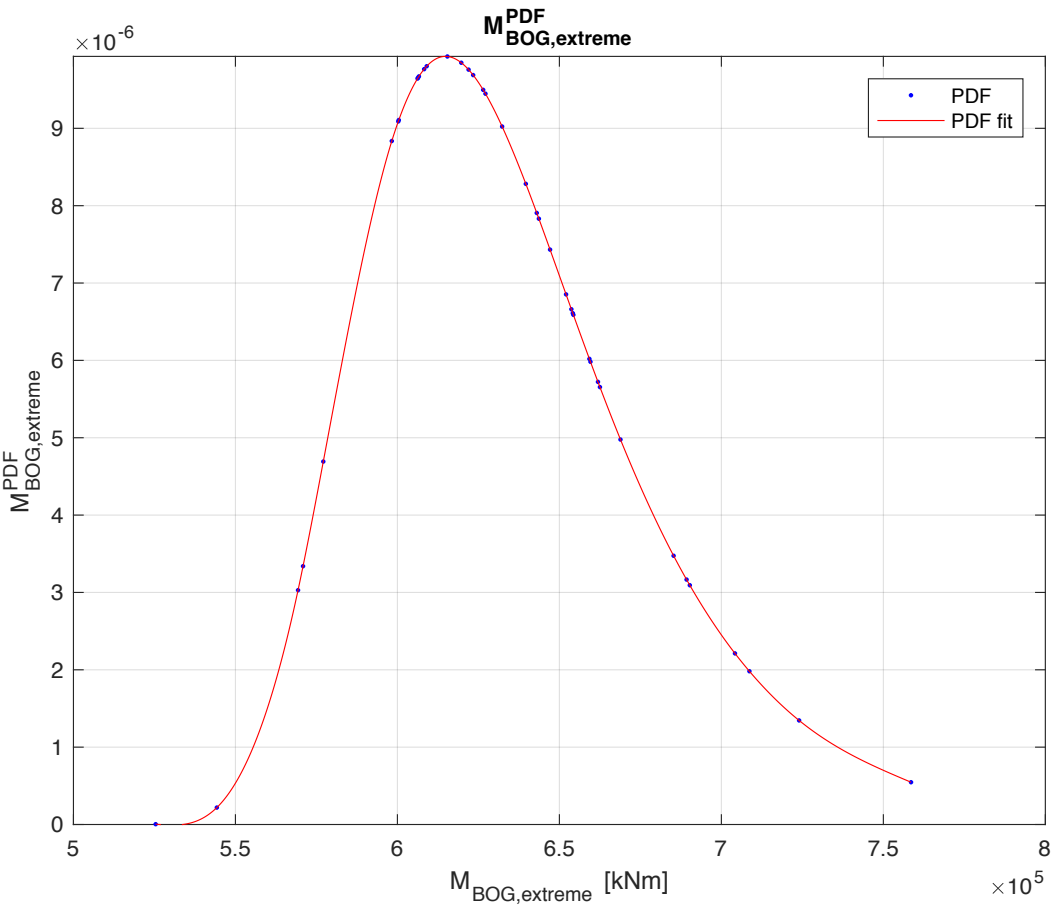

Figure D.2: Probability density function for the moment at bogies, M^{BOG} based on 40 simulations

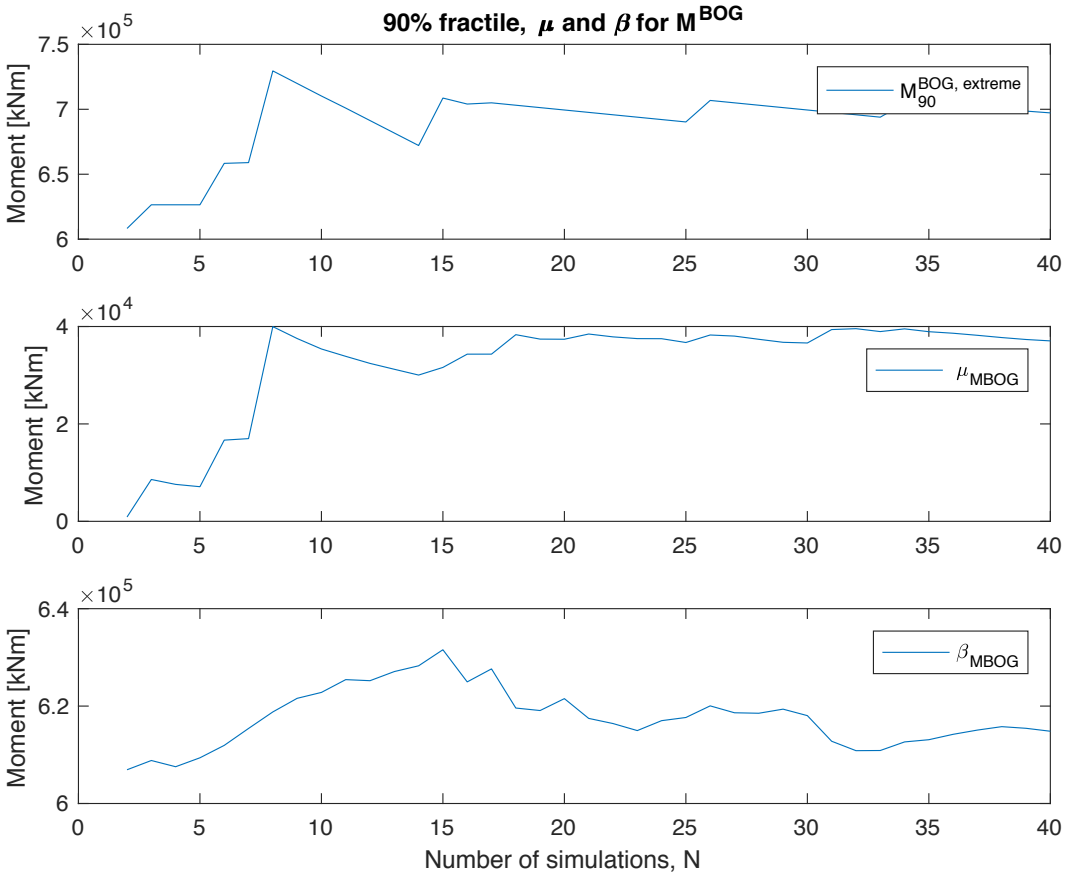

Figure D.3: 90% fractile, μ and β for M^{BOG} based on 40 simulations

Appendix E

Ultimate Limit State Results

The results presented here is not given in tables in the thesis text.

E.1 In-between Collinear All Environments

The following results are based on 14 simulations with different wind and wave seeds for each environmental condition denoted as env 1, env 2 and env 3.

MPM vs 90 % fractile

Inbetween collinear 14 Seeds

	Env 1		Env 2		Env 3	
	MPM Tension [kN]	90% fractile [kN]	MPM Tension [k	90% fractile [kN]	MPM Tension [kN	90% fractile [kN]
Moor1	5793	6388,40	5660	6296,20	5070	5578,00
Moor2	5927	6597,10	5745	6413,00	5156	5680,00
Moor3	6081	6818,70	5845	6596,70	5250	5852,90
Moor4	6240	6949,70	5935	6726,80	5348	6019,50
Moor5	6407	7147,90	6031	6835,30	5490	6213,80
Moor6	6811	7732,60	6258	6842,10	5822	6646,20
Moor7	6618	7445,60	6130	6703,80	5679	6468,30
Moor8	6473	7246,50	6045	6574,20	5576	6301,70
Moor9	6290	7041,30	5926	6442,40	5445	6114,10
Moor10	6139	6812,20	5836	6394,40	5348	5947,00
Moor11	3450	4367,50	3854	4570,80	3372	3975,80
Moor12	3465	4358,40	3860	4566,10	3379	3956,10
Moor13	3441	4333,10	3845	4564,80	3372	3946,00
Moor14	3468	4344,40	3859	4596,80	3376	3949,40
Moor15	3448	4324,10	3831	4548,50	3366	3949,10
Max Tension	6811,30	7732,60	6258,30	6842,10	5822,30	6646,20
Mean Tension	5336,81	6127,17	5243,93	5911,46	4736,55	5373,19
Sf max	3,7	3,255	4,0	3,679	4,3	3,788
Sf margin	1,496	1,055	1,822	1,479	2,124	1,588
SF1 vs Sf2	-21,83276927					

Figure E.1: MPM and 90% fractile values for the three environments

Deviation 90% fractile		
	Env 2	Env 3
Env 1	[%]	[%]
	-4,0	8,4
	-2,4	8,8
	-5,2	7,1

Figure E.2: Deviation between the 90% fractile for the different environments

Deviation between MPM			
		Env 2	Env 3
Env 1	FxRAD_MPM	-0,3	8,2
	FzBOG_MPM	0,4	11,5
	MBOG_MPM	1,2	11,6

Figure E.3: Deviation between the MPM values for the different environments

E.2 Comparison of Directional Distributions

The in-between collinear condition os compared to in-between spread condition. In addition, the in-between collinear condition is compared to the in-line collinear condition.

	Offset:	Inbetween spread	Inbundle collinear
Inbetween	MPM	-0,60 %	23,46 %
col, Env 1	90%frac	-1,59 %	28,81 %

Figure E.4: Offset deviation for the MPM and 90% values for the directional distributions in env 1

Inbetween spread env 1		Inbundle collinear env 1		Inbetween - collinear env 1	
	MPM_Tension_kN		MPM_Tension_kN		MPM_Tension_kN
Moor1	6375,4	Moor1	4156,8	Moor1	5792,9
Moor2	6480,7	Moor2	4230,9	Moor2	5927,4
Moor3	6624,2	Moor3	4292,3	Moor3	6080,7
Moor4	6763,1	Moor4	4376,8	Moor4	6240,2
Moor5	6915,6	Moor5	4445,4	Moor5	6407,2
Moor6	6791,1	Moor6	8995,2	Moor6	6811,3
Moor7	6569,6	Moor7	9103,6	Moor7	6617,6
Moor8	6412,0	Moor8	9398,0	Moor8	6473,1
Moor9	6188,0	Moor9	9477,4	Moor9	6290,1
Moor10	6024,9	Moor10	9757,4	Moor10	6139,2
Moor11	3613,8	Moor11	4486,8	Moor11	3450,0
Moor12	3663,4	Moor12	4416,6	Moor12	3464,6
Moor13	3692,2	Moor13	4340,5	Moor13	3441,1
Moor14	3753,8	Moor14	4263,8	Moor14	3468,4
Moor15	3813,1	Moor15	4168,5	Moor15	3448,3
Max Tension	6915,60		9757,40		6811,30
Mean Tension	5578,727		5994,000		5336,807

Figure E.5: Tension results for the directional distributions in env 1

		Inbetween spread env 1	Inbundle collinear env 1
Inbetween Collinear env 1	Moor1	-10,06	28,24
	Moor2	-9,33	28,62
	Moor3	-8,94	29,41
	Moor4	-8,38	29,86
	Moor5	-7,93	30,62
	Moor6	0,30	-32,06
	Moor7	0,73	-37,57
	Moor8	0,94	-45,19
	Moor9	1,62	-50,67
	Moor10	1,86	-58,94
	Moor11	-4,75	-30,05
	Moor12	-5,74	-27,48
	Moor13	-7,30	-26,14
	Moor14	-8,23	-22,93
	Moor15	-10,58	-20,89

Figure E.6: Tension deviations for the directional distributions in env 1

Deviation		In-between Spread		
		MPM	**90% fractile**	**STD**
In-between Collinear	FxRAD	-5	-1	19
	FzBOG	-5	-8	-3
	MBOG	-6	-5	27

Deviation		In-between collinear		
		MPM	**90% fractile**	**STD**
In-line Collinear	FxRAD	8	13	25
	FzBOG	-2	1	12
	MBOG	7	15	32

Figure E.7: Dynamic turret support forces deviations between the directional distributions

Appendix F

Accidental Limit State Results

Time series partially post-processed in SIMA and MatLab by computing the probability density functions and statistics based on the 14 simulations with different wave and wind seeds. The results from MatLab are then compared in Excel to see the similarities and differences better.

The in-line collinear condition for environment 1 is compared for intact and all ALS analyses.

OFFSET	requirement:		85 m			
ULS			ALS 1			
In-line collinear			**In-line collinear**			
	MPM	**90% fractile**		**MPM**	**90% fractile**	dev ULS
	39,24	44,36		46,489	51,399	7,25 m
						15,59 %
margin	45,76	40,64		38,51	33,60	
sf	2,17	1,92		1,83	1,65	

Figure F.1: Offset for intact and one line failure

	ALS 2				
	Inbundle collinear env 1				
	MPM	**90% fractile**	dev ULS	dev ALS1	
	48,233	53,572	8,99	1,74	m
			18,64	3,62	%
margin	36,77	31,43			
sf	1,76	1,59			

	ALS extreme waves					
	Inbundle collinear env 1					
	MPM	**90% fractile**	dev ULS	dev ALS1	dev ALS2	
	42,072	48,115	2,83	-4,42	-6,16	m
			6,73	-10,50	-14,64	%
margin	42,93	36,89				
sf	2,02	1,77				

Figure F.2: Offset for two line failure and extreme condition (10 000-year sea state)

ULS VS ALS

	Inbundle collinear env 1				
	ULS	**MPM_Tension kN**	**ALS1**	**MPM_Tension** kN	**Dev ULS**
Bundle 1	Moor1	4156,80	Moor1	3873,90	-7,303
	Moor2	4230,90	Moor2	3970,70	-6,553
	Moor3	4292,30	Moor3	4041,90	-6,195
	Moor4	4376,80	Moor4	4144,80	-5,597
	Moor5	4445,40	Moor5	4230,30	-5,085
Bundle 2	Moor6	8995,20	Moor6	11265,00	20,149
	Moor7	9103,60	Moor7	11494,00	20,797
	Moor8	9398,00	Moor8	12004,00	21,709
	Moor9	9477,40	Moor9	0,00	
	Moor10	9757,40	Moor10	12563,00	22,332
Bundle 3	Moor11	4486,80	Moor11	4375,50	-2,544
	Moor12	4416,60	Moor12	4295,00	-2,831
	Moor13	4340,50	Moor13	4182,80	-3,770
	Moor14	4263,80	Moor14	4062,70	-4,950
	Moor15	4168,50	Moor15	3958,40	-5,308
	Max	9757,40		12563,00	22,332
	Mean	5994,00		6318,71	5,139

Second most loaded line
Most loaded line

Figure F.3: Top end tension for intact and one line failure for all mooring lines

ALS2	MPM_Tension kN	Dev ULS	Dev ALS1		waves used as 10 000 ALS extreme MPM_Tensio [kN]	Frac_90_moor_kN [kN]
Moor1	3574,40	-16,294	-8,379	Moor1	5566,70	6388,30
Moor2	3662,60	-15,516	-8,412	Moor2	5651,10	6506,80
Moor3	3731,80	-15,020	-8,310	Moor3	5719,70	6618,10
Moor4	3841,70	-13,929	-7,890	Moor4	5807,90	6743,90
Moor5	3925,50	-13,244	-7,765	Moor5	5884,70	6900,90
Moor6	12911,00	30,329	12,749	Moor6	10415,00	16147,00
Moor7	13127,00	30,650	12,440	Moor7	10508,00	16434,00
Moor8	0,00			Moor8	10857,00	17058,00
Moor9	0,00			Moor9	10925,00	17221,00
Moor10	14253,00	31,541	11,857	Moor10	11250,00	17722,00
Moor11	4022,70	-11,537	-8,770	Moor11	5934,20	6862,10
Moor12	3915,20	-12,806	-9,701	Moor12	5844,80	6769,40
Moor13	3805,30	-14,065	-9,920	Moor13	5738,30	6532,90
Moor14	3726,20	-14,428	-9,031	Moor14	5682,50	6416,00
Moor15	3607,20	-15,561	-9,736	Moor15	5570,40	6295,10
	14253,00	31,541	11,857		11250,00	17722,00
	6007,97	0,233	-5,172		7423,68667	10041,0333

Figure F.4: Top end tension for two line failure and extreme condition for all mooring lines

ULS

Inbundle collinear env 1

	MPM	90% fractile of pdf	dev MPM[%]
FxRAD	18652,00	22158,00	15,82
FzBOG	68592,00	76662,00	10,53
MBOG	675990,00	794780,00	14,95

ALS1

Inbundle collinear env 1

	MPM	90% fractile of pdf	dev MPM[%]	MPMvsMPM dev ULS[%]
FxRAD	18560,00	22010,00	15,67	-0,50
FzBOG	64291,00	71440,00	10,01	-6,69
MBOG	669130,00	788060,00	15,09	-1,03

Figure F.5: Dynamic forces for the intact and one line failure system

ALS2					
Inbundle collinear env 1			**MPMvsMPM**		
	MPM	**90% fractile of pdf**			
			dev MPM[%]	dev ULS[%]	dev ALS1[%]
FxRAD	15651,00	19740,00	20,71	-19,17	-18,59
FzBOG	54875,00	62460,00	12,14	-25,00	-17,16
MBOG	568000,00	695360,00	18,32	-19,01	-17,80

ALS extreme waves						
Inbundle collinear env 1						
	MPM	**90% fractile of pdf**				
			dev MPM[%]	dev ULS[%]	dev ALS1[%]	dev ALS2[%]
FxRAD	22709,00	26443,00	14,12	17,87	18,27	31,08
FzBOG	86718,00	103480,00	16,20	20,90	25,86	36,72
MBOG	815120,00	951380,00	14,32	17,07	17,91	30,32

Figure F.6: Dynamic forces for the two line failure and extreme condition

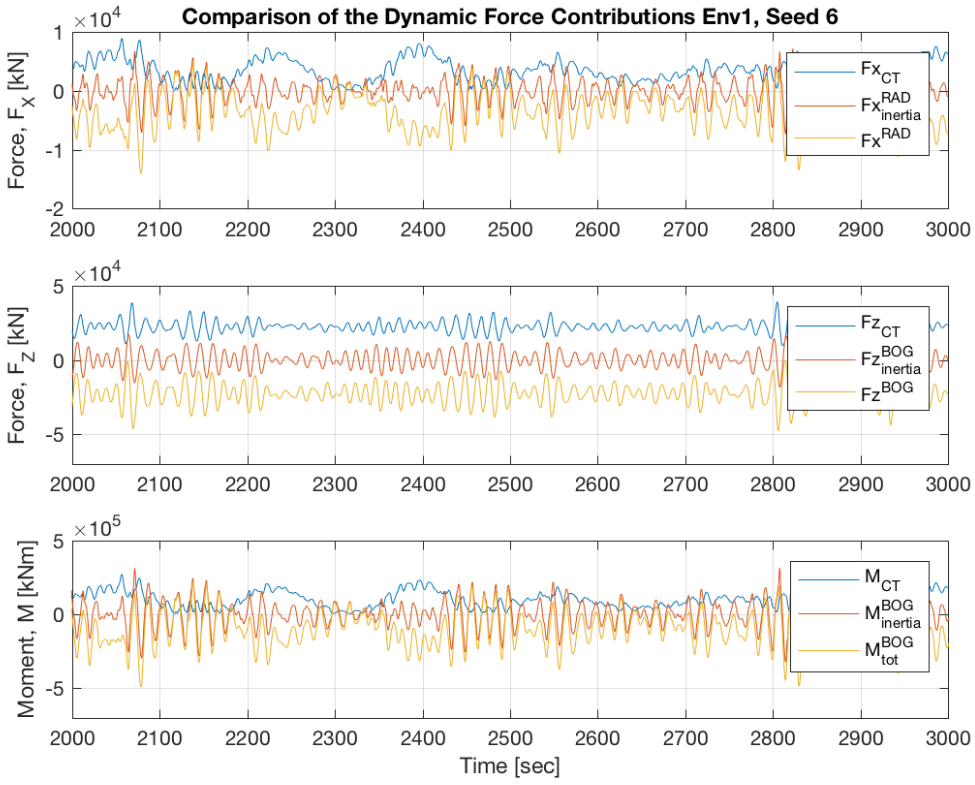

Figure F.7: Comparison of the turret dynamic dynamic support forces for ULS and ALS